Tuukka Petäjä, PhD
Handling Co-Editor
Atmospheric Chemistry and Physics

19 November 2019

Dear Dr. Tuukka Petäjä,

Please find the revised version of the manuscript, entitled "Investigating size-segregated sources of elemental composition of particulate matter in the South China Sea during the 2011 Vasco Cruise" (acp-2019-352, initially submitted on 12 April 2019), for consideration for publication as a research article in Atmospheric Chemistry and Physics.

The authors express their appreciation for the two reviewers and the handling co-editor. We believe that your feedback has improved the quality and clarity of the manuscript. In the following pages, we provide point-by-point replies to the reviewer comments and questions regarding the original manuscript.

While addressing the reviewer comments on the positive matrix factorization (PMF) results, we reviewed our PMF analysis, and found that the uncertainty values should be adjusted for specie concentrations below the detection limit of x-ray fluorescence, following the approach of Han et al. (2006). This was discussed in lines 208-213 in the revised manuscript. There are no changes in the determined sources in the fine and ultrafine modes. However, the revised approach enabled us to further constrain the PMF solution and led to the identification of a third factor in the coarse mode. These coarse mode factors are soil dust, the crustal-marine mixed source, with the addition of fly ash. This change significantly improved the interpretability of the PMF source profiles by re-apportioning heavy metal elements such as Ni, Se, and Pb from the crustal-marine mixed source into its own factor (Fig. 6). The adjusted solution also improved the correspondence between the DRUM sampler and the PMF factors. Comparing the PMF solution and DRUM samples via linear regression, we report higher correlations and a linear regression slope closer to its ideal value of 1.0. We believe that this adjustment to the PMF methodology has improved our results. We have modified the appropriate figures and text in the manuscript to reflect the updated PMF results.

We thank you again for your feedback and handling of the manuscript and we trust that the latest version is now ready for publication in Atmospheric Chemistry and Physics.

Sincerely,

Miguel Ricardo A. Hilario
Corresponding Author
Manila Observatory

Ateneo de Manila University campus, Quezon City, Philippines
miguel.hilario@obf.ateneo.edu

Authors' Response to Reviewers' Comments:

Reviewer 1

General comments:
1) Paper provides some insights into sources; however, the main drawback is the lack of quantitative information on the contribution from the analysed/selected elements to a total aerosol mass or number. How much mass was reconstructed with this elemental analysis and how important it is in the total mass balance?

Thank you for your suggestion to perform mass reconstruction. To provide a more quantitative analysis, we have performed mass reconstruction using the chemically speciated $PM_{2.5}$ filter substrates collected during the cruise. We note that only eight quartz and eight Teflon filters were collected for the entire two-week field campaign. We found that the $PM_{2.5}$ reconstructed mass, of which elements are an important part, make up 53% of the total gravimetric mass. The result is shown in Fig. S1 of the supplementary material. A brief description is provided on lines 228-231 of the revised manuscript.

We estimated the elemental contribution to the total $PM_{2.5}$ mass as the summed contributions of the sulfate, sea salt, and soil components according to formulas from Malm and Hand (2007) and Chow et al. (2015). Reconstructed elemental components derived from the DRUM sampler compose 21.2% of the total $PM_{2.5}$ gravimetric mass. This is approximately twice the value calculated with the filter-based sum of the sulfate, sea salt, and soil components (11.7%). $PM_{2.5}$ Teflon filters have been observed to show lower concentrations than rotating drum impactors for several elements, attributed to insufficient background subtractions (Venecek et al., 2016). A brief discussion is provided on lines 231-238 of the revised manuscript.

We are aware that elemental PM collected by the DRUM does not compose a dominant portion of the total mass; however, we do maintain that, due to their high temporal resolution (174 timestamps, 90-minute resolution), the DRUM elements serve as excellent tracers to identify sources and demonstrate source variability in the region.

Having only eight sets of filter substrates from the cruise, we chose to perform the PMF analysis on the elements from the DRUM sampler due to the higher temporal resolution and additional degrees of freedom through size-resolved measurements (eight stages from 0.10 μm to 10 μm). This enabled us to identify sources and to highlight the source variability present in the South

China Sea region. We have added this explanation of an elements-only PMF analysis to lines 219-225 of the revised manuscript.

2) Source contribution derived from PMF represents only the elemental part of the PM, but, as I wrote above, no quantitative information is provided. Therefore, the main conclusion from this manuscript is very qualitative and just points to an existence of other than biomass burning sources. The main question then is whether this information is new without any quantitative assessment?

The authors agree with the relevant concern of the reviewer that the PMF-calculated source contribution represents only the elemental part of the PM. Although filter data was collected to measure organic and black carbon, only eight filters were collected in the two weeks and only cover the $PM_{2.5}$ size range. Thus, as stated above, we chose to perform the PMF analysis on the elemental PM data because of its higher temporal resolution and size segregation.

While the two week-long intensive research cruise does not allow for a fully quantitative inventory of sources, the dataset presented a unique opportunity to identify aerosol sources and investigate their variability brought by the temporal nature of emissions and the complex meteorology in the region. The research cruise provided the first-ever ship-based measurements of near-surface aerosols in the South China Sea near the Philippines (Reid et al., 2015). Furthermore, these measurements enabled us to test the long-range transport hypothesis proposed in Reid et al. (2012) and provide validation for previous modeling studies on regional aerosol transport (Xian et al. 2013). We have added a short paragraph on this relevant concern in lines 219-225 of the revised manuscript.

3) Also, the text on Line 22 refers to 28 selected elements, what were the criteria for selection?

The "selected elements" refer to the elements measurable by XRF, which range from Na to Pb. We have revised the statement to remove the ambiguity. It now reads as follows "Size-segregated aerosol data was collected using a Davis Rotating-drum Unit size-cut Monitor sampler and analyzed for concentrations of 28 elements measured via X-ray fluorescence (XRF)" on lines 21-23 of the revised manuscript.

4) Figure 5 shows relative contributions to only element mass, but main components such as OM and EC are not included, not even sulphate or nitrate. Lines 498-500: 'Understanding these sources is key to characterizing aerosol composition and transport in the SCS/WPS and, by extension, developing our understanding of aerosol- cloud behavior in the region.' Indeed, but for this you need to include quantitative mass composition information (including OM, SO4, NO3) or/and number distributions.

The authors are aware that the current characterization does not include OM and EC, which are important aerosol species in an aerosol environment influenced by biomass burning. In this study, we use potassium (K) as our main biomass burning tracer with sulfur (S) as a supporting tracer for general combustion. The ionic species, elemental carbon, and black carbon were indeed measured on eight sets of $PM_{2.5}$ filters; however, as stated above, authors favored the size-resolved, high temporal-resolution elemental data collected by the DRUM sampler as its high number of data points is more appropriate for PMF and its size-resolved collection provides an additional degree of freedom for the analysis. This is explained in lines 219-225 of the revised manuscript. An analysis of the speciated data from the filters has been conducted by Reid et al. (2015).

As mentioned above, while the two-week sampling period does not allow for an exhaustive inventory of sources, the elemental dataset enabled us to identify aerosol sources, both local and regional, and investigate the temporal nature of sources present in the South China Sea region.

5) Another problem is mass size distributions provided in the manuscript. Very narrow modes at stages 7 and 5 (260-340 nm and 560-750 nm), but no mass at stage 6, raise many questions. How is this representative of ambient accumulation mode? Can these narrow modes be real? It seems to me, that there was a problem with stage 6, either in sampling or other processes, where accumulation mode peak should have occurred, but the mass is missing there for almost all elements. To conclude, the statement on bimodal distribution is very far from reality and the two narrow modes observed here are never observed with any online size measuring instrumentation.

The sharp decrease in concentrations in stage 6 despite the high concentrations in stages 5 and 7 has been observed in other studies involving the DRUM sampler; this is likely due to DRUM sampling artifacts (Atwood et al., 2013). The authors understand that the bimodal distribution likely does not reflect the true mass of the sampled aerosol, but we are simply stating in lines 220 and 242 of the original manuscript that the DRUM sampler shows a bimodal type of distribution across its stages. To elaborate on this concern and address the low concentrations in stage 6, we have added a description on lines 143-148 of the revised manuscript, which read: "A large difference in the concentrations of stage 6 (0.34-0.56 μm) compared to adjacent stages 5 (0.56-0.75 μm) and 7 (0.26-0.34 μm) was observed. The sharp decrease in concentrations in stage 6 despite the high concentrations in stages 5 and 7 has been observed in other studies involving the DRUM sampler; this is likely due to DRUM sampling artifacts and does not reflect the true aerosol mass distribution (Atwood et al., 2013). In this study, we simply report the mass distributions as sampled by the DRUM." We have removed the term "bimodal distribution" in the revised manuscript for clarity.

6) Some elements are attributed to same source origin, but time evolution is different, e.g. Lines 221-222 claim 'K, S, Al, and Si have very similar mass size distributions over the cruise period which are suggestive of 221 a common source (Fig. 3a-d).', but size distributions change form red to green or blue periods is very different for Si and K, also Al and K. Similarly, for other cases, e.g. the time trend of coarse Cl is quite different from fine, how does this agree with fine and coarse Cl coming from the same source, sea spray? Table 1 shows quite low correlation between PM 2.5 and PM10 for Cl, which is strange for the element form single sea spray source. How do you explain large contributions from other than sea salt origin elements in coarse sea spray factor (Figure 6 a)). Would that point to Cl also originating from other than sea spray sources? Or text on Line 336 claims that Si is originated from different source, which is in contradiction to the text above it.

Thank you for the comment on the size distribution changes. We meant to say that during the last half of the cruise, a regime shift occurred when back-trajectory origins shifted to southern Kalimantan (Fig. 2). This led to enhancements in K, S, and Si, which are indicative of a common source, biomass burning. We have clarified this on lines 256-260 of the revised manuscript. We also note that Figure 3 was edited in response to Reviewer #2 to include the sum of elemental PM. To maintain the eight-plot arrangement, the authors excluded Al since the other elements already provide an excellent description of the air mass evolution during the cruise and the Al size distribution does not contain significant information that cannot be derived from the other elements in the figure (K, S, Si, Fe in Fig. 3b-d, g in the revised manuscript).

Thank you for the comment on factor identification. To better reflect its elemental composition, we have changed the name of the coarse mode factor to "Crustal-Marine Mixed Source" while keeping the fine mode factor as "Sea Spray" due to high apportionments of Cl. The mixed nature in the coarse mode is likely related to covariance between local dust from nearby islands and sea spray. We have added a description of the "Crustal-Marine Mixed Source" in the PMF section, lines 399-410 of the revised manuscript which read:

"Crustal-marine mixed source: The crustal-marine mixed source was resolved in the coarse mode and is characterized by high apportionments for Na, Mg, Cl, P, and S (Fig. 6a). This source explains nearly half of the variation in crustal elements such as Al, Si, and Ca. Na and Cl show the highest contribution to the factor mass which indicate marine influence (Fig. S4, Supplementary material). These elements are indicative of a mix of sea spray and crustal sources (Han et al., 2006; Wang et al., 2014), thus its identification as a crustal-marine mixed source. The mixed nature of the source points to the covariance of local crustal emissions from nearby islands with sea spray emissions. Cl has been treated as the tracer for this factor due to its high factor sum apportionment (Fig. S4, Supplementary material) and is considered marine in origin

under the assumption that the sampled Cl originated from freshly produced sea spray (Atwood et al., 2012). This is likely the case for the cruise as sampling was done over sea water. The factor showed quite high mass contributions to the coarse mode (56.8%) indicating its dominant influence on coarse elemental PM (Fig.5a). Although both this factor and the coarse mode soil dust factor are related to crustal emissions, the crustal-marine mixed source is distinct from the coarse mode soil dust factor in terms of its temporal trend, most apparent during the 28-30 Sept aerosol event (Fig. 7a, b)."

We have clarified the identification and description of fine mode "Sea Spray" in lines 411-417 of the revised manuscript, which read: "Sea Spray: This factor was resolved in the fine mode and shows high apportionments for Na, Mg, Cl, and Ca. The identification of the factor as sea spray is evidenced by the nearly 100% source apportionment of Cl. This factor showed fine (30.4%) modes, attributed to the sampling location over water. As noted prior, the appearance of this factor in the PMF analysis is due to the persistence of Cl in the 0.75-1.15 μm of the DRUM sampler (Fig. 3h). The covariance of the sea spray factor in the fine mode with the crustal-marine mixed source in the coarse mode suggest the influence of marine aerosol to some extent in both fine and coarse modes, as suggested by a moderate correlation (0.67) between PM10 and PM2.5 Cl (Table 1)."

Specific comments:

Lines 36-38: repeating the abstract,

We have reworded the sentence to avoid redundancy. Lines 38-39 of the revised manuscript now read "In the midst of several developing countries, the South China Sea/West Philippine Sea (SCS/WPS) is a receptor for a multitude of natural and anthropogenic sources of aerosol."

Lines 38-48: rewrite to have normal text flow, now it is just a collection of sentences without any strong link.

Thank you for your suggestion; we have revised the paragraph to flow more smoothly. Lines 40-48 of the revised manuscript now read: "Thus, the SCS/WPS hosts one of the world's most complex and sensitive composition and climate regimes (Balasubramanian et al., 2003; Yusef and Francisco, 2009; Atwood et al., 2013; Reid et al., 2012, 2013, 2015). The SCS/WPS is known to be impacted not only by dust storms and industrial pollution from China (Wang et al., 2011; Atwood et al., 2012) but also by biomass burning emissions from the Maritime Continent (Balasubramanian et al., 2003; Lin et al., 2007; Cohen et al., 2010a, 2010b; Wang et al., 2011; Reid et al., 2013, 2015, 2016). The transport of such emissions is enabled by the long atmospheric residence times of fine particles (Cohen et al., 2010a), potentially creating regional and global concerns through their effects on radiative forcing (Nakajima et al., 2007; Boucher et

al., 2013; Lin et al., 2013; Ge et al., 2014) and cloud properties (Sorooshian et al., 2009; Lee et al., 2012; Boucher et al., 2013; Ross et al., 2018)."

Line 60: 'Soil dust and coarse mode biological particles may also play a role in as ice nuclei (O'Sullivan et 60 al., 2014), as biomass burning plumes are known to entrain such particles (Reid et al., 1998; 2005; Schlosser et al., 2017).' Elaborate on what you mean by biological particles from biomass burning.

Thank you for your suggestion; We have reworded the sentence for clarity on lines 61-62 of the revised manuscript which now read: "Coarse mode dust and biogenic particles may also play a role as ice nuclei (O'Sullivan et al., 2014), as biomass burning plumes are known to entrain such particles (Reid et al., 1998; 2005; Schlosser et al., 2017)."

Line 62: Sources do not mixt, aerosol particles do, similarly on line 66, sources do not have complicated chemistry and interactions.

Thank you for the correction; we have corrected the wording accordingly (lines 63, 67 of the revised manuscript). Lines 62-64 of the revised manuscript now read: "As such, a network of interacting sources exists in the region surrounding the SCS/WPS, wherein aerosol particles mix during transport and complicate source apportionment." Lines 67-68 of the revised manuscript now read: "However, the source apportionment of aerosol particles is complicated by their complex chemistry and interactions with the marine environment (Atwood et al., 2012; 2017)."

Line 89: PMF was performed on selected PM elements/tracers, not total PM.

Thank you for the correction; we have reworded the sentence accordingly. Lines 90-91 of the revised manuscript now read: "Positive Matrix Factorization (PMF) was performed on size-segregated, elemental PM to detect possible size-specific sources (Han et al., 2006; van Pinxteren et al., 2016)."

Line 183: how much of the total mass was the sum of the species?

Based on the $PM_{2.5}$ mass reconstruction, the reconstructed mass, of which elements are an important part, accounted for 53% of the gravimetric mass. Due to a lack of PM_{10} filter data, we are unable to perform a full PM_{10} mass reconstruction and thus provide the $PM_{2.5}$ reconstruction instead. As the filters covered the entire $PM_{2.5}$ range, a $PM_{1.15}$ or PM_1 mass reconstruction to ascertain the source contributions from PMF to the total gravimetric mass is not possible. Though the elements by themselves do not compose a dominant portion of the total mass (Fig.

S1), they are useful as tracers to identify sources and demonstrate source variability in the region.

Lines 189-190. Why only selected species and not all that were measured? What were the criteria for selection?

Elements not necessary for improving the interpretability of the PMF results were removed, following the approach in other PMF studies (Liao et al., 2019; Ma et al., 2019). PMF results were found to be more interpretable after the filtering of elements based on their correlations with the total elemental PM mass.

We have reworded the paragraph for clarity. Lines 199-205 of the revised manuscript now read: "Prior to analysis via PMF, the 28 elements measured via XRF were filtered based on their Pearson's R correlation with the total elemental PM mass per mode in order to improve the interpretability of PMF factors. A minimum Pearson's R value of 0.0 was used, which removed elements that were negatively correlated with the total elemental PM. From the 28 elements identified by XRF, 20 elements in the coarse mode, 22 elements in the fine mode, and 19 elements in the ultrafine mode were included in the PMF analysis. Comparing profiles with and without the correlation-based filtering, there was no significant change in factor interpretation. This indicates that the removed elements were unnecessary for improving the PMF results (Liao et al. 2019; Ma et al., 2019)."

Lines 190-192. The method is not clear here. What was done?

Please see the response above. We have reworded the paragraph for clarity (lines 199-205 of the revised manuscript).

Line 196: What do you mean by 'Below detection limit (BDL) values were replaced with half the detection limit (Han 196 et al., 2006).'

We meant that elemental concentrations below the XRF detection limits were replaced with the half of the detection limit following the approach of Han et al. (2006). We have reworded the paragraph for clarity. Lines 211-213 of the revised manuscript now read: "Measured elemental concentrations below the detection limit of XRF were replaced with half the detection limit and their relative uncertainties were set to 100% as done in Han et al. (2006)."

Figure 3: add more ticks to y axis. It is difficult to read now. Missing mass at stage 6 is unrealistic in ambient terms.

Thank you for your suggestion; gridlines have been added across the plot for clarity (Fig. 3). We agree that the drop in stage 6 is unrealistic in terms of mass. This is likely a sampling artifact as it has been observed in previous studies using the same type of sampler. Please see our discussion on Stage 6 as a sampling artifact in the general comments section. We added this discussion in lines 143-148 in the revised manuscript.

Lines 220-221: what is sigma of such narrow modes?

Stages 5, 6, and 7 have sigma values of 0.292, 0.499, and 0.268, respectively. We note though that the sampled bimodal distribution is likely not reflective of the true mass distribution. The low concentrations in stage 6 of the DRUM sampler has been observed in other studies involving the sampler (Atwood et al. 2013). We have provided a short discussion on the sampling artifact on lines 143-148 of the revised manuscript.

Line 258: add 'element' to mass concentrations in 'PM1.15 and PM10 mass concentrations';

Thank you for the correction. Lines 293-295 of the revised manuscript now read: "Table 1 shows the ratios of elemental PM1.15/PM10 mass concentrations. As in Atwood et al. (2013a), the ratio-slope was computed by taking the slope of the linear regression line between elemental PM1.15 and PM10 mass concentrations, accompanied by r^2 values."

Line 305: What do you wanted to say by this 'likely through wet deposition processes', elaborate.

We meant that the low concentrations of anthropogenic tracers (K, S, V) are associated with wet deposition related to precipitation (Reid et al., 2015, their Fig 7d). We elaborated on the wet deposition processes for better clarity. Lines 342-344 of the revised manuscript now read: "Wet deposition processes are likely responsible for the suppressed anthropogenic aerosol concentrations as precipitation was prevalent during these periods (Reid et al., 2015). Inversely, peaks in the concentrations of anthropogenic aerosol occurred during dry periods of the cruise when precipitation was low: 24-26 Sept and 28-30 Sept."

Lines 409-410: elaborate on what you mean by 'However, as PMF is an unsupervised technique, it may miss significant aerosol events, particularly transient ones' what do you base your statement that PMF can miss events on? Reference?

Thank you for your suggestion; we meant that PMF may merge consecutive but distinct aerosol events. We have elaborated on this for better clarity. Lines 468-471 of the revised manuscript now read: "However, as PMF is an unsupervised technique, it may not sufficiently disaggregate

significant, consecutive aerosol events. Visually, two distinct ultrafine events occur between 18 Sept and 19 Sept in Si (Fig. 4b) and V, Ni (Fig. 4d) which are merged by PMF in its oil combustion factor (Fig. 7d). The disproportionate enhancement of ultrafine-mode Si over V and Ni suggests a source apart from oil combustion. ”

Line 535: how much of the total mass is these 34

As described earlier, the $PM_{2.5}$ reconstructed mass, of which elements are an important part, make up 53% of the total gravimetric mass. Thus the elemental PMF is expected to resolve sources detectable from the known portion (53% of the total $PM_{2.5}$ mass). Due to a lack of PM_{10} filter data, we are unable to perform a full PM_{10} mass reconstruction and thus provide the $PM_{2.5}$ reconstruction instead. We are aware that elemental PM does not compose a dominant portion of the total mass (Fig. S1); however, we do maintain that they serve as useful tracers to identify sources and demonstrate source variability in the region.

Reviewer 2

Major comments:
1) Mass concentration: What are the typical mass size distributions for the total mass? This would be helpful to show at the beginning.

Thank you for your suggestion to include the summed elemental PM mass; we have added the total elemental mass distribution as Fig. 3a and have adjusted the figure lettering accordingly in-figure and in-text. The size distribution shows a distinct coarse mode peak apart from the submicron peaks, which indicate the presence of both biogenic and anthropogenic sources. Changes in the total mass size distribution shows that, over time, a regime-change occurred around 24 Sept during which the general back-trajectory origin shifted to southern Kalimantan (Fig. 2), bringing smoke-enriched air masses to the sampling area. We have added a description of the total mass distribution on lines 252-256 of the revised manuscript, which reads: “The mass distribution of summed elemental PM (Fig. 3a) is informative as it shows distinct peaks in the coarse and submicron ranges, pointing to a combustion or anthropogenic signal during the cruise. The total mass size distribution shows that, over time, a regime-change occurred around 24 Sept during which the general back-trajectory origin shifts to the Maritime Continent. Comparing the magnitude of the summed mass distribution to those of the key species, it is clear that S contributed a significant part of the submicron mass.”

To maintain the 8-subplot figure while retaining the information on size distributions, we have removed Al from Fig. 3 (formerly Fig. 3d) since the other elements already provide an excellent description of the air mass evolution during the cruise and the Al size distribution does not

contain significant information that cannot be derived from the other elements in the figure (K, S, Si, Fe in Fig. 3b-d, g in the revised manuscript).

2) Why is there such a drastic difference between stages 5,6 and 7? Is this a sampling artefact or real? Is there mass on the stage 6, which seems to be drastically lower in many of the mass distribution of specific elementals (Figure 2).

Thank you for your question. The sharp decrease in concentrations in stage 6 despite the high concentrations in stages 5 and 7 has been observed in other studies involving the DRUM sampler; this is likely due to DRUM sampling artifacts (Atwood et al., 2013). The authors understand that the bimodal distribution likely does not reflect the true mass of the sampled aerosol, but we are simply stating in lines 220 and 242 of the original manuscript that the DRUM sampler shows a bimodal type of distribution across its stages. To elaborate on this concern and address the low concentrations in stage 6, we have added a description on lines 143-148 of the revised manuscript, which read: "A large difference in the concentrations of stage 6 (0.34-0.56 μm) compared to adjacent stages 5 (0.56-0.75 μm) and 7 (0.26-0.34 μm) was observed. The sharp decrease in concentrations in stage 6 despite the high concentrations in stages 5 and 7 has been observed in other studies involving the DRUM sampler; this is likely due to DRUM sampling artifacts and does not reflect the true aerosol mass distribution (Atwood et al., 2013). In this study, we simply report the mass distributions as sampled by the DRUM." We have removed the term "bimodal distribution" in the revised manuscript for clarity.

Minor/technical comments:

L 17-18: On what grounds the area has the most complex aerosol-meteorological system?

The area hosts a number of developing countries with increasing aerosols emissions over time associated with economic development and rapid urbanization. In addition to emissions from urban activity, seasonal practices such as agricultural burning also contribute to aerosol loadings in the region. These aerosols, when subject to local and regional meteorological phenomena, produce a complex aerosol-climate system. The role of topography in aerosol transport and meteorology is also well-studied, adding a third feedback in this already-complex environment. The original statement has been reworded for clarity. Lines 17-19 of the revised manuscript now read: "A combination of several developing countries, archipelagic/peninsular terrain, a strong Asian monsoon climate, and a host of multi-scale meteorological phenomena make the SCS/WPS one of the most complex aerosol-meteorological systems in the world."

L 32-34: The source analysis of aerosol mass and tracers is very far from understanding the regional aerosol-cloud interactions.

Thank you for raising this point. We are aware that source identification does not directly improve our understanding of aerosol-cloud interactions; however, improving our understanding of regional aerosol sources is a step towards this goal as aerosol composition and size are important factors in determining aerosol impacts on cloud properties (Dusek et al., 2006). We have rephrased the statement for clarity. Lines 33-35 of the revised manuscript now read: "Identifying these sources is not only key for characterizing the chemical profile of the SCS/WPS but, by improving our picture of aerosol sources in the region, is also a step forward in developing our understanding of aerosol-meteorology feedbacks in this complex environment."

L 128: Figure 2: AGL and UTC/LST not defined in the text.

Thank you for the correction; we have added definitions in lines 126-127 of the revised manuscript which now read: "Back trajectories were run for 72 hours ending at 00:00 Coordinated Universal Time (UTC)/08:00 Local Time (LT) and constrained to isobaric, 300m above ground level (AGL)."

L 72, L107, L 225: boreal summer monsoon? Northern hemisphere summer? The term boreal is very specific in my field connecting to a specific vegetation type, which I think is very far from the environment pertinent to this paper.

Thank you for pointing that out; we have reworded "boreal summer monsoon" to "Asian summer monsoon" (lines 73, 108, 263 of the revised manuscript).

L 73: Although MC is defined earlier, the message would be much clearer, if the name of the area would be spelled out.

Thank you for your suggestion. We have spelled out MC in line 74 of the revised manuscript, which now reads: "In particular, the cruise aimed to observe that emissions from the Maritime Continent were reaching the southwest monsoon trough."

L 76: Please include year for the date of the typhoon as well.

We have revised the sentence accordingly. Line 77 of the revised manuscript now has the date of the typhoon as "26 September 2011".

L 150: Driving meteorology from a model or reanalysis? Please specify.

Thank you for the suggestion. We have elaborated on the model meteorology. Lines 161-163 of the revised manuscript now read: "The Navy Aerosol Analysis and Prediction System (NAAPS)

reanalysis product (Lynch et al., 2016) with driving meteorology from the Navy Global Environmental Model (NAVGEM) was used to provide overall aerosol and meteorological context to the analysis."

L 160: MODIS is spelled out here for the first time.

We have revised the sentence accordingly to use the acronym MODIS (line 164 of the revised manuscript) and have spelled out MODIS the first time it is mentioned in the text (line 123 of the revised manuscript).

L 187: Does the modes here refer to size distribution or to source specific modes? Please clarify. How much do you lose data due to filtering? This could also be an indication of some problems with sampling.

Thank you for your question. To clarify: by modes, we meant size distribution. From filtering, we removed eight elements (out of 28) in the coarse mode, six in the fine mode, and nine in the ultrafine mode. We have revised the sentence for clarity on the filtered data and process. Lines 199-205 of the revised manuscript now read: "Prior to analysis via PMF, the 28 elements measured via XRF were filtered based on their Pearson's R correlation with the total elemental PM mass per mode in order to improve the interpretability of PMF factors. A minimum Pearson's R value of 0.0 was used, which removed elements that were negatively correlated with the total elemental PM. From the 28 elements identified by XRF, 20 elements in the coarse mode, 22 elements in the fine mode, and 19 elements in the ultrafine mode were included in the PMF analysis. Comparing profiles with and without the correlation-based filtering, there was no significant change in factor interpretation. This indicates that the removed elements were unnecessary for improving the PMF results (Liao et al. 2019; Ma et al., 2019)."

L 226: a.g.l. was earlier AGL. Please be consistent

Thank you for the correction; we have revised the sentence accordingly on line 264 of the revised manuscript.

L 267-L289: A good discussion. Why is the concentration on stage 6 so much lower than on the steges 5 and 7?

Thank you; please see our discussion on Stage 6 as a sampling artifact in the general comments section of the authors' response and on lines 143-148 of the revised manuscript, which reads: "A large difference in the concentrations of stage 6 (0.34-0.56 μm) compared to adjacent stages 5 (0.56-0.75 μm) and 7 (0.26-0.34 μm) was observed. The sharp decrease in concentrations in

stage 6 despite the high concentrations in stages 5 and 7 has been observed in other studies involving the DRUM sampler; this is likely due to DRUM sampling artifacts and does not reflect the true aerosol mass distribution (Atwood et al., 2013). In this study, we simply report the mass distributions as sampled by the DRUM."

L 315-316: Please correct the sentence: During this period, plume concentration dropped sharply before recovering due to the passage of squall lines sharp, . . .

Thank you for the correction; we have removed the word "sharp" after squall lines on line 356 of the revised manuscript.

L 318: What do you mean by aerosol-convection interactions? How do you connect elementary composition to these interactions?

We meant that frequent, short-term events such as cold pools and squall lines must be accounted for in modeling studies in order to properly capture aerosol-convection interaction. Reid et al. (2015) observed sudden changes in aerosol concentrations in response to these short-term events which are not as well studied as larger circulation types. Lines 357-358 of the revised manuscript now read: "As concluded in Reid et al. (2015), frequent, short-term events such as cold pools and squall lines must be accounted for in modeling studies in order to properly capture aerosol-convection interaction."

L 337: Section 4 is well written and informative.

Thank you.

L 380: Figure 7: I would show the mass concentrations in units ug m-3. How does these numbers correspond to the integrated mass concentrations from the filters (total mass)?

We have converted the mass concentrations to μg m^{-3} in Figure 7. Mass reconstruction on the $PM_{2.5}$ filters showed that the reconstructed mass, of which elements are an important part, accounts for 53% of the total $PM_{2.5}$ (gravimetric) mass. As the filters covered the entire $PM_{2.5}$ range, a $PM_{1.15}$ or PM_1 mass reconstruction to ascertain the source contributions from PMF to the total gravimetric mass is not possible.

To further elucidate on the contribution of the elemental dataset to the total $PM_{2.5}$ mass, we estimated the elemental contribution to the total $PM_{2.5}$ mass as the summed contributions of the reconstructed sulfate, sea salt, and soil components according to formulas from Malm and Hand (2007) and Chow et al. (2015). Reconstructed elemental components derived from the DRUM

sampler compose 21.2% of the total $PM_{2.5}$ gravimetric mass. This is approximately twice the value calculated with filter-collected elemental concentrations (11.7%). $PM_{2.5}$ Teflon filters have been observed to show lower concentrations than rotating drum impactors for several elements, attributed to insufficient background subtractions (Venecek et al., 2016). A brief discussion is provided on lines 231-238 of the revised manuscript.

We are aware that elemental PM collected by the DRUM does not compose a dominant portion of the total mass; however, we do maintain that, due to their high temporal resolution (174 timestamps, 90-minute resolution), the DRUM elements serve as excellent tracers to identify sources and demonstrate source variability in the region.

L 411: Please summarize the results of the regression results at the end of the section. In the current form it is difficult to see the importance of the findings (Sulfur and connection to biomass burning, V/Ni ratio in connection with oil combustion and discussion on Si-enhancement). Maybe a reorganization with Sect 5 would help to convey the message? In the current form, Sect 5 is very short and it could be integrated with the earlier section.

Thank you for your suggestion. We have rephrased the section to more clearly describe the importance of the linear regression analysis and added a paragraph to summarize the results of the linear regression. Lines 511-519 of the revised manuscript now read: "The regression analysis showed an early-cruise enhancement in ultrafine Si that was merged by PMF with a V, Ni enhancement that occurred soon after, highlighting the importance of the regression analysis in addition to PMF to investigate the temporal characteristics of sources via elemental tracers. We suggest a local source en route to the main sampling area to be the cause of the enhancement but fly ash is unlikely the source due to low correlations with its tracers As, Pb, and Se. The analysis also showed the strong associations of S with biomass burning and oil combustion; however, S was shown to covary more significantly with the former. Oil combustion was determined to originate from shipping as indicated by a V/Ni ratio within the range of that measured by a previous shipping emission study. Finally, we infer multiple sources of soil dust between the coarse and fine modes due to distinct Si-Al ratios between modes; however, we are unable to determine the exact sources due to lack of information regarding local and regional soil dust ratios."

L 430: Supplementary material.

Thank you for the correction; we have revised the sentence accordingly on line 494 of the revised manuscript.

L 444: What do you mean by "timestamp"? A specific concentration at a given time?

Yes, that is correct. Each point of the scatter plot is colored by the concentration of sulfur at that given time. We clarified this in line 494-496 of the revised manuscript, which read: "fine and ultrafine mode linear regressions of K and V, colored by the concentration of S per given time, were constructed to show the relationships between the three species (Fig. 8a, b)."

L502: See my comment on the stage 6. Is it feasible to have such a drastic difference between three adjacent size ranges (stages 5,6,7)?

Thank you for raising this point; we agree that the drop in mass at Stage 6 is likely a sampling artifact as it has been observed in previous studies using the same type of sampler and probably does not reflect the true mass distribution of the aerosol environment. Please see our discussion on Stage 6 as a sampling artifact in the general comments section and on lines 143-148 of the revised manuscript.

L 511: . . . evidence of high levels of MC burning? Please clarify.

Thank you for the suggestion; we have revised the sentence for clarity. Line 586-588 of the revised manuscript now read: "The strong peaks of these biomass burning tracers, in combination with the rapid spread of high AOD and NAAPS-modelled smoke concentration across the region, provide evidence for intensive emissions from the MC."

L 514: Please remind the reader that TC is a tropical cyclone.

Thank you for the suggestion; we have revised the sentence accordingly on line 590 of the revised manuscript.

L 528: three size modes

Thank you for the correction; we have revised the sentence accordingly on line 606 of the revised manuscript.

L 571: Rapid nucleation event is brought up only in the conclusions. Also secondary formation during transport is brought up at the end. Please clarify. Is there data to support this?

Thank you for raising this point. We meant that the sudden ultrafine silicon enhancement noted at the start of the cruise may be related to a rapid nucleation process, as even submicron dust can be an important source of cloud condensation nuclei in a marine/coastal environment (Twohy et al., 2009). We have added clarification in the results section regarding the rapid nucleation event

to lines 482-485 of the revised manuscript, which now read: “As the Vasco was travelling near islands, the source of the ultrafine Si enhancement is likely a local source en route to Palawan. The sudden enhancement may be related to a rapid nucleation event as even submicron dust can be an important source of CCN in marine/coastal environments (Twohy et al. 2009).”

By secondary formation during transport, we meant that research using trace gases collected during the same research cruise may give us an idea on the chemical transformations that occur during transport to produce secondary species. We have revised the final paragraph for clarity on lines 651-655 of the revised manuscript, which now read: “In addition to the findings of this study on the elemental PM, future research on other species collected during the 2011 and 2012 Vasco campaigns such as trace gases may complement and deepen our current understanding of the aerosol environment in the SCS/WPS through additional degrees of freedom, specifically utilizing the lifetimes of trace gases and inferring the potential for secondary aerosol formation during transport.”

References

Atwood, S. A., Reid, J. S., Kreidenweis, S. M., Cliff, S. S., Zhao, Y., Lin, N.-H., Tsay, S.-C., Chu, Y.-C. and Westphal, D. L.: Size resolved measurements of springtime aerosol particles over the northern South China Sea, Atmos. Environ., 78, 134–143, doi:10.1016/j.atmosenv.2012.11.024, 2013.

Dusek, U., Frank, G. P., Hildebrandt, L., Curtius, J., Schneider, J., Walter, S., Chand, D., Drewnick, F., Hings, S., Jung, D., Borrmann, S. and Andreae, M. O.: Size Matters More Than Chemistry for Cloud-Nucleating Ability of Aerosol Particles, Science, 312(5778), 1375–1378, doi:10.1126/science.1125261, 2006.

Liao, H.-T., Chang, J.-C., Tsai, T.-T., Tsai, S.-W., Chou, C. C.-K. and Wu, C.-F.: Vertical distribution of source apportioned PM 2.5 using particulate-bound elements and polycyclic aromatic hydrocarbons in an urban area, J Expo Sci Environ Epidemiol, 1–11, doi:10.1038/s41370-019-0153-2, 2019.

Ma, L., Dadashazar, H., Braun, R. A., MacDonald, A. B., Aghdam, M. A., Maudlin, L. C. and Sorooshian, A.: Size-resolved characteristics of water-soluble particulate elements in a coastal area: Source identification, influence of wildfires, and diurnal variability, Atmos. Environ., 206, 72–84, doi:10.1016/j.atmosenv.2019.02.045, 2019.

Reid, J. S., Lagrosas, N. D., Jonsson, H. H., Reid, E. A., Sessions, W. R., Simpas, J. B., Uy, S. N., Boyd, T. J., Atwood, S. A., Blake, D. R., Campbell, J. R., Cliff, S. S., Holben, B. N., Holz, R. E., Hyer, E. J., Lynch, P., Meinardi, S., Posselt, D. J., Richardson, K. A., Salinas, S.

V., Smirnov, A., Wang, Q., Yu, L. and Zhang, J.: Observations of the temporal variability in aerosol properties and their relationships to meteorology in the summer monsoonal South China Sea/East Sea: the scale-dependent role of monsoonal flows, the Madden–Julian Oscillation, tropical cyclones, squall lines and cold pools, Atmospheric Chem. Phys., 15(4), 1745–1768, doi:10.5194/acp-15-1745-2015, 2015.

Twohy, C. H., Kreidenweis, S. M., Eidhammer, T., Browell, E. V., Heymsfield, A. J., Bansemer, A. R., Anderson, B. E., Chen, G., Ismail, S., DeMott, P. J. and Van Den Heever, S. C.: Saharan dust particles nucleate droplets in eastern Atlantic clouds, Geophys. Res. Lett., 36(1), L01807, doi:10.1029/2008GL035846, 2009.

Venecek, M. A., Zhao, Y., Mojica, J., McDade, C. E., Green, P. G., Kleeman, M. J. and Wexler, A. S.: Characterization of the 8-stage Rotating Drum Impactor under low concentration conditions, Journal of Aerosol Science, 100, 140–154, doi:10.1016/j.jaerosci.2016.07.007, 2016.

Xian, P., Reid, J. S., Atwood, S. A., Johnson, R., Hyer, E. J., Westphal, D. L., and Sessions, W.: Smoke transport patters over the Maritime Continent, Atmos. Res., 122, 469–485, doi:10.1016/j.atmosres.2012.05.006, 2013

Investigating size-segregated sources of elemental composition of particulate matter in the South China Sea during the 2011 *Vasco* Cruise

Miguel Ricardo A. Hilario[a, +], **Melliza T. Cruz**[b], **Maria Obiminda L. Cambaliza**[a,b], **Jeffrey S. Reid**[c], **Peng Xian**[c], **James B. Simpas**[a,b], **Nofel D. Lagrosas**[b, *], **Sherdon Niño Y. Uy**[b], **Steve Cliff** [d], **Yongjing Zhao**[d]

[a] Department of Physics, Ateneo de Manila University, Quezon City, Philippines

[b] Manila Observatory, Ateneo de Manila University campus, Quezon City, Philippines

[c] Marine Meteorology Division, Naval Research Laboratory, Monterey, CA, USA

[d] Air Quality Research Center, University of California Davis, CA, USA

[+]Now with Manila Observatory, Ateneo de Manila University campus, Quezon City, Philippines

[*] Now with Center for Environmental Remote Sensing, Chiba University, Japan

Correspondence: Maria Obiminda L. Cambaliza (mcambaliza@ateneo.edu)

Abstract

The South China Sea/West Philippine Sea (SCS/WPS) is a receptor of numerous natural and anthropogenic aerosol species from throughout greater Asia. A combination of several developing countries, archipelagic/peninsular terrain, a strong Asian monsoon climate, and a host of multi-scale meteorological phenomena make the SCS/WPS one of the most complex aerosol-meteorological systems in the world. However, aside from the well-known biomass burning emissions from Indonesia and Borneo, the current understanding of aerosol sources is limited-especially in remote marine environments. In September 2011, a 2-week research cruise was conducted near Palawan, Philippines to sample the remote SCS/WPS environment. Size-segregated aerosol data was collected using a Davis Rotating-drum Unit size-cut Monitor sampler and analyzed for concentrations of 28 elements measured via X-ray fluorescence (XRF). Positive Matrix Factorization (PMF) was performed separately on the coarse, fine, and ultrafine size ranges to determine possible sources and their contributions to the total elemental particulate matter mass. The PMF analysis resolved six sources across the three size ranges: biomass burning, oil combustion, soil dust, a crustal-marine mixed source, sea spray, and fly ash. Additionally, size distribution plots, time series plots, back trajectories and satellite data were used in interpreting factors. The multi-technique source apportionment revealed

the presence of biogenic sources such as soil dust, sea spray and a crustal-marine mixed source; anthropogenic sources were identified as well: biomass burning, oil combustion, and fly ash. Mass size distributions showed elevated aerosol concentrations towards the end of the sampling period which coincided with a shift of air mass back trajectories to Southern Kalimantan. Covariance between coarse mode soil dust and fine mode biomass burning aerosols were observed. Agreement between the PMF and the linear regression analyses indicates that the PMF solution is robust. While biomass burning is indeed a key source of aerosol, the study shows the presence of other important sources in the SCS/WPS. Identifying these sources is not only key for characterizing the chemical profile of the SCS/WPS but, by improving our picture of aerosol sources in the region, is also a step forward in developing our understanding of aerosol-meteorology feedbacks in this complex environment.

1. Introduction

In the midst of several developing countries, the South China Sea/West Philippine Sea (SCS/WPS) is a receptor for a multitude of natural and anthropogenic sources of aerosol. At the same time, the region exhibits some of the world's most complicated meteorology due to its archipelagic/peninsular terrain and strong Asian monsoon climate. Thus, the SCS/WPS hosts one of the world's most complex and sensitive composition and climate regimes (Balasubramanian et al., 2003; Yusef and Francisco, 2009; Atwood et al., 2013a, b; Reid et al., 2012, 2013, 2015). It is known to be impacted not only by dust storms and industrial pollution from China (Wang et al., 2011; Atwood et al., 2013a) but also by biomass burning emissions from the Maritime Continent (Balasubramanian et al., 2003; Lin et al., 2007; Cohen et al., 2010a, 2010b; Wang et al., 2011; Reid et al., 2013, 2015, 2016). The transport of such emissions is enabled by the long atmospheric residence times of fine particles (Cohen et al., 2010a), potentially creating regional and global concerns through their effects on radiative forcing (Nakajima et al., 2007; Boucher et al., 2013; Lin et al., 2013; Ge et al., 2014) and cloud properties (Sorooshian et al., 2009; Lee et al., 2012; Boucher et al., 2013; Ross et al., 2018).

Highlighting the unique combination of terrain and sea that feeds into the complexity of the meteorological environment of the region, Reid et al. (2012) and Xian et al. (2013) posed the long-range hypothesis that monsoonal flows and higher-frequency meteorological phenomena are a major factor in seasonal aerosol dispersion. Biomass burning plumes are known to cause severe haze episodes due to these monsoonal flows, raising concentrations of particulate matter (PM) to impact cloud physics and, in some cases, to dangerous air quality levels across large areas, particularly in association with positive phases of the El Niño-Southern Oscillation (ENSO) (Engling et al., 2014; Fujii et al., 2015). Likewise, biomass burning is a significant contributor to the region's cloud condensation nuclei (CCN) budget in all years as are the region's significant anthropogenic emissions (Balasubramanian et al., 2003; Field et al., 2008; Reid et al., 2012; 2013; 2015; 2016; Atwood et al., 2017).

Partly due to the emphasis on dramatic biomass burning as the primary source of aerosol particles in the region, the contributions of other regional sources are not well understood or perhaps underappreciated. As the SCS/WPS is host to major population centers, industry, major ports, and coal and oil combustion are expected to be an important regional source of aerosol particles in the MC. Coarse mode dust and biogenic particles may also play a role as ice nuclei (O'Sullivan et al., 2014), as biomass burning plumes are known to entrain such particles (Reid et al., 1998; 2005; Schlosser et al., 2017). As such, a network of interacting sources exists in the region surrounding the SCS/WPS, wherein aerosol particles mix during transport and complicate source apportionment. Understanding the nature of sources in the remote MC and their contributions is key to characterizing the aerosol environment in the SCS/WPS and its relationship with cloud behavior and precipitation patterns in the region; this is particularly true given the higher sensitivity of clouds to particle perturbations at lower concentrations. However, the source apportionment of aerosol particles is complicated by their complex chemistry and interactions with the marine environment (Atwood et al., 2013a; 2017).

As part of the Seven South East Asian Studies program (7-SEAS), a research cruise (Reid et al., 2015) was conducted in late September 2011 onboard the Philippine-flagged M/Y *Vasco* in the vicinity of the northern Palawan archipelago. The goal of this cruise was to observe the behavior of aerosol particles in the SCS/WPS and test the transport hypothesis proposed in Reid et al. (2012) that the Philippines is a long-range receptor of aerosol species transported across the SCS/WPS during the Asian summer monsoon from Borneo, Sumatra, and the Malay Peninsula. In particular, the cruise aimed to observe that emissions from the Maritime Continent were reaching the southwest monsoon trough. The Palawan archipelago is a good receptor site for regional emissions due to its largely rural settlements and its location upwind relative to the rest of the Philippines. The sampling period coincided with the passage of one tropical storm and two tropical cyclones (TC). Of particular importance is the passage of super typhoon Nesat beginning on 26 September 2011 as TC inflow arms are known to cause abrupt changes in regional flows.

As part of the 2011 *Vasco* cruise, particulate matter was collected using a size segregated Davis-Rotating Uniform Size-Cut Monitor (DRUM) impactor analyzed for elemental composition. While Reid et al. (2015) noted the presence of smoke plumes in two episodes during the cruise, their initial analysis of the region's atmospheric chemistry also suggested the events were a mix of biomass burning and oil or shipping emissions due to elevated levels of vanadium. Additionally, differences in elemental ratios, mass fractions and back trajectory origins between the two events support the presence of other sources besides biomass burning. From the initial analysis of aerosol chemistry presented by Reid et al. (2015), this study aims to identify aerosol sources in the SCS/WPS, to highlight the source variability present in the region, and to further develop the current understanding of the effect of regional meteorological phenomena on aerosol dispersion. The paper shows that, though biomass burning is a major source of aerosols in the SCS, anthropogenic sources such as oil combustion also play an important role in the chemical profile of the region. As we report, soil transport was observed as well.

In this paper we expand on the original 2011 *Vasco* cruise analysis to quantitatively apportion sampled biomass burning and anthropogenic aerosol species. Positive Matrix Factorization (PMF) was performed on size-segregated, elemental PM to detect possible size-specific sources (Han et al., 2006; van Pinxteren et al., 2016). Indeed, the relationship between the aerodynamic diameter of a particle and its source has been well-established in literature (Reid et al., 1993; Balasubramanian et al., 2003; Han et al., 2006; Lestari et al., 2009; Wimolwattanapun et al., 2010; Santoso et al., 2010; Karanisiou et al., 2009; Seneviratne et al., 2010; Atwood et al., 2013a; Lin et al., 2015; Cahill et al., 2016). Aerosol factors and characteristics were then used to spawn back trajectories to identify individual island emissions areas.

2. Sampling and Methods

2.1. Overall cruise sampling and environment

A general overview of the 2011 cruise can be found in Reid et al. (2015) and a brief summary is provided here. Sampling was conducted around the Palawan archipelago, an island chain located at the southwestern edge of the Philippines in between the SCS/WPS and the Sulu Sea. Sampling was performed between Manila and the northern tip of Palawan Island onboard the M/Y *Vasco* which left Manila Bay on 17 September 2011 and returned on 30 September 2011 (Fig. 1). Majority of samples were collected around the areas of El Nido and Malampaya Sound (111.1° N, 119.3° E) where the vessel was on station from 21-28 Sept. The largely rural population of Palawan made it an ideal receptor for regional rather than local emissions.

Figure 1. Path taken by the M/Y *Vasco* for 17-20 September (red), 20-28 September (black), 28-30 Sept (blue). Majority of sampling was done at the northern end of Palawan island. Image courtesy of Google Maps (map data ©2018 Google).

The cruise was conducted at the end of the Asian summer monsoon which usually lasts from June through September (Loo et al., 2014; Chang et al., 2005). The Asian monsoon is caused by the annual march of the sun and asymmetrical heating of air masses due to the complex terrain of Southeast Asia (Chang et al., 2005). The campaign coincided with the peak burning season in Southern Kalimantan and Southern Sumatra, which have been measured to be the highest emitters of biomass burning plumes in the MC (Reid et al., 2012). As the southwest monsoon is characterized by winds travelling southwest to northeast, Reid et al. (2015) proposed that the Philippines was an excellent receptor for regional emissions from the MC.

Although 2011 was a moderate La-Niña year, it was noted that fire activity and precipitation levels resembled a neutral year (Reid et al., 2015). The cruise took place when the Madden-Julian Oscillation (MJO) was transitioning from the wet phase to the dry phase, which is expected to enhance burning activity and transport. With the passage of tropical cyclones (TCs), significant aerosol events were observed to propagate across the region.

Reid et al. (2015) described three tropical events that occurred during the cruise, specifically tropical storm (TS) Haitang, super-TC Nesat, and super-TC Nalgae. The presence of inflow arms in the SCS has been suggested to affect the aerosol environment by bringing more MC air into the region (Reid et al., 2015). The passage of Nesat was observed to abruptly affect air mass trajectories coinciding with an enhancement of several elements during the last two days of the cruise.

Figure 2 shows the evolution of the meteorological environment over the cruise period with comparisons between satellite-derived aerosol optical depth (AOD) derived from the Moderate Resolution Imaging Spectroradiometer (MODIS) onboard the Terra and Aqua satellites, back trajectories from NOAA Hybrid Single Particle Lagrangian Integrated Trajectory Model (HYSPLIT) and 850 hPa smoke concentrations from the Navy Aerosol Analysis and Prediction System (NAAPS). Back trajectories were run for 72 hours ending at 00:00 Coordinated Universal Time (UTC)/08:00 Local Time (LT) and constrained to isobaric, 300m above ground level (AGL).

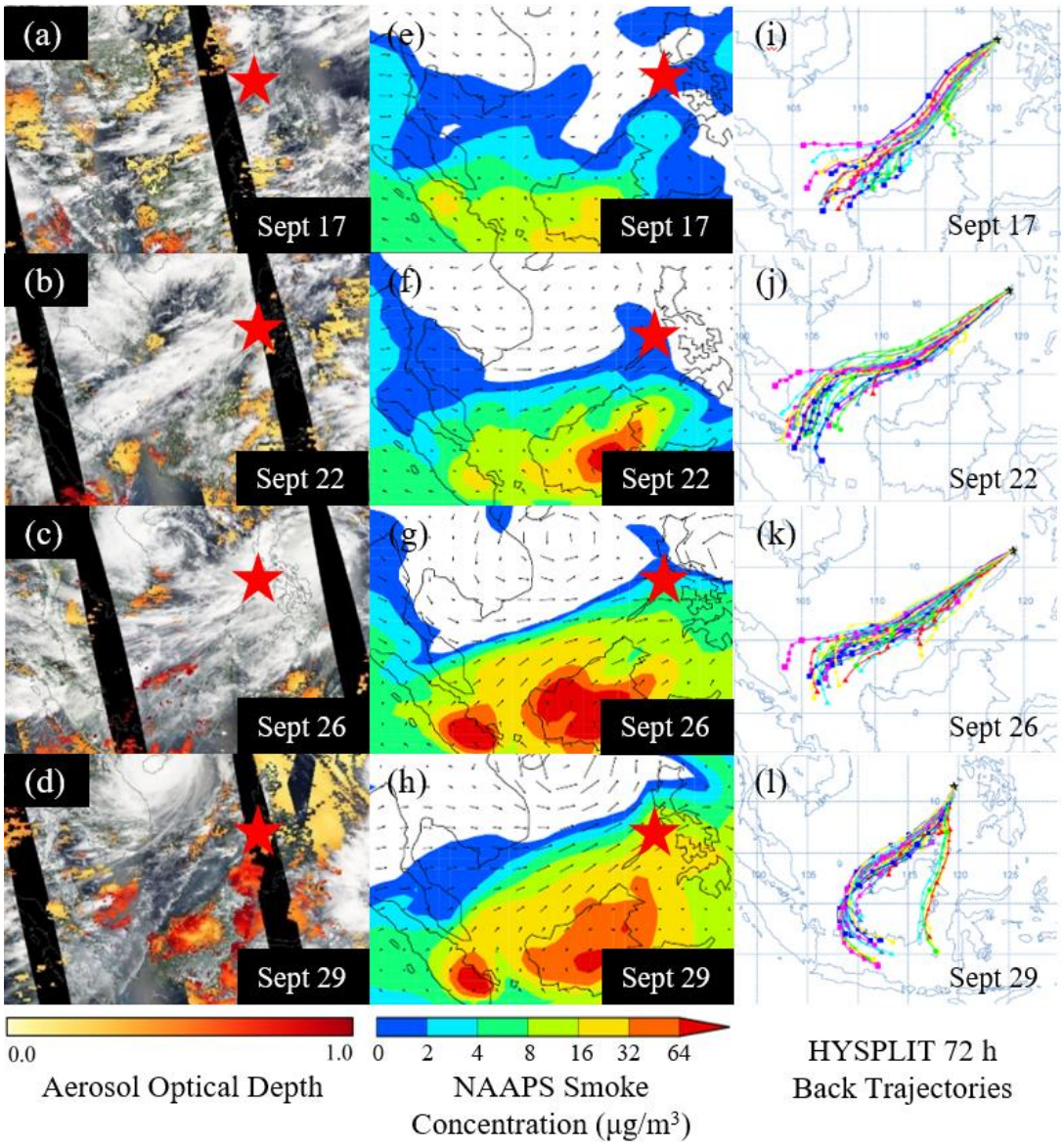

Figure 2. Satellite images of the SCS/WPS region taken from (a-d) NASA Worldview with overlaid AOD, (e-h) NAAPS smoke concentration plots ($\mu g/m^3$; 850 hPa) and (i-l) HYSPLIT ensemble back trajectories during the cruise for 18, 22, 26 and 29 Sept (isobaric; 300m AGL; 72 hours; ending at 00:00 UTC/08:00 LT). Red star indicates location of the *Vasco*.

2.2. Aerosol sampling and analysis

Size-resolved aerosol samples were collected during the cruise using a Davis-Rotating Unit for Monitoring (DRUM) continuously sampling cascade impactor. Samples were collected with a 10 μm inlet and eight size cuts at 5, 2.5, 1.15, 0.75, 0.56, 0.34, 0.26, 0.10 μm at a 90-minute time resolution from noontime 17 September until noontime 30 September local-time. Particles were collected on Mylar strips coated with Apiezon grease. The eight drums were rotated at a consistent rate to create a temporal record of mass concentration (Raabe et al., 1988). X-ray fluorescence (XRF) was performed on the DRUM samples at the Advanced Light Source (ALS) of Lawrence Berkeley National Laboratory to measure mass concentrations of 28 elements ranging from Na to Pb. In this study, data was filtered based on location notes from the cruise such that samples

collected in the vicinity of Manila Bay were excluded from the analysis. Additionally, samples during an 8-hour pump failure that occurred on 20 September were also excluded from the dataset. In the analysis, the stages were aggregated into three modes: coarse (1.15-10 μm), fine (0.34-1.15 μm) and ultrafine (0.10-0.34 μm) modes. A large difference in the concentrations of stage 6 (0.34-0.56 μm) compared to adjacent stages 5 (0.56-0.75 μm) and 7 (0.26-0.34 μm) was observed. The sharp decrease in concentrations in stage 6 despite the high concentrations in stages 5 and 7 has been observed in other studies involving the DRUM sampler; this is likely due to DRUM sampling artifacts and does not reflect the true aerosol mass distribution (Atwood et al., 2013a). Nevertheless, the two size resolved modes lend themselves to size segregated analysis. In this study, we simply report the mass distributions as sampled by the DRUM.

In addition to the DRUM sampler, eight sets of $PM_{2.5}$ filters were collected during the cruise and were chemically analyzed for information on species such as sulfate, nitrate, and organic carbon. The $PM_{2.5}$ filters were described more fully in Reid et al. (2015). Mass reconstruction was performed on the $PM_{2.5}$ filter data according to the methodology of Malm and Hand (2007). Results are shown in Fig. S1 and discussed briefly in Section 3.1.

2.3. Model and satellite data

NOAA Hybrid Single Particle Lagrangian Integrated Trajectory Model (HYSPLIT) back trajectories (Draxler et al., 1998, 1999) were generated throughout the cruise period to investigate locations of aerosol emission. HYSPLIT back trajectories have been used in several studies to establish air mass source regions (Lin et al., 2007; Cohen et al., 2010a; Atwood et al. 2013a, 2017). Back trajectories were run for 72 hours for heights of 500 m and 300 m to investigate possible vertical inhomogeneity that has been noted in other SCS/WPS papers (Atwood et al., 2013a). Trajectory endpoints corresponded to cruise coordinates. Trajectories were constrained isobarically to limit vertical wind velocity since our area of interest is surface-level emission.

The Navy Aerosol Analysis and Prediction System (NAAPS) reanalysis product (Lynch et al., 2016) with driving meteorology from the Navy Global Environmental Model (NAVGEM) was used to provide overall aerosol and meteorological context to the analysis. This reanalysis utilizes a modified version of the NAAPS as its core and assimilates quality controlled retrievals of aerosol optical depth (AOD) from MODIS on Terra and Aqua and the Multi-angle Imaging SpectroRadiometer (MISR) on Terra (Zhang et al., 2006; Hyer et al., 2011; Shi et al., 2014). NAAPS characterizes anthropogenic and biogenic fine (including sulfate, and primary and secondary organic aerosols), dust, biomass burning smoke and sea salt aerosols. Smoke from biomass burning is derived from near-real time satellite based thermal anomaly data to construct smoke source functions (Reid et al., 2009), with additional orbital corrections on MODIS based emissions and regional tunings. The system has been successfully used to monitor biomass burning plumes and to study the relationship of aerosol lifecycle to weather systems over the MC (Reid et al., 2012, 2015, 2016; Atwood et al., 2013b; Xian et al., 2013).

Active fire hotspot data was downloaded from the Fire Information for Resource Management System (FIRMS) (https://firms.modaps.eosdis.nasa.gov/). Active fire hotspots and aerosol optical depth (AOD) at a wavelength of 550 nm were tracked throughout the cruise via MODIS. MODIS detects thermal anomalies across a region to identify possible fire activity. MODIS-derived AOD was used to derive large-scale estimates of $PM_{2.5}$ in some studies (e.g., Zheng et al., 2017). In the study, MODIS was used to track burning emissions which were found to be particularly prevalent in Eastern Malaysia and Indonesia. The use of MODIS to track active fire hotspots has been used in other studies to understand seasonal trends in agricultural burning (Reid et al., 2012) and to identify and locate burning-related sources when used in conjunction with HYSPLIT back trajectories (Atwood et al., 2017).

The NASA Worldview site (www.worldview.nasa.gov), an application operated by the NASA/Goddard Space Flight Center Earth Science Data and Information System (ESDIS) project, was used to supplement the satellite data by providing true color images of the region and is particularly useful in demonstrating sudden changes of cloud environment or monsoon flow caused by tropical cyclones.

2.4. Positive Matrix Factorization

Positive Matrix Factorization (PMF) was used to study the covariance of elemental species. PMF is a multivariate factor analysis technique used in source apportionment that resolves a sample matrix $\mathbf{X}$ ($i \times j$) of i samples and j species into matrices $\mathbf{G}$ ($i \times k$), $\mathbf{F}$ ($k \times j$), and $\mathbf{E}$ ($i \times j$), the source contribution matrix, source profile matrix and residual matrix, respectively, with the assumption of k factors:

$$X_{ij} = G_{ik}F_{kj} + E_{ij}$$

The goal of PMF is to determine the number of factors or sources k such that the solution will be physically interpretable. Developed by Paatero and Tapper (Paatero and Tapper, 1994), PMF is a well-established approach used in previous source apportionment studies (Polissar et al., 1998; Lee et al., 1999; Han et al., 2006; Chan et al., 2008; Karanisiou et al., 2009; Lestari et al., 2009; Santoso et al., 2010; Wimolwattanapun et al., 2010). PMF provides more physically realistic results compared to other factor analysis techniques due to non-negative constraints in the model and better treatment of missing or below detection limit (BDL) values by increasing the associated uncertainty (Paterson et al., 1999).

PMF outputs source profiles (F) and source contributions (G). PMF source profiles were normalized to the percent of species sum, defined as the percent concentration of an element apportioned to a source. An outlier threshold distance α was used to reduce the effect of extremely large data points and was set at a value of 4.0 to be consistent with other PMF studies (Lee et al., 1999; Han et al., 2006).

Prior to analysis via PMF, the 28 elements measured via XRF were filtered based on their Pearson's R correlation with the total elemental PM mass per mode in order to improve the interpretability of PMF factors. A minimum Pearson's R value

of 0.0 was used, which removed elements that were negatively correlated with the total elemental PM. From the 28 elements identified by XRF, 20 elements in the coarse mode, 22 elements in the fine mode, and 19 elements in the ultrafine mode were included in the PMF analysis. Comparing profiles with and without the correlation-based filtering, there was no significant change in factor interpretation. This indicates that the removed elements were unnecessary for improving the PMF results (Liao et al. 2019; Ma et al., 2019). Tables S1-3 (Supplementary material) show the correlation coefficients of coarse-, fine-, and ultrafine-mode elements. The filtering of elements through correlation with total PM per mode was observed to improve the interpretability of the PMF outputs and remove the need for the matrix rotation parameter, F_{peak}.

Data screening was performed based on the approach of Polissar et al. (1998) and Han et al. (2006) to ensure that no erroneous data points were included in the analysis. BDL values were replaced by half the detection limit and relative uncertainties were set to 100% (Han et al., 2006). Signal-to-noise ratios were determined and elements with low ratios (less than 0.2) were excluded from the data set (Paatero and Hopke, 2003). Measured elemental concentrations below the detection limit of XRF were replaced with half the detection limit and their relative uncertainties were set to 100% as done in Han et al. (2006). Detection limit values and error values were based on values provided by the Lawrence Berkeley National Laboratory.

The current study employs a size-resolved PMF approach as a supplement to the other analysis methods. PMF is a powerful tool that quantifies the contributions of PM sources and is useful for forming an initial understanding of the possible sources from the data. However, PMF may neglect important events, particularly short-term ones, that can reveal insightful interactions between identified sources and is unable to dissociate covarying sources as it assumes orthogonality between factors (Van Pinxteren et al., 2016).

For this study, we included only the DRUM elemental data for PMF analysis. Speciated data from the $PM_{2.5}$ filter was excluded due to the limited number of filters available (eight quartz and eight Teflon filters). The much higher temporal resolution (174 timestamps) from the DRUM sampler, in addition to its collection across eight size ranges, provided the necessary data resolution for PMF while offering the additional degree of freedom of size-resolved collection. Due to the limitations inherent in a two-week-long research cruise, the collected dataset is not expected to provide a full quantitative inventory of sources but rather provides an opportunity to study short-term aerosols events to gain a better understanding of source variability in the SCS region.

3. Results I: Mass distributions and time series of selected elements

3.1. Reconstructed mass and DRUM mass distributions

Mass reconstruction performed on the $PM_{2.5}$ filters shows an increasing trend in aerosol loadings towards the end of the cruise (Fig. S1a). A large event beginning on 28 Sept is characterized by heightened contributions of particulate organic matter. A smaller aerosol event was also detected by the 23 Sept and 25 Sept filters. The mass reconstruction shows that 53% of the

total $PM_{2.5}$ gravimetric mass is accounted for by the reconstructed components which include organic carbon (Fig. S1b). The elemental contribution to the total $PM_{2.5}$ mass was estimated as the summed contributions of the reconstructed sulfate, sea salt, and soil components according to formulas from Malm and Hand (2007) and Chow et al. (2015). Reconstructed elemental components derived from the DRUM sampler compose 21.2% of the total $PM_{2.5}$ mass. This is approximately twice the value calculated with filter-collected elemental concentrations (11.7%). $PM_{2.5}$ Teflon filters have been observed to show lower concentrations than rotating drum impactors for several elements, attributed to insufficient background subtractions when computing for filter concentrations (Venecek et al., 2016). Other potential factors in this discrepancy include a complicated sampling environment that may result in filter losses during collection and the long filter collection times during the cruise.

Elemental mass size distributions show normalized species concentrations (dM/dlogDp) across all eight DRUM stages and can be used to validate the signal of a mode-specific tracer. In addition to isolating the signal of a tracer, changes in the mass distributions of key elements over time indicate periods when mode-specific sources are present. Figure 3 depicts the mass size distributions of the (a) summed elemental PM, and key elements (b) potassium (K) as a tracer for biomass burning in the fine and ultrafine modes; (c) sulfur (S), a general indicator of combustion; (d) silicon (Si) for soil dust; (e) vanadium (V) and (f) nickel (Ni), which are often paired as tracers of oil combustion; (g) iron (Fe), another key tracer for dust; and (h) chlorine (Cl), a reasonable tracer for sea spray given the sampling location. Figure 3 is further divided into time periods, distinguished by color: 18-19 September (red), 19-24 September (blue), 24-27 September (green) and 27-30 September (black).

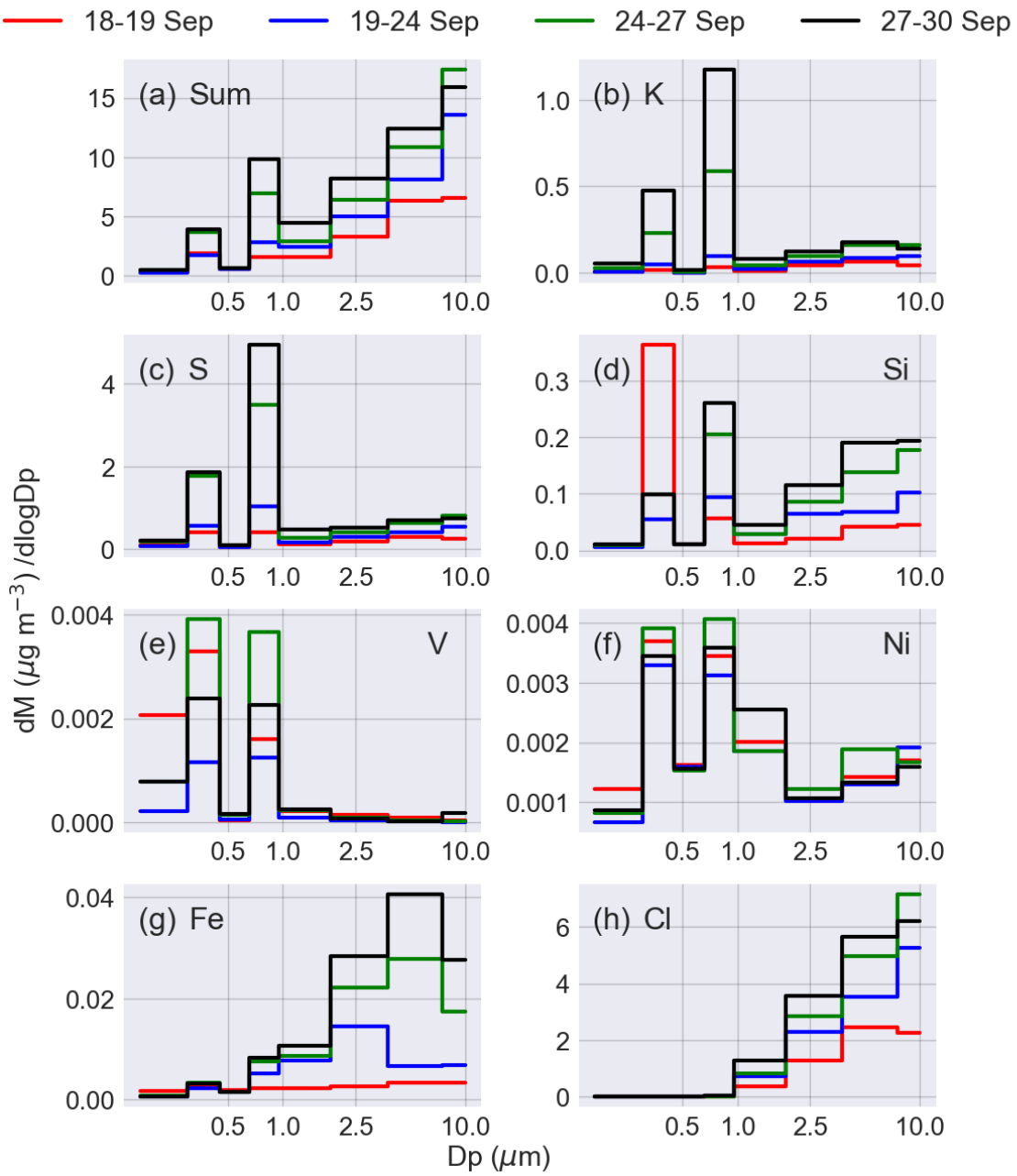

Figure 3. Time evolution of mass size distributions over the cruise period. (a) Sum of all measured elements, (b) potassium, (c) sulfur, (d) silicon, (e) vanadium, (f) nickel, (g) iron, and (h) chlorine. Time periods are colored: 18-19 Sept (red), 19-24 Sept (blue), 24-27 Sept (green), 27-30 Sept (black). Stage numbers are depicted in (a).

The mass distribution of summed elemental PM (Fig. 3a) is informative as it shows distinct peaks in the coarse and submicron ranges, pointing to a combustion or anthropogenic signal during the cruise. The total mass size distribution shows that, over time, a regime-change occurred around 24 Sept during which the general back-trajectory origin shifts to the Maritime Continent. Comparing the magnitude of the summed mass distribution to those of the key species, it is clear that S contributed a significant part of the submicron mass. Elements associated with combustion showed peaks in stage 5 (0.56-0.75 μm) and stage 7 (0.26-0.34 μm). K, S, and Si have very similar changes in their mass size distributions over the cruise period which are

suggestive of a common source (Fig. 3b-d). During the latter half of the cruise, a regime shift occurred wherein back-trajectory origins shifted to southern Kalimantan (Fig. 2). We observe coincident enhancements in K, S, and Si – indicative of a common source, likely biomass burning. These elements have strong peaks in stages 5 and 7 during the whole cruise but particularly high values are observed during the last days of the sampling period (27-30 Sept). A general enhancement late in the cruise is likely related to the increase in the number of active fire hotspots reported by Reid et al. (2015), who attributed these hotspots primarily to Indonesian Kalimantan and Southern Sumatra. As the cruise took place during the end of the Asian summer monsoon, 300 m AGL winds were predominantly southwesterly. A shift in back trajectories at the end of the cruise to the western and southern coasts of Borneo is observable in Fig. 2l, suggesting the source of the late-cruise enhancement to be the MC, which hosts elevated aerosol background levels during this time of year from seasonal burning (Reid et al., 2013). The advection of this large aerosol event can be observed in the NAAPS smoke model over the region (Fig. 2g, h). The attribution of late-cruise aerosol enhancement to the MC is in agreement with Reid et al. (2015) who noted that the AOD maps and southwesterly flows towards the end of the cruise were suggestive of southwesterly transport from the MC to SCS/WPS.

Covariance of Si (Fig. 3d) with K and S suggest possible fine soil entrainment caught in burning updraft (Reid et al., 2015). The stage 5 and stage 7 peaks in S are similar to those observed for northern SCS/WPS in the springtime (Atwood et al., 2013a); however, we report enhanced values, attributed to the timing of the sampling period during the MC burning season.

Interestingly, Si shows a strong peak early in the cruise (18-19 Sept) unique to the ultrafine mode which indicates this particular signal may not originate from soil dust but fly ash (Xie et al., 2009). As the *Vasco* was travelling past the islands of Mindoro and Coron en-route to Palawan, local sources are likely the cause of the ultrafine Si enhancement. This early-cruise Si signal is further examined through later time series and regressions.

V shows a mass distribution characteristic of a combustion source with strong peaks in stage 5, stage 7, and stage 8 (0.10-0.26 μm) (Fig. 3e). Almost no contribution was observed for coarser stages 1 through 4 (0.75 -10 μm), indicating that V did not originate from soil (Lin et al., 2015) and can be treated as a tracer for oil combustion. Ni shows a similar mass distribution (Fig. 3f) but had a larger spread over the eight stages than V, which may be due to contributions from other sources such as fly ash (Davison et al., 1974).

Fe and Cl, well-known tracers for soil dust and sea spray, respectively, showed coarse-mode distributions that taper off considerably in the submicron stages (Fig. 3g, h). Cl shows a purely coarse distribution, indicative of the influence of sea spray considering the sample location (Viana et al., 2008; Gugamsetty et al., 2012; Farao et al., 2014). Fe shows small peaks in stage 4 (0.75-1.15 μm), stage 5, and stage 7; however, these do not constitute a significant signal relative to its coarse mode concentrations. As such, we treat Fe as our coarse mode soil dust tracer. The mass distribution of Fe is observed to increase across stages 1 through 3 (2.5-10 μm) over the cruise period. The increase in coarse Fe coincides with the NAAPS-simulated transport of smoke (Fig. 2g, h) and mirrors the enhancements of K, S, Si (Fig. 4a, b), and Al (Fig. S2a, b). These patterns

suggest that coarse soil dust accompanies smoke emissions, possibly through entrainment. The presence of soil dust is further corroborated by Fig. 3d, which show the presence of Si in the coarse mode. The distinct coarse and fine mode peaks of Al and Si indicate separate soil dust sources. As fine mode particles have longer residence times (Cohen et al., 2010a), the fine peaks may be an indicator of long-range transport of fine soil dust through the SCS/WPS.

Interpreting DRUM data reveals insights about the composition and interpretation of sources. Table 1 shows the ratios of elemental $PM_{1.15}/PM_{10}$ mass concentrations. As in Atwood et al. (2013a), the ratio-slope was computed by taking the slope of the linear regression line between elemental $PM_{1.15}$ and PM_{10} mass concentrations, accompanied by r^2 values. Direct averages of per-timestamp ratios of $PM_{1.15}$ and PM_{10} were also taken to compute for ratio-averages, accompanied by the standard deviation of the ratios. Fe and Cl both had ratios of 0.06, which confirm the predominantly coarse nature of these species. As commonly used tracers of soil dust, Al and Si show moderate ratio-slope values of 0.51 and 0.29, respectively, suggesting that Al resides in both coarse and fine ($PM_{1.15}$) modes while Si is predominantly coarse. As expected, elements commonly associated with anthropogenic species such as V, K, and S show high $PM_{1.15}/PM_{10}$ ratios (0.8 and above) which indicate that these elemental particles largely reside in the fine and ultrafine modes. The high ratios of V, K, and S provide evidence for the presence of anthropogenic emissions from sources such as oil combustion and biomass burning while the low ratios of Fe and Cl support their treatment as tracers for soil dust and sea spray, respectively.

The time-resolved DRUM data is important for showing variations in species which may be representative of important aerosol events. Thus, observations on the time-resolved DRUM data can aid in our analysis. At the beginning of the cruise, between 18 to 19 Sept, V, Ni, and Si show enhancements in stages 5, 7, and 8. The stage 7 Si peak during this time is the maximum concentration over the entire cruise period, so this warrants further analysis through later time series and regressions. The period of 19-24 Sept shows a low point in the DRUM peaks of several elements, most notably combustion tracers K and V (Fig. 3b, e), while Cl (Fig. 3h) shows higher peaks in the coarse-mode which suggests a period of clean marine aerosol. This period was described by Reid et al. (2015) as the cleanest of the cruise. The NAAPS model shows nearly zero smoke concentration at the sampling site (Fig. 2f) while 72-h HYSPLIT back trajectories indicate that air masses originate from central SCS/WPS (Fig. 2j). From 24 to 27 Sept, we observed the first major aerosol event characterized by the stage 5 and 7 enhancements of several combustion elements: K, S, Si, V, and Ni (Fig. 3b-f). Fe, our coarse-mode soil dust tracer, shows enhancements in stages 1 to 3 (Fig. 3g), which points to combustion-related entrainment of soil dust in the coarse mode. The NAAPS model (Fig. 2g) depicts the intensification and spread of a smoke-related aerosol event that had been escalating in southern Kalimantan since 22 Sept, reaching the *Vasco* around 26 Sept. During this mid-cruise period, concentrations of biomass burning species K, S, Si, Al are elevated, and oil combustion tracers V and Ni show their maximum concentrations for the cruise in stages 5 and 7 (Fig. 4e, f). The last period, 28 to 30 Sept, depicts the highest concentrations of elements associated with biomass burning (Fig. 4a, b; Fig. S2a, b). As seen in the NAAPS smoke model (Fig. 2h) and HYSPLIT model (Fig. 2l), the westward movement of TC Nesat across the region alters back trajectories to wind around Borneo island, reaching

southern Kalimantan which hosted a high active fire hotspot density during the time (Reid et al., 2015), thus bringing polluted air masses toward the sampling site. Stage 5 and 7 peaks of K and S are quite notable as no other stages show significant enhancements in response to this event. Fe and Si show similar changes but for the coarser stages 1 to 3 (Fig. 3d, g), indicating a covariance of soil dust and biomass burning tracers. The temporal trends from the DRUM data serve as an entry point into the time series analysis. By identifying key DRUM stages and time periods per element based on their mass size distributions, we can then examine these stages to observe aerosol events over the cruise period.

3.2. Time series of selected elements

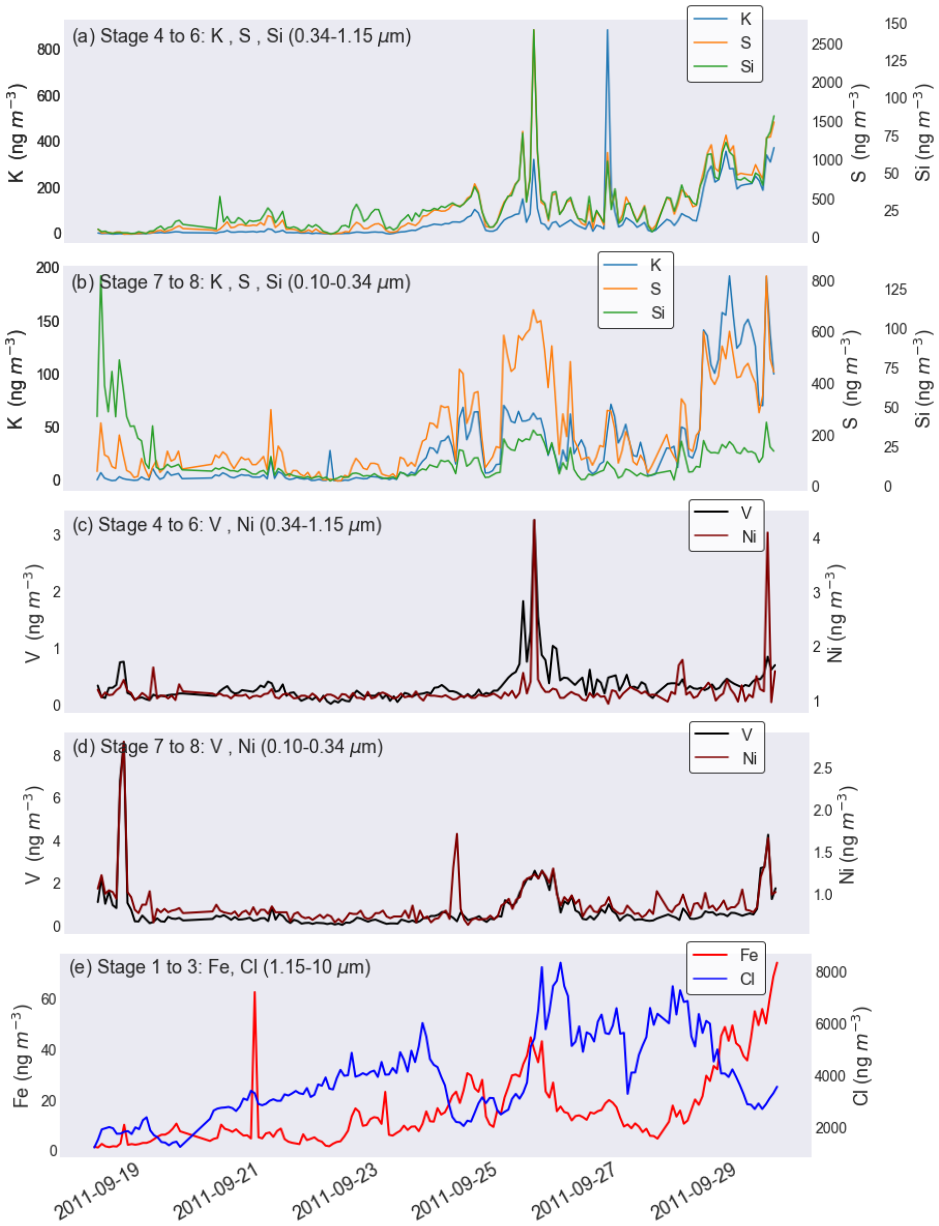

Figure 4. Time series of (a) Stage 4-6 K, S, Si, (b) Stage 7-8 K, S, Si, (c) Stage 4-6 V, Ni, (d) Stage 7-8 V, Ni, and (e) Stage 1-3 Fe, Cl.

The first few days of the cruise showed an 18 Sept event in oil combustion tracers V and Ni in the ultrafine mode (Fig. 4d) with a coincident but lower-magnitude response in the fine mode (Fig. 4c). Ultrafine mode V and Ni show their maxima for the cruise period during this time, expanded further in Section 5. High concentrations of ultrafine Si were sampled during this time from the beginning of the cruise until 19 Sept when it dropped to stable background levels. This early-cruise enhancement was also seen in its mass distribution plot (Fig. 3d). As the *Vasco* was traveling among islands, the Si signal may be due to local sources en-route to the El Nido sampling site.

Reid et al. (2015) noted periods of clean regime after departing Manila Bay through midday 22 Sept, observable in the consistently low concentrations of various elements (Fig. 4). Chlorine shows a gradual increase in concentration from 20 Sept until 24 Sept. Chlorine, although it ages into HCl, is assumed to be fresh due to the sampling location and can therefore be used as an indicator of sea spray. Interestingly, coarse-mode Cl (Fig. 4e) showed peak concentration times during low points in the concentrations of anthropogenic aerosol species (Fig. 4a-d), marking periods of clean marine aerosol on 22-24 Sept and 26-28 Sept. Wet deposition processes are likely responsible for the suppressed anthropogenic aerosol concentrations as precipitation was prevalent during these periods (Reid et al., 2015). Conversely, peaks in the concentrations of anthropogenic aerosol occurred during dry periods of the cruise when precipitation was low: 24-26 Sept and 28-30 Sept. During the periods of clean marine aerosol, back trajectories shift away from source regions and traverse open sea (Fig. 2j, k) which also hosts a lower shipping route density compared to coastal regions (Fig. S3, Supplementary material). The first half of the cruise also saw the lowest concentrations from species associated with biomass burning, specifically submicron K, S, Si, (Fig. 4a, b), and Al (Fig. S2a, b, Supplementary material). These species track each other quite well throughout the cruise period indicating a common source.

The event between 24 Sept and 26 Sept is observable on the time series of several key elements. The plume was the first of two distinct plume events reported by Reid et al. (2015) with the later plume occurring on 29 Sept. The enhancement of all elements in Fig. 4 suggests a mix of biomass burning, oil combustion and soil dust influences within the 24-26 Sept plume. Fine mode V and Ni show their maximum concentrations for the cruise during this event (Fig. 4c). Although these two plumes appeared as one uniform progression across the SCS/WPS region on the NAAPS smoke model (Fig. 2h), the time series showed the presence of two distinct events (Fig. 4), which is corroborated by observations from Reid et al. (2015). During this period, aerosol concentrations dropped sharply before recovering due to the passage of squall lines, observed in the time series for K, S, Si, Fe, and Cl (Fig. 4a, b, e). As concluded in Reid et al. (2015), frequent, short-term events such as cold pools and squall lines must be accounted for in modeling studies in order to properly capture aerosol-convection interaction.

The period between plumes (26-28 Sept) is characterized by an overall drop in the aerosol concentration of species associated with anthropogenic sources (K, S, V, Ni; Fig. 4a-d). As Cl concentrations show peak values during this period (Fig. 4d), this indicates a period of pure marine aerosol sampling similar to the 22-24 Sept clean period. Coinciding with the passage

of TC Nesat through the SCS/WPS, the observed drop in aerosol concentration is attributed to a possible restriction of shipping traffic in response to the TC and scavenging of aerosols by precipitation along the TC inflow arm (Fig. 2c) (Reid et al., 2015).

The last days of the cruise were particularly eventful as the largest aerosol event of the cruise period was visible on the NAAPS model in the form of smoke (Fig. 2h), accompanied by the spread of high AOD values throughout the SCS/WPS (Fig. 2d). Although the large areas of cloud cover created by TC Nesat hinders the detection of AOD on 26 Sept, the region is free of cloud cover by 29 Sept that significant AOD values were observed to visibly stretch from Southern Kalimantan towards the *Vasco* sampling site (Fig. 2d). In general, the NAAPS smoke transport model agrees with the spatial distribution of high AOD. Here, NAAPS modelling of smoke transport is useful in demonstrating the event's northward advection and the severity of smoke concentration in Borneo island on 26 Sept (Fig. 2h). Time series plots of elements associated with biomass burning (K, S, Si; Fig. 4a, b) and coarse mode soil dust (Fe; Fig. 4d) show significant enhancements during this time which were also observed on their mass distributions (Fig. 3). HYSPLIT back trajectories show that air masses originate from Southern Kalimantan during this period as opposed to mainland Malaysia during the first half (Fig. 2j, l). The shift in air mass trajectories is attributed to the passage of TC Nesat through the region as inflow arms from TCs have been observed to accelerate air mass advection across the SCS/WPS, bringing more MC air into the region (Reid et al., 2012; 2015). The observed transport of emissions from Borneo indicates that TC-enhanced long-range transport is a significant factor in SCS/WPS aerosol dispersion.

4. Results II: positive matrix factorization and regressions

4.1. Source apportionment via positive matrix factorization

To verify groupings of key elements and aid in source identification, size-resolved PMF was performed. As described in Section 2, the eight-stage DRUM data were combined into coarse (1.15-10 μm), fine (0.34-1.15 μm) and ultrafine (0.10-0.34 μm) modes and the species included in the PMF analysis were then filtered based on their correlation to the aggregated PM concentration per mode. The PMF analysis resolved six sources across the three size ranges: biomass burning, oil combustion, soil dust, a crustal-marine mixed source, sea spray, and fly ash (Table 2). Due to the similarities in composition and temporal trends of the crustal-marine mixed source in the coarse mode and the sea spray factor in the fine mode, they are depicted together in Fig. 5-7 for simplicity.

One strength of PMF is its quantification of a source's contribution. Figure 5 shows the percent contribution of each source relative to the total elemental PM mass. As expected, natural sources such as the crustal-marine mixed source and soil dust mainly contribute to the coarse mode while combustion-related sources such as biomass burning and oil combustion contribute to the fine and ultrafine modes. The identification of sea spray in the fine mode is likely due to the existence of Cl in stage 4 of the DRUM sampler (Fig. 3h). The existence of these sources in their expected modes is an indicator of the successful implementation of PMF. The following sections describe the observed characteristics of sources determined by PMF.

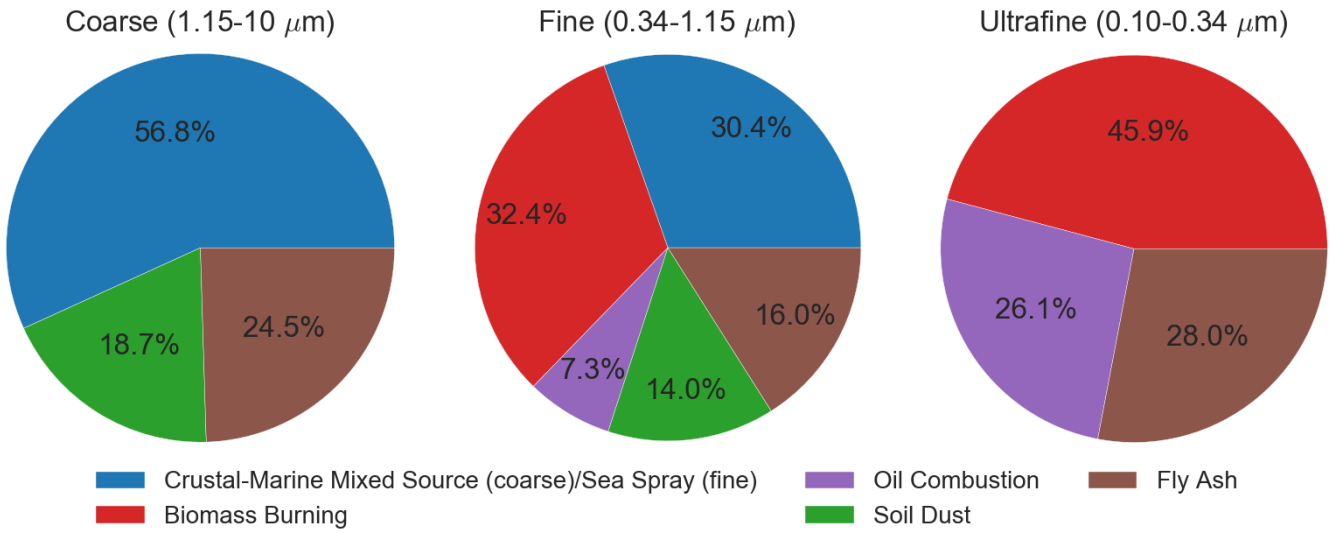

392

393 **Figure 5. Contributions of factors to the total elemental PM mass. The crustal-marine mixed source (coarse mode) and**

394 **sea spray (fine mode) share the same color to reflect their similar chemical compositions.**

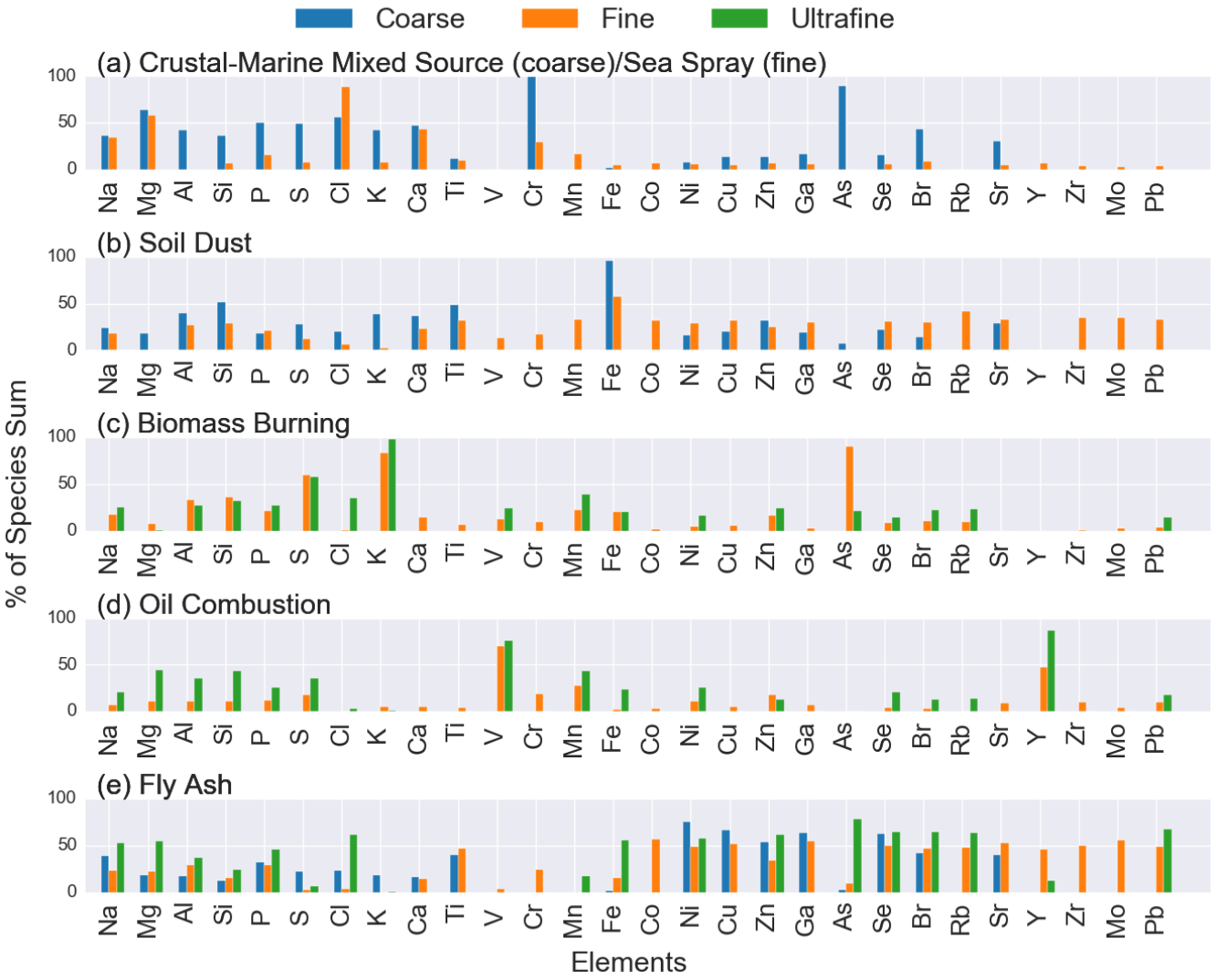

395

Figure 6. PMF source profiles across different size ranges displayed by percent of species sum for (a) crustal-marine mixed source, (b) soil dust, (c) biomass burning, (d) oil combustion, and (e) fly ash. Coarse: Stage 1-3 (1.15-10 μm; blue), Fine: Stage 4-6 (0.34-1.15 μm; orange), Ultrafine: Stage 7-8 (0.10-0.34 μm; green).

Crustal-marine mixed source: The crustal-marine mixed source was resolved in the coarse mode and is characterized by high apportionments for Mg, Cl, P, Al, Si, S and Ca (Fig. 6a). This source explains nearly half of the variation in crustal elements such as Al, Si, and Ca. Na and Cl show the highest contribution to the factor mass which indicate marine influence (Fig. S4, Supplementary material). These elements are indicative of a mix of marine and crustal emissions (Han et al., 2006; Wang et al., 2014), thus its identification as a crustal-marine mixed source. The mixed nature of the source points to the covariance of local crustal emissions from islands of the Maritime Continent and those nearby with sea spray. Cl has been treated as the tracer for this factor due to its high factor sum apportionment (Fig. S4, Supplementary material) and is considered marine in origin under the assumption that the sampled Cl originated from freshly produced sea spray (Atwood et al., 2013a). This is likely the case for the cruise as sampling was done over sea water. The factor showed quite high mass contributions to the coarse mode (56.8%) indicating its dominant influence on coarse elemental PM (Fig.5a). Although both this factor and the coarse mode soil dust factor are related to crustal emissions, the crustal-marine mixed source is distinct from the coarse mode soil dust factor in terms of its temporal trend, most apparent during the 28-30 Sept aerosol event (Fig. 7a, b).

Sea Spray: This factor was resolved in the fine mode and shows high apportionments for Na, Mg, Cl, and Ca. The identification of the factor as sea spray is evidenced by the nearly 100% source apportionment of Cl. This factor showed fine (30.4%) modes, attributed to the sampling location over water. As noted above, the appearance of this factor in the PMF analysis is due to the persistence of Cl in the 0.75-1.15 μm of the DRUM sampler (Fig. 3h). The covariance of the sea spray factor in the fine mode with the crustal-marine mixed source in the coarse mode point to the influence of marine emissions to some extent in both the fine and coarse modes, as suggested by a moderate correlation coefficient (0.67) between PM_{10} and $PM_{2.5}$ Cl (Table 1).

Soil dust: This factor was characterized by the presence of Fe, Al, Si, K, Ca, Ti, and Zn in the coarse mode and Fe, Cr, Mn, and Y in the fine mode (Fig. 6b; Table 2). Several of these elements are associated with soil dust (Artaxo et al., 1990, 1998; Lestari et al., 2009; Wimolwattanapun et al., 2010; Gugamsetty et al., 2012). Soil dust may originate from the nearby island of Palawan but also can potentially come from Borneo. The PMF model was able to distinguish between the crustal-marine mixed source and soil dust factors. As crustal-marine mixed emissions are assumed to be freshly sampled during the cruise and the temporal trends of the two sources are distinct (Fig. 7a, b), this suggests the possibility of a long-range transport mechanism for coarse mode soil dust. The time series of coarse soil dust (Fig. 7b) tracks the fine biomass burning factor well (Fig. 7c), indicative of coarse soil dust particles entrained in biomass burning plumes. Fe serves as our tracer for soil dust due to its high apportionment in both soil dust modes. This factor showed mass contributions of 18.7% and 14.0% in the coarse and fine modes, respectively, which indicates the predominantly coarse mode contribution of the factor (Fig. 5a, b).

Biomass burning: This factor was characterized by high levels of K and S, and moderate levels of Al, As, and Si which were found to be associated with biomass burning in previous studies (Artaxo et al., 1998; Han et al., 2006; Lestari et al., 2009; Atwood et al., 2013a; Alam et al., 2014) (Fig. 6c; Table 2). The factor showed the highest percent contributions to the PM mass: 32.4% and 45.9% in the fine and ultrafine modes, respectively. The sources of the 26 Sept and 28-30 Sept events (Fig. 7c) will be investigated in Section 5. The presence of crustal elements Fe, Si, and Al in the source profile and the covariance of the coarse soil dust factor (Fig. 7b) with this factor (Fig. 7c) indicate possible soil dust entrainment during burning updraft (Reid et al., 2015; Schlosser et al., 2017).

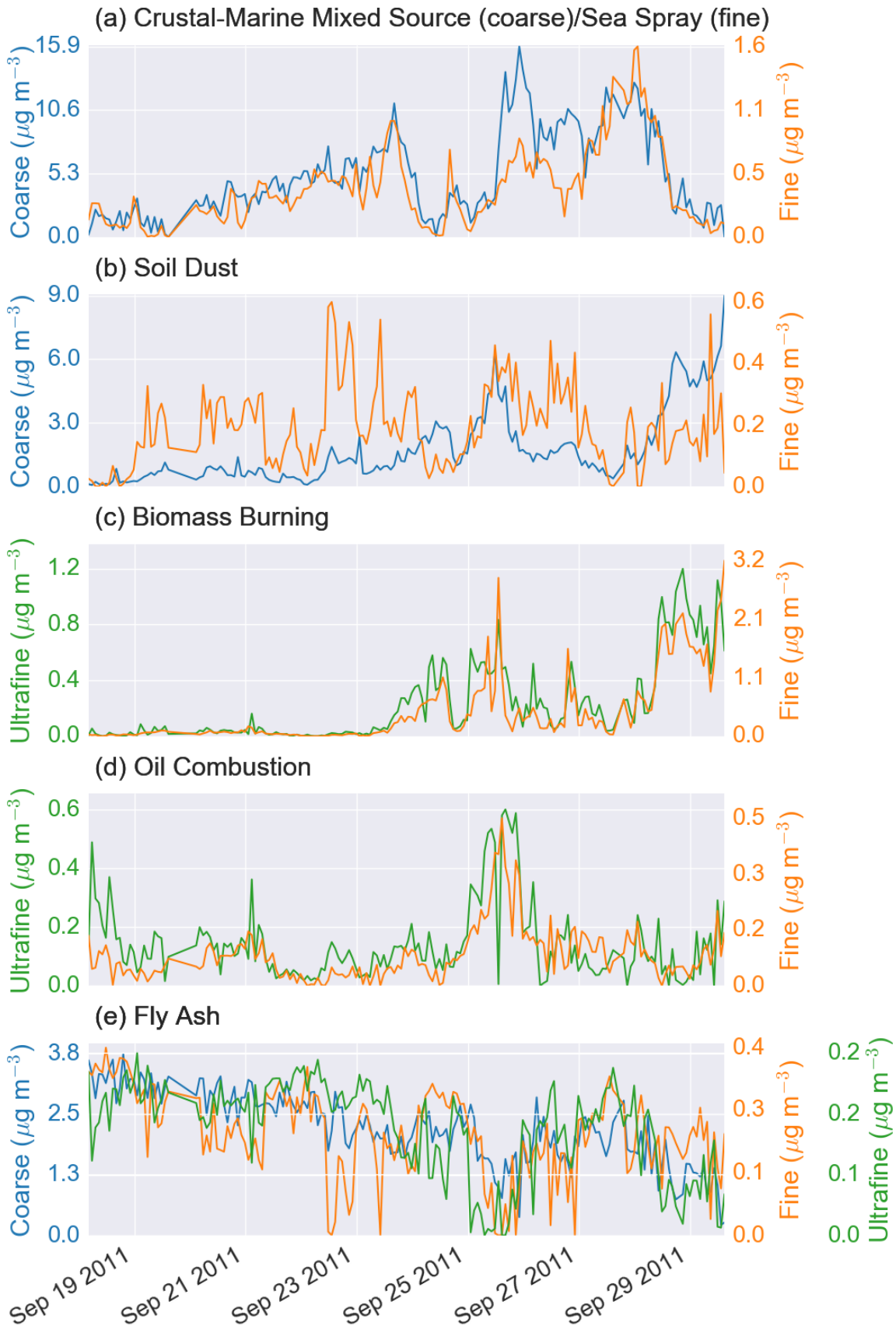

435

436 **Figure 7. Temporal distribution of PMF source contributions (μg/m^3) for (a) crustal-marine mixed source, (b) soil dust,**
437 **(c) biomass burning, (d) oil combustion, and (e) fly ash. Coarse: Stage 1-3 (1.15-10 μm; blue), Fine: Stage 4-6 (0.34-1.15**
438 **μm; orange), Ultrafine: Stage 7-8 (0.10-0.34 μm; green).**

Oil combustion: This factor was characterized by high levels of V (Fig. 7d; Table 2), a well-documented tracer for oil combustion (Hedberg et al., 2005; Mazzei et al., 2008; Becagli et al., 2012). As shown in Fig. 5, the oil combustion factor only appeared in the fine and ultrafine sizes, contributing 7.3% and 26.1%, respectively, to the total elemental PM mass. The increasing contribution towards finer stages corroborates the identification of the factor as an anthropogenic source. The presence of oil combustion is expected as the SCS/WPS hosts high shipping volume, particularly in parts of the Borneo coast (Fig. S3, Supplementary material).

Fly ash: This factor was observed in all size modes, characterized by high levels of trace metals Ni, Ga, Zn, Se, Br, Rb, Pb across modes with slight differences in composition per mode (Fig. 6e); and a source contribution without distinct events (Fig. 7e). The dominance of Ni, Zn, Se, and Br are indicative of fly ash (Davison et al., 1974; Markowski et al., 1985; Deonarine et al., 2015). Moderate apportionments of crustal elements Na, Mg, Al, Si, P, and Ti are also observed, suggestive of entrained soil. The source contribution time series shows a background-type signal. The factor contributed 24.5%, 16.0% and 28.0% to the total elemental PM mass for the coarse, fine, and ultrafine modes, respectively (Fig. 5). Long-range transport of fly ash from coal-fired power plants in Indonesia or mainland Malaysia may be responsible for the appearance of the factor as no local coal-fired power plants could be found upwind of the sampling site in 2011.

The PMF analysis resolved the presence of six sources across the ultrafine, fine and coarse modes which aids in directing further analysis by identifying key species in the source profiles. Pearson correlation heatmaps (Fig. S5-7, Supplementary material) and matrices with numerical values (Tables S1-S3, Supplementary material) were constructed to examine the relationships between species. The first column of the correlation outputs (Fig. S5-7, Tables S1-S3, Supplementary material) shows the correlation coefficient of the element when compared to the summed elemental PM for that mode. Similar groupings of elements were observed when compared to the PMF source profiles, indicating the robustness of the analysis. In the coarse mode (Fig. S5, Table S1, Supplementary material), we observe high correlations between Na, Mg, Cl, P, S, K, Ca, Br, and Sr, which are associated with sea spray and crustal sources (Han et al., 2006; Wang et al., 2014). Fe, Ti, Mn, Si, and Zn show moderate to high correlations in the coarse mode, indicative of dust (Karanisiou et al., 2009; Wimolwattanapun et al., 2010; Lin et al., 2015; Landis et al., 2017). In the fine mode, moderate to high correlations between Al, Si, P, S, K, Br are observed (Fig. S6, Table S2, Supplementary material). Several of these biomass burning elements show similarly strong correlations in the ultrafine mode (Fig. S7, Table S3, Supplementary material). V and Ni show a high correlation coefficient (0.91) in the ultrafine mode, indicative of oil combustion.

The excellent correspondence between the observed groupings of elements based on correlation (Tables S2-4, Supplementary material) and the sources resolved by PMF (Table 2) adds confidence to the identification of key sources during the cruise. However, as PMF is an unsupervised technique, it may not sufficiently disaggregate significant, consecutive aerosol events. Visually, two distinct ultrafine events occur between 18 Sept and 19 Sept in Si (Fig. 4b) and V, Ni (Fig. 4d) which are

merged by PMF in its oil combustion factor (Fig. 7d). The disproportionate enhancement of ultrafine-mode Si over V and Ni suggests a source apart from oil combustion. Thus, to further expand on the relationships between elements, we turn to regression analysis.

4.2. Regressions of selected elements

An ultrafine Si event between 18 Sept and 19 Sept was shown in the mass size distribution (Fig. 3d) and the time series (Fig. 4b) of ultrafine Si. Fly ash was the hypothesized source of the ultrafine Si signal; however, although the PMF analysis suggested the presence of fly ash, ultrafine Si was not significantly apportioned to the fly ash factor (Fig. 6e). Additionally, none of the factor contributions from PMF showed a similar trend between 18-19 Sept as that of ultrafine Si. This suggests that PMF may have mishandled the early Si enhancement (Fig. 4b) by merging it with an enhancement in V, Ni that occurred soon after (Fig. 4d). Regressions show that, between 18 Sept and 19 Sept, Si had distinct ratio slopes and moderate correlations with P (r^2 = 0.76), S (r^2 = 0.73), and Al (r^2 = 0.61) (Fig. 8; Table S4, Supplementary material) but poor correlations with fly ash tracers (As, Se, Pb; r^2 < 0.12). The high correlations of Si with P, Al, and S suggest a distinct source of Si between 18 Sept and 19 Sept versus the rest of the cruise; but the low correlations with fly ash tracers rule out fly ash as a possible source. As the *Vasco* was travelling near islands, the source of the ultrafine Si enhancement is likely a local source en-route to Palawan. The sudden enhancement may be related to a rapid nucleation event as even submicron dust can be an important source of CCN in marine/coastal environments (Twohy et al. 2009).

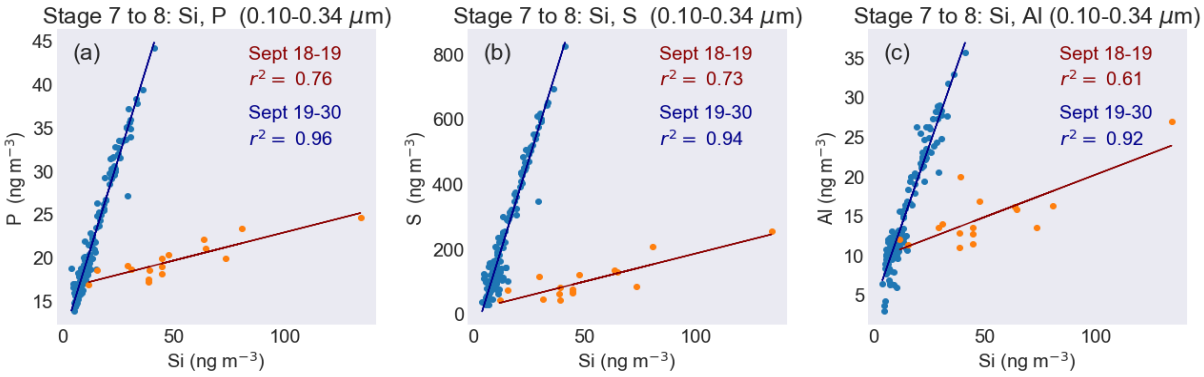

Figure 8. Linear regressions of ultrafine Si and its most highly correlated elements (a) P, (b) S, (c) Al, divided by cruise period before Sept 19 (red) and after Sept 19 (blue).

As S is an indicator of general combustion (Atwood et al., 2013a), it is important to elucidate its relationship with tracers of other combustion sources. Multiple linear regression was performed on S on the fine and ultrafine modes (Fig. S8, Supplementary material). It was found that K and V were excellent predictors of S for most of the cruise but the model required the addition of Al to capture the variance in S between 24 Sept and 26 Sept, suggesting an additional source during this period separate from biomass burning or oil combustion. A detailed description of the multiple linear regression analysis can be found in the Supplementary material. Further examining the relationships of S to these combustion sources, fine and ultrafine mode

linear regressions of K and V, colored by the concentration of S per given time, were constructed to show the relationships between the three species (Fig. 9a, b). S covaries more with K than V as seen with the clearer color gradient along the K-axis, suggesting the origin of S during the cruise to be more dominantly from biomass burning rather than oil combustion.

The ratio between V and Ni is often used as an indicator of the type of oil combustion source (Hedberg et al., 2005; Nigam et al., 2006; Mazzei et al., 2008; Becagli et al., 2012; Lin et al., 2015). Linear regression plots of V and Ni have a slope of 3.64 in the ultrafine mode (Fig. 9c). Nigam et al. (2006) measured a V/Ni ratio of 3.5-4 when sampling shipping emissions directly from the exhausts of various ship engines which suggests shipping to be the main source of ultrafine mode oil combustion during the cruise.

As soil composition varies geographically, soil dust ratios are excellent indicators of a plume's origin (Prospero et al., 1999; Song et al., 2006; Witt et al., 2006). Figure 8d shows linear regressions of soil dust elements in the coarse and fine modes. Al and Si, well-known indicators of dust (Viana et al., 2008; Tian et al., 2016; Landis et al., 2017), show moderate correlations with each other in the coarse and fine modes but slightly differ in ratio-slopes between the fine (Al/Si ~ 1.3; r^2 = 0.94) and coarse (Al/Si ~ 0.93; r^2 = 0.78) modes (Fig. 9d). This is indicative of varying sources of fine and coarse mode soil, with coarse mode soil dust enriched in Si; however, this could also be a matrix effect from the XRF analysis. As the *Vasco* remained near Palawan island, local dust could be the source of coarse-mode Si-enrichment; however, soil dust from Borneo is also a possibility.

The regression analysis showed an early-cruise enhancement in ultrafine Si that was merged by PMF with a V, Ni enhancement that occurred soon after, highlighting the importance of the regression analysis in addition to PMF to investigate the temporal characteristics of sources via elemental tracers. We suggest a local source en-route to the main sampling area to be the cause of the enhancement but fly ash is unlikely the source due to low correlations with its tracers As, Pb, and Se. The analysis also showed the strong associations of S with biomass burning and oil combustion; however, S was shown to covary more significantly with the former. Oil combustion was determined to originate from shipping as indicated by a V/Ni ratio within the range of that measured by a previous shipping emission study. Finally, we infer multiple sources of soil dust between the coarse and fine modes due to distinct Si-Al ratios between modes; however, we are unable to determine the exact sources due to lack of information regarding local and regional soil dust ratios.

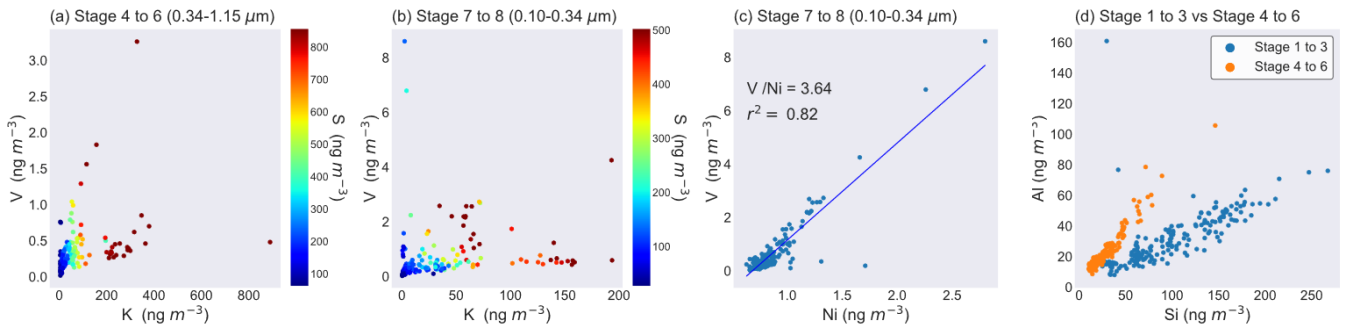

Figure 9. Scatter plot of key species during the cruise. (a) fine mode K, V colored by the concentrations of S at a given time, (b) ultrafine mode K, V likewise colored by concentrations of S at a given time, (c) ultrafine mode V, Ni, and (d) coarse and fine mode Al, Si.

5. Results III: Back trajectory analysis

5.1. 18-19 Sept: Ultrafine V, Ni enhancement from Sandakan, Sabah

As described in Section 3**,** ultrafine mode V and Ni show a maximum around 18 Sept (Fig. 4d). As the *Vasco* was traveling near local islands, the event may originate from a local source; however, back trajectories propose an oil combustion source in Borneo. Back trajectories were generated every hour between 14:00 to 18:00 UTC (corresponding to 22:00 to 02:00 LT) on 18 September and show a westward shift along the eastern coast of Borneo (Fig. 10a). The coast of Borneo is largely forest (Fig. 10b) but hosts the city of Sandakan, one of Sabah's major ports (Fig. 10c, d). In addition to shipping traffic (Fig. 10d), Sandakan contains oil depots which are a major source of industry in the area. During the westward shift of the back trajectories, air masses pass through Sandakan at around 16:00 UTC, approximately the time of the sampled spike in V. The shipping activity and oil depots present in this area may be responsible for the spike in oil combustion tracers, indicating the complexity of aerosol transport in the region as small cities like Sandakan may be a source of significant spikes in aerosol.

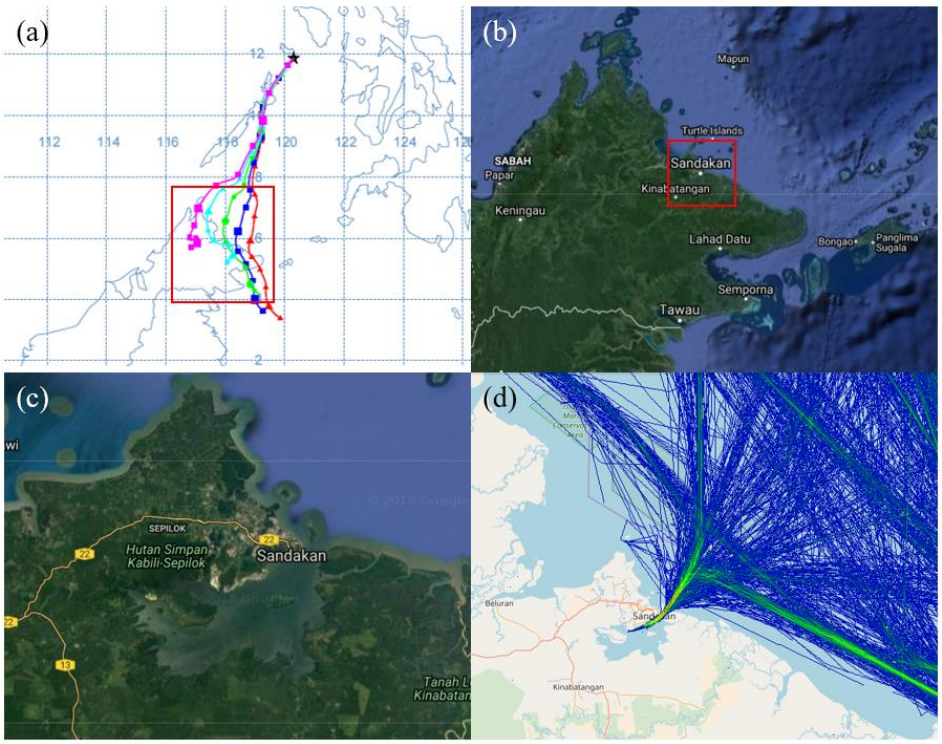

Figure 10. Determination of 18 September event using (a) HYSPLIT back trajectories, (b, c) Google Maps view of the northeastern coast of Borneo (map data ©2018 Google), (d) Density of shipping traffic from Sandakan, Sabah (source: MarineTraffic). Red squares indicate the location of the succeeding plot.

5.2. 20-24 Sept: Clean marine period

The first half of the cruise showed the lowest concentrations of elements associated with biomass burning K, S, Si, and Al. Back trajectories during this early period originate from the northern part of Borneo and do not penetrate deeply into the MC until late into the cruise (Fig. 2l). During this period, HYSPLIT back trajectories show that air mass pathways shift away from the Borneo coasts towards open sea (Fig. 2j). In addition to the shift away from biomass burning sites, back trajectories between 22 and 24 Sept pass through areas of open sea that host lower levels of shipping traffic (Fig. S3, Supplementary material).

5.3. 24-26 Sept: Large mixed aerosol event from northwest Borneo

Around 26 Sept, increases in fine mode V and Ni occurred when air masses passed through the northwest coast of Borneo, suggesting the presence of ports or oil depots like with the aforementioned spike on 18 Sept from Sandakan. Back trajectories generated every 6 hours starting from 24 Sept 15:00 UTC until 26 Sept 09:00 UTC show little change over this period (not shown) and intersect with the shipping route hub located along northwest Borneo which would explain the V and Ni spikes (Fig. 2k, S1, Supplementary material). The enrichments of biomass burning and combustion tracers K and S in the sampled air mass span a wider period beginning on 24 Sept until 26 Sept. This may be due to burning activity along the coast of Borneo which hosts several MODIS-detected active fire hotspots. Late-night land breeze from the island may have advected polluted air masses towards the coast.

5.4. 28-30 Sept: Large biomass burning event from Southern Kalimantan

Enhancements of these elements after 28 Sept coincide with a regional increase in AOD (Fig. 2d) and are captured by the NAAPS model in the form of a large smoke event advected northeast (Fig. 2h). Linear regressions show this large aerosol event at the end of the cruise as a distinct group of points with enhanced concentrations of K and S (Fig. S9, Supplementary material), suggesting an increase in biomass burning activity during this time. Reid et al. (2015) observed a sharp increase in the number of active fire hotspots, particularly in Sumatra and Southern Kalimantan. As discussed prior and depicted in Fig. 2, TC Nesat played a major in role in synoptic wind patterns during the cruise, causing a shift in back trajectories after 28 Sept to the southwest coast of Borneo island. Thus, the enhancements of submicron K, S, Si and Al likely originate from biomass burning in the MC.

6. Summary and conclusions

This study describes the size-resolved aerosol elemental composition of particles collected by a DRUM rotating impactor during the 17 to 30 September 2011 M/Y *Vasco* cruise in the vicinity of the Palawan island of the Philippines. This region was chosen due to its location as a receptor for MC aerosol sources, such as biomass burning, oil combustion and soil dust. Meteorological conditions during the cruise were conducive to southwesterly long range transport for seasonal burning aerosol which was observed in the concentration time series of tracers and satellite-derived AOD. Size-resolved aerosol composition in the coarse (1.15-10 μm), fine (0.34- 1.15 μm) and ultrafine (0.10-0.34 μm) modes were used as key tracers to ascertain

source contributions. Despite the meteorological complexity of the SCS/WPS, we can gain insights into aerosol sources by focusing on key elemental species. The time series of key elements showed distinct events on 18-19 Sept, 24-26 Sept, and 28-30 Sept, with clean aerosol periods between events. These aerosol events served as case studies of sources in the region. While biomass burning is indeed a key source of aerosol, other sources such as oil combustion, crustal-marine mixed source, fly ash, and soil dust contribute to the chemical profile of the SCS/WPS during the southwest monsoon. Understanding these sources is key to characterizing aerosol composition and transport in the SCS/WPS and, by extension, developing our understanding of aerosol-cloud behavior in the region. As back trajectory analysis and aerosol chemistry showed the presence of multiple key sources, the general conclusions of the study show that:

1. Mass distributions of key elements showed the evolution of aerosol chemistry throughout the cruise and interesting covariances between modes. Stage 5 (0.56-0.75 μm) and stage 7 (0.26-0.34 μm) showed enhanced peaks in several elements associated with combustion. Throughout the cruise, mass distributions of V and Ni track each other well both temporally and across DRUM stages, indicative of oil combustion. Mass distributions of V and Ni show higher values in the ultrafine mode between 18-19 September, indicative of an early oil combustion-enriched air mass which was identified to possibly originate from Sandakan, Sabah in Borneo. Mass distributions of K, Al and S show large enhancements in the fine and ultrafine modes after 27 September, corroborated by a reported large aerosol event from Reid et al. (2015). The strong peaks of these biomass burning tracers, in combination with the rapid spread of high AOD and NAAPS-modelled smoke concentration across the region, provide evidence for intensive emissions from the MC. Coarse-mode soil dust elements such as Fe and Si showed similarly-timed enhancements, attributed to soil particle entrainment during burning.
2. Short-term meteorological events such as the tropical cyclone (TC) Nesat played a key role in long-range transport as they propagated through the region, expediting the northeastward advection of aerosol emissions, an effect observed in previous studies (Atwood et al., 2013a; Reid et al., 2012, 2015). The sudden variations in aerosol concentration after 24 Sept can be connected to the movement of TC Nesat through the region. Prior to these events, aerosol concentrations remained at generally low levels as NAAPS shows smoke was largely constrained to the southern hemisphere. The passage of TC Nesat advected air masses more northward, allowing them to penetrate deep enough into the northern hemisphere to be sampled by the *Vasco*. The TC's passage coincided with a shift in air mass origin from mainland Malaysia prior to 24 Sept to areas known for intense burning activity, most notably Southern Kalimantan by the end of the cruise. This corresponded to a mixed aerosol event from 24 to 26 Sept attributed to Brunei, Borneo and a significant increase in biomass burning tracer concentrations from 28 to 30 Sept attributed to Southern Kalimantan. Between these aerosol events, a clean marine event from 26 until 28 Sept was characterized by high concentrations of Cl and low levels of elements associated with anthropogenic sources. Back trajectories showed that air masses travelled through the open,

603 central SCS/WPS which suggest a good signal of sea spray was sampled. As the ship route brought the *Vasco*
604 near islands, local crustal emissions covaried with sea spray aerosol which resulted in the crustal-marine mixed
605 source during the PMF analysis.
606 3. Six sources across the three size modes were resolved by the PMF analysis: biomass burning, oil combustion,
607 soil dust, crustal-marine mixed source, sea spray, and fly ash. A threshold Pearson R coefficient of 0.0 was used
608 to filter species included in the PMF analysis to improve the interpretability of the PMF solution. Results show
609 that natural sources – the crustal-marine mixed source and soil dust factors - were observed in only the coarse
610 and fine modes while anthropogenic sources, biomass burning, oil combustion, and fly ash, were resolved purely
611 in the fine and ultrafine modes. A strong correspondence between key elements seen on the PMF source profiles
612 and groupings of these elements on the correlation matrices adds confidence to the PMF solution. The biomass
613 burning PMF factor showed the highest percent contributions to total elemental PM mass in the fine and ultrafine
614 modes: 32.4% in the fine mode, and 45.9% in the ultrafine mode. It is interesting to note that the relative
615 contribution of the oil combustion factor increased significantly towards finer modes, 7.3% in the fine mode but
616 26.1% in the ultrafine mode, corroborating its anthropogenic identification. In terms of aerosol events, PMF
617 source contributions were able to capture the most events seen in the raw elemental concentrations. Differences
618 in the temporal variations between PMF-resolved sources suggest these sources are distinct. However, PMF did
619 not differentiate between an early ultrafine Si spike from a distinct, subsequent spike in V which demonstrates
620 that PMF may merge events, leading to a loss in resolution as observed in other studies (Van Pinxteren et al.,
621 2016). This, however, can be ameliorated with an in-depth, supervised analysis of the data as done in this study.
622 4. As stated above, spikes in oil combustion tracers V and Ni were observed on 18 Sept in the fine and ultrafine
623 modes. HYSPLIT back trajectories suggest the origin of the air mass as Sandakan, an industrial area and port
624 city of Sabah known for its oil depots and shipping activity located along the northeastern coast of Borneo. The
625 spike in oil combustion suggest that a small city can cause drastic increases in tracer concentration depending on
626 air mass trajectories. The strong presence of ultrafine mode Si from 18-19 September was also observed but the
627 time series of Si is distinct from the time series of V and Ni, suggestive of a source distinct from oil combustion.
628 5. The 24 to 26 September event coincided with the arrival of TC Nesat east of Luzon (northeast of the *Vasco*'s
629 location). Enhancements of multiple key tracers for biomass burning, oil combustion and soil dust were observed,
630 indicative of aerosols mixing within an air mass during transport. Biomass burning tracers K, S, Si, Al show
631 enhancements over a wider period (24-26 Sept) than that of oil combustion tracers V and Ni, which spiked at the
632 end of the period. Furthermore, aerosol-convection interactions were observed as sharp dips in the concentrations
633 of biomass burning and soil dust tracers around 25 Sept before recovery. Interestingly, this dip was not observed
634 for oil combustion tracers V, Ni. This cold pool event was reported in detail by Reid et al. (2015) and this study

further elaborated on its impact on PM of different elemental composition. This case demonstrates the effect of short-term or high frequency phenomena on aerosol transport in the MC. HYSPLIT back trajectories show that air masses begin to travel from the southwest MC in response to TC Nesat's inflow arm. Air masses during the 24-26 September event pass through Brunei, a shipping hub located along the northeastern coast of Borneo, which explains the increase in oil combustion tracers V and Ni. The coast was also observed to host a number of active fire hotspots. Land breeze may lead to the entrainment of burning plumes into the traveling air mass which would explain the enrichment.

6. The 28-30 September aerosol event showed an enrichment in K and S that coincided with a shift in back trajectory origin to Southern Kalimantan, which hosts a high fire hotspot density. MC burning may be characterized by an elevated K/S ratio and strong fine and ultrafine mode peaks in the mass distributions of S and K. The 28-30 September event also coincided with the enhancement of soil dust elements in the coarse mode, indicative of soil particle entrainment during burning activity (Reid et al., 2015).

The study identified source locations of aerosol and characterized the plumes during the *Vasco* 2011 cruise; however, unanswered questions remain such as the origin of the strong ultrafine Si signal detected early in the cruise (18-19 Sept) which may be connected to a rapid local nucleation event. The source location of the PMF-resolved fly ash factor also remains unidentified due to its complicated source contribution time series and unclear elemental profile. Investigation into cloud nuclei (CN) properties during the cruise may be done to further validate the intensity and timing of plumes. In addition to the findings of this study on the elemental PM, future research on other species collected during the 2011 and 2012 *Vasco* campaigns such as trace gases may compliment and deepen our current understanding of the aerosol environment in the SCS/WPS through additional degrees of freedom, specifically utilizing the lifetimes of trace gases and inferring the potential for secondary aerosol formation during transport.

Author contribution

MRAH performed the analysis and prepared the manuscript. MTC supervised the analysis, especially for the PMF section. MOLC supervised the analysis and provided input for the manuscript. JSR collected the data onboard the *Vasco*, supervised the analysis, provided input for the manuscript. PX provided the NAAPS Smoke model outputs for Fig. 2 and provided input for the manuscript. JBS, NDL, SNYU collected the data onboard the *Vasco*. SC, YJZ performed the XRF analysis on the data.

Data availability

The Vasco ship data is available through correspondence with Jeffrey S. Reid, jeffrey.reid@nrlmry.navy.mil. MODIS AOD images were obtained from the NASA Worldview application: https://worldview.earthdata.nasa.gov/. HYSPLIT data is

accessible through the NOAA READY website (http://www.ready.noaa.gov). NAAPS aerosol reanalysis data can be accessed at the US GODAE server: http://www.usgodae.org/.

Competing Interests

The authors declare that they have no conflict of interest.

Acknowledgements

We acknowledge the use of imagery from the NASA Worldview application (https://worldview.earthdata.nasa.gov/), part of the NASA Earth Observing System Data and Information System (EOSDIS). The authors gratefully acknowledge the NOAA Air Resources Laboratory (ARL) for the provision of the HYSPLIT transport and dispersion model and/or READY website (http://www.ready.noaa.gov) used in this publication.

References

Alam, K., Mukhtar, A., Shahid, I., Blaschke, T., Majid, H., Rahman, S., Khan, R. and Rahman, N.: Source apportionment and characterization of particulate matter (PM10) in urban environment of Lahore, Aerosol Air Qual. Res., 14(7), 1851–1861, doi:10.4209/aaqr.2014.01.0005, 2014.

Artaxo, P. and Maenhaut, W.: Aerosol Characteristics and Sources for the Amazon Basin During the Wet Season, J. Geophys. Res., 95(D10), 16971–16985, 1990.

Artaxo, P., Fernandas, E. T., Martins, J. V., Yamasoe, M. A., Maenhaut, W., Longo, K. M., Castanho, A. and Hobbs, P. V.: Large-scale aerosol source apportionment in Amazonia, J. Geophys. Res. Atmos., 103(D24), 31837–31847, doi:10.1029/98jd02346, 1998.

Atwood, S. A., Reid, J. S., Kreidenweis, S. M., Cliff, S. S., Zhao, Y., Lin, N.-H., Tsay, S.-C., Chu, Y.-C. and Westphal, D. L.: Size resolved measurements of springtime aerosol particles over the northern South China Sea, Atmospheric Environment, 78, 134–143, doi:10.1016/j.atmosenv.2012.11.024, 2013a.

Atwood, S. A., Salinas, S. V., Chew, B. N., Reid, J. S., Balasubramanian, R., Yu, L. E. and Kreidenweis, S. M.: Analysis of source regions for smoke events in Singapore for the 2009 El Nino burning season, Atmos. Environ., 78, 219–230, doi:10.1016/j.atmosenv.2013.04.047, 2013b.

Atwood, S. A., Reid, J. S., Kreidenweis, S. M., Blake, D. R., Jonsson, H. H., Lagrosas, N. D., Xian, P., Reid, E. A., Sessions, W. R. and Simpas, J. B.: Size-resolved aerosol and cloud condensation nuclei (CCN) properties in the remote marine South China Sea-Part 1: Observations and source classification, Atmos. Chem. Phys., 17(2), 1105–1123, doi:10.5194/acp-17-1105-2017, 2017.

693 Baker, K. R., Simon, H. and Kelly, J. T.: Challenges to modeling "cold pool" meteorology associated with high pollution
694 episodes, Environ. Sci. Technol., 45(17), 7118–7119, doi:10.1021/es202705v, 2011.

695 Balasubramanian, R., Qian, W.-B., Decesari, S., Facchini, M. C. and Fuzzi, S.: Comprehensive characterization of PM 2.5
696 aerosols in Singapore, J. Geophys. Res., 108(D16), doi:10.1029/2002jd002517, 2003.

697 Becagli, S., Sferlazzo, D. M., Pace, G., Di Sarra, A., Bommarito, C., Calzolai, G., Ghedini, C., Lucarelli, F., Meloni, D.,
698 Monteleone, F., Severi, M., Traversi, R. and Udisti, R.: Evidence for heavy fuel oil combustion aerosols from chemical
699 analyses at the island of Lampedusa: A possible large role of ships emissions in the Mediterranean, Atmos. Chem. Phys.,
700 12(7), 3479–3492, doi:10.5194/acp-12-3479-2012, 2012.

701 Boucher, O., D. Randall, P. Artaxo, C. Bretherton, G. Feingold, P. Forster, V.-M. Kerminen, Y. Kondo, H. Liao, U.
702 Lohmann, P. Rasch, S.K. Satheesh, S. Sherwood, B. Stevens and X.Y. Zhang: Clouds and Aerosols. In: Climate Change
703 2013: The Physical Science Basis. Contribution of Working Group I to the Fifth Assessment Report of the
704 Intergovernmental Panel on Climate Change [Stocker, T.F., D. Qin, G.-K. Plattner, M. Tignor, S.K. Allen, J. Boschung,
705 A. Nauels, Y. Xia, V. Bex and P.M. Midgley (eds.)]. Cambridge University Press, Cambridge, United Kingdom and New
706 York, NY, USA, 2013.

707 Cahill, T. A., Barnes, D. E., Lawton, J. A., Miller, R., Spada, N., C, R. D. W. and Kimbrough, S.: Transition metals in
708 coarse, fine, very fine and ultra-fine particles from an interstate highway transect near Detroit, , doi:10.1016/S0065-
709 3454(07)37008-3, 2007.

710 Chan, Y. C., Christensen, E., Golding, G., King, G., Gore, W., Cohen, D. D., Stelcer, E., Simpson, R., Denison, L. and
711 Wong, N.: Source Apportionment of Ambient Volatile Organic Compounds in Major Cities in Australia By Positive
712 Matrix Factorisation , 42(2), 22–29, 2008.

713 Chang, C. P., Zhuo, W., John, M. and Ching-Hwang, L.: Annual Cycle of Southeast Asia — Maritime Continent Rainfall
714 and the Asymmetric, J. Clim., 18, 287–301, doi:10.1175/JCLI-3257.1, 2005.

715 Chow, J. C., Lowenthal, D. H., Chen, L.-W. A., Wang, X. and Watson, J. G.: Mass reconstruction methods for PM2.5: a
716 review, Air Qual Atmos Health, 8(3), 243–263, doi:10.1007/s11869-015-0338-3, 2015.

717 Cohen, D. D., Crawford, J., Stelcer, E. and Bac, V. T.: Long range transport of fine particle windblown soils and coal fired
718 power station emissions into Hanoi between 2001 to 2008, Atmos. Environ., 44(31), 3761–3769,
719 doi:10.1016/j.atmosenv.2010.06.047, 2010a.

720 Cohen, D. D., Crawford, J., Stelcer, E. and Bac, V. T.: Characterisation and source apportionment of fine particulate sources
721 at Hanoi from 2001 to 2008, Atmos. Environ., 44(3), 320–328, doi:10.1016/j.atmosenv.2009.10.037, 2010b.

Davison, R. L., Natusch, D. F. S. and Wallace, J. R.: Trace Elements in Fly Ash, , 8(13) [online] Available from: https://pubs.acs.org/doi/pdf/10.1021/es60098a003?src=recsys, 1974.

Deonarine, A., Kolker, A. and Doughten, M.: Trace Elements in Coal Ash, Usgs, (May), 1–6, doi:10.1002/9781119199090.fmatter, 2015.

Draxler, R. R. and Hess, G. D.: An overview of the HYSPLIT_4 modelling system for trajectories, Aust. Meteorol. Mag., 47, 295–308, 1998.

Draxler, R. R.: HYSPLIT4 user's guide. NOAA Tech. Memo. ERL ARL-230, NOAA Air Resources Laboratory, Silver Spring, MD., 1999.

Duncan, B. N., Martin, R. V., Staudt, A. C., Yevich, R. and Logan, J. A.: Interannual and seasonal variability of biomass burning emissions constrained by satellite observations, J. Geophys. Res., 108(D2), doi:10.1029/2002jd002378, 2003.

Engling, G., He, J., Betha, R. and Balasubramanian, R.: Assessing the regional impact of Indonesian biomass burning emissions based on organic molecular tracers and chemical mass balance modeling, Atmos. Chem. Phys., 14(15), 8043–8054, doi:10.5194/acp-14-8043-2014, 2014.

Farao, C., Canepari, S., Perrino, C. and Harrison, R. M.: Sources of PM in an industrial area: Comparison between receptor model results and semiempirical calculations of source contributions, Aerosol Air Qual. Res., 14(6), 1558–1572, doi:10.4209/aaqr.2013.08.0281, 2014.

Field, R. D. and Shen, S. S. P.: Predictability of carbon emissions from biomass burning in Indonesia from 1997 to 2006, J. Geophys. Res. Biogeosciences, 113(4), 1–17, doi:10.1029/2008JG000694, 2008.

Fujii, Y., Tohno, S., Amil, N., Latif, M. T., Oda, M., Matsumoto, J. and Mizohata, A.: Annual variations of carbonaceous PM2.5in Malaysia: Influence by Indonesian peatland fires, Atmos. Chem. Phys. Discuss., 15(16), 22419–22449, doi:10.5194/acpd-15-22419-2015, 2015.

Ge, C., Wang, J. and Reid, J. S.: Mesoscale modeling of smoke transport over the Southeast Asian maritime continent: Coupling of smoke direct radiative effect below and above the low-level clouds, Atmos. Chem. Phys., 14(1), 159–174, doi:10.5194/acp-14-159-2014, 2014.

Gugamsetty, B., Wei, H., Liu, C. N., Awasthi, A., Tsai, C. J., Roam, G. D., Wu, Y. C. and Chen, C. F.: Source Characterization and Apportionment of PM10, PM2.5 and PM0.1 by Using Positive Matrix Factorization, Aerosol Air Qual. Res., 12(4), 476–491, doi:10.4209/aaqr.2012.04.0084, 2012.

749 Han, J. S., Moon, K. J., Lee, S. J., Ryu, S. Y., Cliff, S. S., Kim, Y. J. and Yi, S. M.: Size-resolved source apportionment of
750 ambient particles by positive matrix factorization at Gosan background site in East Asia, Atmos. Chem. Phys., 6(1), 211–
751 223, doi:10.5194/acp-6-211-2006, 2006.

752 Hedberg, E., Gidhagen, L. and Johansson, C.: Source contributions to PM10 and arsenic concentrations in Central Chile
753 using positive matrix factorization, Atmos. Environ., 39(3), 549–561, doi:10.1016/j.atmosenv.2004.11.001, 2005.

754 Higgins, R. W. and Shi, W.: Intercomparison of the principal modes of interannual and intraseasonal variability of the North
755 American Monsoon System, J. Clim., 14(3), 403–417, doi:10.1175/1520-0442(2001)014<0403:IOTPMO>2.0.CO;2,
756 2001.

757 Hoek, G., Krishnan, R. M., Beelen, R., Peters, A., Ostro, B., Brunekreef, B. and Kaufman, J. D.: Long-term air pollution
758 exposure and cardio-respiratory mortality: A review, Environ. Heal. A Glob. Access Sci. Source, 12(1),
759 doi:10.1186/1476-069X-12-43, 2013.

760 Hsu, S. C., Tsai, F., Lin, F. J., Chen, W. N., Shiah, F. K., Huang, J. C., Chan, C. Y., Chen, C. C., Liu, T. H., Chen, H. Y.,
761 Tseng, C. M., Hung, G. W., Huang, C. H., Lin, S. H. and Huang, Y. T.: A super Asian dust storm over the East and South
762 China Seas: Disproportionate dust deposition, J. Geophys. Res. Atmos., 118(13), 7169–7181, doi:10.1002/jgrd.50405,
763 2013.

764 Hyer, E. J., Reid, J. S. and Zhang, J.: An over-land aerosol optical depth data set for data assimilation by filtering, correction,
765 and aggregation of MODIS Collection 5 optical depth retrievals, Atmos. Meas. Tech., 4(3), 379–408, doi:10.5194/amt-4-
766 379-2011, 2011.

767 Karanasiou, A. A., Siskos, P. A. and Eleftheriadis, K.: Assessment of source apportionment by Positive Matrix Factorization
768 analysis on fine and coarse urban aerosol size fractions, Atmos. Environ., 43(21), 3385–3395,
769 doi:10.1016/j.atmosenv.2009.03.051, 2009.

770 Kecorius, S., Madueno, L., Vallar, E., Alas, H., Betito, G., Birmili, W., Cambaliza, M. O., Catipay, G., Gonzaga-Cayetano,
771 M., Galvez, M. C., Lorenzo, G., Müller, T., Simpas, J. B., Tamayo, E. G. and Wiedensohler, A.: Aerosol particle mixing
772 state, refractory particle number size distributions and emission factors in a polluted urban environment: Case study of
773 Metro Manila, Philippines, Atmos. Environ., 170, 169–183, doi:10.1016/j.atmosenv.2017.09.037, 2017.

774 Landis, M. S., Pancras, J. P., Graney, J. R., White, E. M., Edgerton, E. S., Legge, A. and Percy, K. E.: Source apportionment
775 of ambient fine and coarse particulate matter at the Fort McKay community site, in the Athabasca Oil Sands Region,
776 Alberta, Canada, Sci. Total Environ., 584–585, 105–117, doi:10.1016/j.scitotenv.2017.01.110, 2017.

Lareau, N. P., Crosman, E., Whiteman, C. D., Horel, J. D., Hoch, S. W., Brown, W. O. J. and Horst, T. W.: The persistent cold-air pool study, Bull. Am. Meteorol. Soc., 94(1), 51–63, doi:10.1175/BAMS-D-11-00255.1, 2013.

Lee, E., Chan, C. K. and Paatero, P.: Application of positive matrix factorization in source apportionment of particulate pollutants in Hong Kong, Atmos. Environ., 33(19), 3201–3212, doi:10.1016/S1352-2310(99)00113-2, 1999.

Lee, S.-S., Feingold, G. and Chuang, P. Y.: Effect of Aerosol on Cloud–Environment Interactions in Trade Cumulus, J. Atmos. Sci., 69(12), 3607–3632, doi:10.1175/jas-d-12-026.1, 2012.

Lestari, P. and Mauliadi, Y. D.: Source apportionment of particulate matter at urban mixed site in Indonesia using PMF, Atmos. Environ., 43(10), 1760–1770, doi:10.1016/j.atmosenv.2008.12.044, 2009.

Li, T., Wang, Y., Li, W. J., Chen, J. M., Wang, T. and Wang, W. X.: Concentrations and solubility of trace elements in fine particles at a mountain site, southern China: Regional sources and cloud processing, Atmos. Chem. Phys., 15(15), 8987–9002, doi:10.5194/acp-15-8987-2015, 2015.

Liao, H.-T., Chou, C. C.-K., Chow, J. C., Watson, J. G., Hopke, P. K. and Wu, C.-F.: Source and risk apportionment of selected VOCs and PM2.5 species using partially constrained receptor models with multiple time resolution data, Environ. Pollut., 205, 121–130, doi:10.1016/j.envpol.2015.05.035, 2015.

Liao, H.-T., Chang, J.-C., Tsai, T.-T., Tsai, S.-W., Chou, C. C.-K. and Wu, C.-F.: Vertical distribution of source apportioned PM 2.5 using particulate-bound elements and polycyclic aromatic hydrocarbons in an urban area, J Expo Sci Environ Epidemiol, 1–11, doi:10.1038/s41370-019-0153-2, 2019.

Lin, C.-Y., Wang, Z., Chen, W.-N., Chang, S.-Y., Chou, C. C. K., Sugimoto, N. and Zhao, X.: Long-range transport of Asian dust and air pollutants to Taiwan: observed evidence and model simulation, Atmos. Chem. Phys. Discuss., 6(5), 10183–10216, doi:10.5194/acpd-6-10183-2006, 2007.

Lin, Y.-C., Tsai, C.-J., Wu, Y.-C., Zhang, R., Chi, K.-H., Huang, Y.-T., Lin, S.-H. and Hsu, S.-C.: Characteristics of trace metals in traffic-derived particles in Hsuehshan Tunnel, Taiwan: size distribution, potential source, and fingerprinting metal ratio, Atmos. Chem. Phys., 15(8), 4117–4130, doi:10.5194/acp-15-4117-2015, 2015.

Loo, Y. Y., Billa, L. and Singh, A.: Effect of climate change on seasonal monsoon in Asia and its impact on the variability of monsoon rainfall in Southeast Asia, Geosci. Front., 6(6), 817–823, doi:10.1016/j.gsf.2014.02.009, 2015.

Lynch, P., Reid, J. S., Westphal, D. L., Zhang, J., Hogan, T. F., Hyer, E. J., Curtis, C. A., Hegg, D. A., Shi, Y., Campbell, J. R., Rubin, J. I., Sessions, W. R., Turk, F. J. and Walker, A. L.: An 11-year global gridded aerosol optical thickness reanalysis (v1.0) for atmospheric and climate sciences, Geosci. Model Dev., 9(4), 1489–1522, doi:10.5194/gmd-9-1489-2016, 2016.

Ma, L., Dadashazar, H., Braun, R. A., MacDonald, A. B., Aghdam, M. A., Maudlin, L. C. and Sorooshian, A.: Size-resolved characteristics of water-soluble particulate elements in a coastal area: Source identification, influence of wildfires, and diurnal variability, Atmospheric Environment, 206, 72–84, doi:10.1016/j.atmosenv.2019.02.045, 2019.

Malm, W. C. and Hand, J. L.: An examination of the physical and optical properties of aerosols collected in the IMPROVE program, Atmospheric Environment, 41(16), 3407–3427, doi:10.1016/j.atmosenv.2006.12.012, 2007.

Maloney, E. D. and Hartmann, D. L.: The Madden–Julian Oscillation, Barotropic Dynamics, and North Pacific Tropical Cyclone Formation. Part I: Observations, J. Atmos. Sci., 58(17), 2545–2558, doi:10.1175/1520-0469(2001)058<2545:TMJOBD>2.0.CO;2, 2001.

Mazzei, F., D'Alessandro, A., Lucarelli, F., Nava, S., Prati, P., Valli, G. and Vecchi, R.: Characterization of particulate matter sources in an urban environment, Sci. Total Environ., 401(1–3), 81–89, doi:10.1016/j.scitotenv.2008.03.008, 2008.

Markowski, G. R. and Filby, R.: Trace Element Concentration as a Function of Particle Size in Fly Ash from a Pulverized Coal Utility Boiler, Environ. Sci. Technol., 19(9), 796–804, doi:10.1021/es00139a005, 1985.

Nakajima, T., Yoon, S. C., Ramanathan, V., Shi, G. Y., Takemura, T., Higurashi, A., Takamura, T., Aoki, K., Sohn, B. J., Kim, S. W., Tsuruta, H., Sugimoto, N., Shimizu, A., Tanimoto, H., Sawa, Y., Lin, N. H., Lee, C. Te, Goto, D. and Schutgens, N.: Overview of the Atmospheric Brown Cloud East Asian Regional Experiment 2005 and a study of the aerosol direct radiative forcing in east Asia, J. Geophys. Res. Atmos., 112(24), 1–23, doi:10.1029/2007JD009009, 2007.

Nigam, A., Welch, W., Wayne Miller, J., and Cocher III, D. R.: Effect of fuel sulphur content and control technology on PM emission from ship's auxiliary engine. Proceeding international aerosol conference, St. Paul, USA, 10–15 September 2006, 1531–1532, 2006.

Oanh, Nguyen Thi Kim. Integrated air quality management: Asian case studies. Boca Raton, FL: Taylor & Francis, 2013. Print.

O'Sullivan, D.Murray, B. J., Malkin, T. L., Whale, T. F., Umo, N. S., Atkinson, J. D., Price, H. C., Baustian, K. J., Browse, J. and Webb, M. E.: Ice nucleation by fertile soil dusts: relative importance of mineral and biogenic components, Atmos. Chem. Phys., 14(4), 1853–1867, doi:10.5194/acp-14-1853-2014, 2014.

Paatero, P. and Tapper, U.: Positive matrix factorization: A non-negative factor model with optimal utilization of error estimates of data values, Environmetrics, 5(2), 111–126, doi:10.1002/env.3170050203, 1994.

Paatero, P. and Hopke, P. K.: Discarding or downweighting high-noise variables in factor analytic models, Anal. Chim. Acta, 490(1–2), 277–289, doi:10.1016/S0003-2670(02)01643-4, 2003.

Paterson, K. G., Sagady, J. L., Hooper, D. L., Bertman, S. B., Carroll, M. A. and Shepson, P. B.: Analysis of air quality data using positive matrix factorization, Environ. Sci. Technol., 33(4), 635–641, doi:10.1021/es980605j, 1999.

Polissar, A. V., Hopke, P. K., Paatero, P., Malm, W. C. and Sisler, J. F.: Atmospheric aerosol over Alaska 2. Elemental composition and sources, J. Geophys. Res. Atmos., 103(D15), 19045–19057, doi:10.1029/98JD01212, 1998.

Prospero, J. M.: Long-range transport of mineral dust in the global atmosphere: Impact of African dust on the environment of the southeastern United States, Proc. Natl. Acad. Sci., 96(7), 3396–3403, doi:10.1073/pnas.96.7.3396, 1999.

Qi, L., Chen, M., Ge, X., Zhang, Y. and Guo, B.: Seasonal variations and sources of 17 aerosol metal elements in suburban Nanjing, China, Atmosphere (Basel)., 7(12), 1–21, doi:10.3390/atmos7120153, 2016.

Qian, J.-H., Robertson, A. W. and Moron, V.: Interactions among ENSO, the Monsoon, and Diurnal Cycle in Rainfall Variability over Java, Indonesia, J. Atmos. Sci., 67(11), 3509–3524, doi:10.1175/2010jas3348.1, 2010.

Querol, X., Viana, M., Alastuey, A., Amato, F., Moreno, T., Castillo, S., Pey, J., Rosa, J. de la, Campa, A. S. de la, Artinano, B., Salvador, P., Santos, S. G. Dos, Fernandez-Patier, R., Moreno-Grau, S., Negral, L., Minguillon, M. C., Monfort, E., Gil, J. I., Inza, A., Ortega, L. A., Santamaria, J. M. and Zabalza, J.: Source origin of trace elements in PM from regional background, urban and industrial sites of Spain, Atmos. Environ., 41(34), 7219–7231, doi:10.1016/j.atmosenv.2007.05.022, 2007.

Raabe, O. G., Braaten, D. A., Axelbaum, R. L., Teague, S. V and Cahill, T. A.: Calibration studies of the drum impactor, J. Aerosol Sci., 19(2), 183–195, doi:10.1016/0021-8502(88)90222-4, 1988.

Reid, J. S., Flocchini, R. G., Cahill, T. A., Ruth, R. S. and Salgado, D. P.: Local meteorological, transport, and source aerosol characteristics of late autumn Owens Lake (dry) dust storms, Atmos. Environ., 28(9), 1699–1706, doi:10.1016/1352-2310(94)90315-8, 1994.

Reid, J. S., Hyer, E. J., Prins, E. M., Westphal, D. L., Zhang, J., Wang, J., Christopher, S. A., Curtis, C. A., Schmidt, C. C., Eleuterio, D. P., Richardson, K. A. and Hoffman, J. P.: Global monitoring and forecasting of biomass-burning smoke: Description of and lessons from the fire Locating and Modeling of Burning Emissions (FLAMBE) program, IEEE J. Sel. Top. Appl. Earth Obs. Remote Sens., 2(3), 144–162, doi:10.1109/JSTARS.2009.2027443, 2009.

Reid, J. S., Xian, P., Hyer, E. J., Flatau, M. K., Ramirez, E. M., Turk, F. J., Sampson, C. R., Zhang, C., Fukada, E. M. and Maloney, E. D.: Multi-scale meteorological conceptual analysis of observed active fire hotspot activity and smoke optical depth in the Maritime Continent, Atmos. Chem. Phys., 12(4), 2117–2147, doi:10.5194/acp-12-2117-2012, 2012.

Reid, J., Hyer, E., Johnson, R., Holben, B. N., Yokelson, R., Zhang, J., Campbell, J., Christopher, S., DiGirolamo, L., Giglio, L., Holz, R., Kearney, C., Miettinen, J., Reid, E., Turk, F. J., Wang, J., Xian, P., Zhao, G., Balasubramanian, R., Chew,

B. N., Janjai, S., Lagrosas, N., Lestari, P., Lin, N.-H., Mahmud, M., Nguyen, A. X., Norris, B., Oanth, N. T. K., Oo, M., Salinas, S. V., Welton, E. J. and Liew, S. C.: Observing and understanding the Southeast Asian aerosol system by remote sensing: An initial review and analysis for the Seven Southeast Asian Studies (7SEAS) program, Atmos. Res., 122, 403–468, doi:10.1016/j.atmosres.2012.06.005, 2013.

Reid, J. S., Lagrosas, N. D., Jonsson, H. H., Reid, E. A., Sessions, W. R., Simpas, J. B., Uy, S. N., Boyd, T. J., Atwood, S. A., Blake, D. R., Campbell, J. R., Cliff, S. S., Holben, B. N., Holz, R. E., Hyer, E. J., Lynch, P., Meinardi, S., Posselt, D. J., Richardson, K. A., Salinas, S. V., Smirnov, A., Wang, Q., Yu, L. and Zhang, J.: Observations of the temporal variability in aerosol properties and their relationships to meteorology in the summer monsoonal South China Sea/East Sea: the scale-dependent role of monsoonal flows, the Madden–Julian Oscillation, tropical cyclones, squall lines and cold pools, Atmos. Chem. Phys., 15(4), 1745–1768, doi:10.5194/acp-15-1745-2015, 2015.

Reid, J. S., Xian, P., Holben, B. N., Hyer, E. J., Reid, E. A., Salinas, S. V., Zhang, J., Campbell, J. R., Chew, B. N., Holz, R. E., Kuciauskas, A. P., Lagrosas, N., Posselt, D. J., Sampson, C. R., Walker, A. L., Welton, E. J. and Zhang, C.: Aerosol meteorology of the Maritime Continent for the 2012 7SEAS southwest monsoon intensive study – Part 1: regional-scale phenomena, Atmos. Chem. Phys., 16(22), 14041–14056, doi:10.5194/acp-16-14041-2016, 2016.

Ross, A. D., Holz, R. E., Quinn, G., Reid, J. S., Xian, P., Turk, F. J. and Posselt, D. J.: Exploring the First Aerosol Indirect Effect over the Maritime Continent Using a Ten-Year Collocated MODIS, CALIOP, and Model Dataset, Atmos. Chem. Phys. Discuss., (March), 1–28, doi:10.5194/acp-2018-4, 2018.

Rolph, G., Stein, A., and Stunder, B. Real-time Environmental Applications and Display sYstem: READY. Environmental Modelling & Software, 95, 210-228, https://doi.org/10.1016/j.envsoft.2017.06. 2017.

Santoso, M., Lestiani, D. D., Mukhtar, R., Hamonangan, E., Syafrul, H., Markwitz, A. and Hopke, P. K.: Preliminary study of the sources of ambient air pollution in Serpong, Indonesia, Atmos. Pollut. Res., 2(2), 190–196, doi:10.5094/apr.2011.024, 2011.

Schlosser, J. S., Braun, R. A., Bradley, T., Dadashazar, H., MacDonald, A. B., Aldhaif, A. A., Aghdam, M. A., Mardi, A. H., Xian, P. and Sorooshian, A.: Analysis of aerosol composition data for western United States wildfires between 2005 and 2015: Dust emissions, chloride depletion, and most enhanced aerosol constituents, J. Geophys. Res. Atmos., 122(16), 8951–8966, doi:10.1002/2017JD026547, 2017.

Seneviratne, M. C. S., Waduge, V. A., Hadagiripathira, L., Sanjeewani, S., Attanayake, T., Jayaratne, N. and Hopke, P. K.: Characterization and source apportionment of particulate pollution in Colombo, Sri Lanka, Atmos. Pollut. Res., 2(2), 207–212, doi:10.5094/apr.2011.026, 2011.

Shi, Y., Zhang, J., Reid, J. S., Liu, B., and Hyer, E. J.: Critical evaluation of cloud contamination in the MISR aerosol products using MODIS cloud mask products, Atmos. Meas. Tech., 7, 1791-1801, 2014.

Song, Y., Xie, S., Zhang, Y., Zeng, L., Salmon, L. G. and Zheng, M.: Source apportionment of PM2.5 in Beijing using principal component analysis/absolute principal component scores and UNMIX, Sci. Total Environ., 372(1), 278–286, doi:10.1016/j.scitotenv.2006.08.041, 2006.

Sorooshian, A., Feingold, G., Lebsock, M. D., Jiang, H., and Stephens, G. L.: On the precipitation susceptibility of clouds to aerosol perturbations, Geophys. Res. Lett., 36, L13803, doi:10.1029/2009GL038993, 2009.

Sowlat, M. H., Hasheminassab, S. and Sioutas, C.: Source apportionment of ambient particle number concentrations in central Los Angeles using positive matrix factorization (PMF), Atmos. Chem. Phys., 16(8), 4849–4866, doi:10.5194/acp-16-4849-2016, 2016.

Stein, A.F., Draxler, R.R, Rolph, G.D., Stunder, B.J.B., Cohen, M.D., and Ngan, F. NOAA's HYSPLIT atmospheric transport and dispersion modeling system, Bull. Amer. Meteor. Soc., 96, 2059-2077, http://dx.doi.org/10.1175/BAMS-D-14-00110.1, 2015.

Thurston, G. D., Ito, K. and Lall, R.: A Source Apportionment of U.S. Fine Particulate Matter Air Pollution, Atmos. Environ., 45(24), 3831–3840, doi: 10.1016/j.atmosenv.2011.04.070, 1994.

Tian, S. L., Pan, Y. P. and Wang, Y. S.: Size-resolved source apportionment of particulate matter in urban Beijing during haze and non-haze episodes, Atmos. Chem. Phys., 16(1), 1–19, doi:10.5194/acp-16-1-2016, 2016.

Twohy, C. H., Kreidenweis, S. M., Eidhammer, T., Browell, E. V., Heymsfield, A. J., Bansemer, A. R., Anderson, B. E., Chen, G., Ismail, S., DeMott, P. J. and Van Den Heever, S. C.: Saharan dust particles nucleate droplets in eastern Atlantic clouds, Geophys. Res. Lett., 36(1), L01807, doi:10.1029/2008GL035846, 2009.

Van Pinxteren, D., Fomba, K. W., Spindler, G., Müller, K., Poulain, L., Iinuma, Y., Löschau, G., Hausmann, A. and Herrmann, H.: Regional air quality in Leipzig, Germany: Detailed source apportionment of size-resolved aerosol particles and comparison with the year 2000, Faraday Discuss., 189, 291–315, doi:10.1039/c5fd00228a, 2016.

Venecek, M. A., Zhao, Y., Mojica, J., McDade, C. E., Green, P. G., Kleeman, M. J. and Wexler, A. S.: Characterization of the 8-stage Rotating Drum Impactor under low concentration conditions, Journal of Aerosol Science, 100, 140–154, doi:10.1016/j.jaerosci.2016.07.007, 2016.

Viana, M., Kuhlbusch, T. A. J., Querol, X., Alastuey, A., Harrison, R. M., Hopke, P. K., Winiwarter, W., Vallius, M., Szidat, S., Prévôt, A. S. H., Hueglin, C., Bloemen, H., Wåhlin, P., Vecchi, R., Miranda, A. I., Kasper-Giebl, A., Maenhaut, W.

and Hitzenberger, R.: Source apportionment of particulate matter in Europe: A review of methods and results, J. Aerosol Sci., 39(10), 827–849, doi:10.1016/j.jaerosci.2008.05.007, 2008.

Visser, S., Slowik, J. G., Furger, M., Zotter, P., Bukowiecki, N., Canonaco, F., Flechsig, U., Appel, K., Green, D. C., Tremper, A. H., Young, D. E., Williams, P. I., Allan, J. D., Coe, H., Williams, L. R., Mohr, C., Xu, L., Ng, N. L., Nemitz, E., Barlow, J. F., Halios, C. H., Fleming, Z. L., Baltensperger, U. and Prévôt, A. S. H.: Advanced source apportionment of size-resolved trace elements at multiple sites in London during winter, Atmos. Chem. Phys., 15(19), 11291–11309, doi:10.5194/acp-15-11291-2015, 2015.

Wang, B., Wu, R. and Fu, X.: Pacific–East Asian Teleconnection: How Does ENSO Affect East Asian Climate?, J. Clim., 13(9), 1517–1536, doi:10.1175/1520-0442(2000)013<1517:PEATHD>2.0.CO;2, 2000.

Wang, S.-H., Tsay, S.-C., Lin, N.-H., Hsu, N. C., Bell, S. W., Li, C., Ji, Q., Jeong, M.-J., Hansell, R. A., Welton, E. J., Holben, B. N., Sheu, G.-R., Chu, Y.-C., Chang, S.-C., Liu, J.-J. and Chiang, W.-L.: First detailed observations of long-range transported dust over the northern South China Sea, Atmos. Environ., 45(27), 4804–4808, doi:10.1016/j.atmosenv.2011.04.077, 2011.

Wang, Z., Sorooshian, A., Prabhakar, G., Coggon, M. M. and Jonsson, H. H.: Impact of emissions from shipping, land, and the ocean on stratocumulus cloud water elemental composition during the 2011 E-PEACE field campaign, Atmos. Environ., 89, 570–580, doi:10.1016/j.atmosenv.2014.01.020, 2014.

Webster, P. J., Magana, V. O., Palmer, T. N., Shukla, J., Tomas, R. A., Yanai, M. and Yasunari, T.: Monsoons : Processes , predictability , and the prospects for prediction 2 . Description of the Monsoons, Weather, 103(C7), 14451–14510, 1998.

Weichenthal, S., Villeneuve, P. J., Burnett, R. T., Donkelaar, A. van, Martin, R. V., Jones, R. R., DellaValle, C. T., Sandler, D. P., Ward, M. H. and Hoppin, J. A.: Long-Term Exposure to Fine Particulate Matter: Association with Nonaccidental and Cardiovascular Mortality in the Agricultural Health Study Cohort, Environ. Health Perspect., 122(6), 609–615, doi:10.1289/ehp.1307277, 2014.

Wimolwattanapun, W., Hopke, P. K. and Pongkiatkul, P.: Source apportionment and potential source locations of PM2.5 and PM2.5–10 at residential sites in metropolitan Bangkok, Atmos. Pollut. Res., 2(2), 172–181, doi:10.5094/apr.2011.022, 2011.

Witt, M., Baker, A. R. and Jickells, T. D.: Atmospheric trace metals over the Atlantic and South Indian Oceans: Investigation of metal concentrations and lead isotope ratios in coastal and remote marine aerosols, Atmos. Environ., 40(28), 5435–5451, doi:10.1016/j.atmosenv.2006.04.041, 2006.

949 Wu, C., Larson, T. V., Wu, S., Williamson, J., Westberg, H. H. and Liu, L.-J. S.: Source apportionment of PM2.5 and
950 selected hazardous air pollutants in Seattle, Sci. Total Environ., 386(1–3), 42–52, doi:10.1016/j.scitotenv.2007.07.042,
951 2007.

952 Xian, P., Reid, J. S., Atwood, S. A., Johnson, R. S., Hyer, E. J., Westphal, D. L. and Sessions, W.: Smoke aerosol transport
953 patterns over the Maritime Continent, Atmos. Res., 122, 469–485, doi:10.1016/j.atmosres.2012.05.006, 2013.

954 Xie, R. K., Seip, H. M., Liu, L. and Zhang, D. S.: Characterization of individual airborne particles in Taiyuan City, China,
955 Air Qual. Atmos. Heal., 2(3), 123–131, doi:10.1007/s11869-009-0039-x, 2009.

956 Xing, Y. F., Xu, Y. H., Shi, M. H. and Lian, Y. X.: The impact of PM2.5 on the human respiratory system, J. Thorac. Dis.,
957 8(1), E69–E74, doi:10.3978/j.issn.2072-1439.2016.01.19, 2016.

958 Yuan, B., Shao, M., Gouw, J. de, Parrish, D. D., Lu, S., Wang, M., Zeng, L., Zhang, Q., Song, Y., Zhang, J. and Hu, M.:
959 Volatile organic compounds (VOCs) in urban air: How chemistry affects the interpretation of positive matrix
960 factorization (PMF) analysis, J. Geophys. Res. Atmos., 117(D24), 1-17, doi:10.1029/2012jd018236, 2012.

961 Yusuf, A. A. and Francisco, H.: Climate change vulnerability mapping for Southeast Asia, Economy and Environment
962 Program for Southeast Asia (EEPSEA) report, available at: http://www. eepsea.net (last access: July 2014), 32 pp., 2009.

963 Zhang, C.: Madden-Julian Oscillation, Rev. Geophys., 43, RG2003, doi:10.1029/2004RG000158, 2005.

964 Zhang, J. and Reid, J. S.: MODIS Aerosol Product Analysis for Data Assimilation: Assessment of Level 2 Aerosol Optical
965 Thickness Retrievals, J. Geophys. Res.-Atmos., 111, 22207, doi:10.1029/2005JD006898, 2006.

966 Zheng, C., Zhao, C., Zhu, Y., Wang, Y., Shi, X., Wu, X., Chen, T., Wu, F. and Qiu, Y.: Analysis of influential factors for the
967 relationship between PM2.5 and AOD in Beijing, Atmos. Chem. Phys., 17(21), 13473–13489, doi:10.5194/acp-17-
968 13473-2017, 2017.

969 Zivanovic, V.: XRF analysis of mineralogical matrix effects and differences between pulverized and fused ferromanganese
970 slag, Chem. Ind. Chem. Eng. Q., 17(2), 231–237, doi:10.2298/ciceq101104008z, 2011.

971 **Table 1. PM1.15/PM10 ratio slopes for elements ordered by ratio-slope.**

	Ratio slope	*R-squared correlation*	*Ratio average*	*Standard deviation*
V	0.94	0.99	0.95	0.07
K	0.82	0.94	0.35	0.21
S	0.8	0.92	0.49	0.17
Zn	0.74	0.94	0.62	0.04
Y	0.7	0.7	0.53	0.11
Zr	0.7	0.63	0.65	0.07
Mo	0.7	0.67	0.65	0.04
Ti	0.68	0.7	0.53	0.08
Rb	0.61	0.64	0.73	0.09
Al	0.51	0.68	0.55	0.12
Pb	0.47	0.44	0.67	0.06
Cu	0.4	0.42	0.63	0.05
Ni	0.31	0.33	0.61	0.08
As	0.31	0.36	0.33	0.26
Mn	0.3	0.62	0.49	0.19
Si	0.29	0.56	0.32	0.13
Se	0.2	0.24	0.59	0.06
P	0.19	0.32	0.27	0.08
Na	0.16	0.57	0.17	0.03
Sr	0.16	0.11	0.49	0.08
Br	0.13	0.17	0.47	0.08
Ca	0.07	0.59	0.1	0.05
Cl	0.06	0.67	0.04	0.02
Fe	0.06	0.38	0.24	0.12
Mg	0.03	0.29	0.07	0.03
Co	0.03	0.03	0.57	0.1
Ga	0.03	0.04	0.56	0.09
Cr	0.01	0.02	0.19	0.19

972

973 **Table 2. Sources identified in each size range with PMF. Coarse (1.15-10 μm), fine (0.34-1.15 μm) and ultrafine (0.10-**

974 **0.34 μm).**

Source	Major Components	Coarse	Fine	Ultrafine
Biomass Burning	K, S, Si, Al, As		+	+
Oil Combustion	V		+	+
Crustal-Marine Mixed Source	Mg, Cl, P, Al, Si, S, Ca	+		
Sea Spray	Na, Mg, Cl, Ca		+	
Soil Dust	Fe, Al, Si, Ca, Ti, Zn	+	+	
Fly ash	As, Se, Pb, Zn, Ti	+	+	+

975

976

Supplementary material

Manuscript Title: Investigating size-segregated sources of elemental composition of particulate matter in the South China Sea during the 2011 Vasco Cruise

Miguel Ricardo A. Hilario[a, +], **Melliza T. Cruz**[b], **Maria Obiminda L. Cambaliza**[a,b], **Jeffrey S. Reid**[c], **Peng Xian**[c], **James B. Simpas**[a,b], **Nofel D. Lagrosas**[b, *], **Sherdon Niño Y. Uy**[b], **Steve Cliff**[d], **Yongjing Zhao**[d]

[a] Department of Physics, Ateneo de Manila University, Quezon City, Philippines

[b] Manila Observatory, Ateneo de Manila University campus, Quezon City, Philippines

[c] Marine Meteorology Division, Naval Research Laboratory, Monterey, CA, USA

[d] Air Quality Research Center, University of California Davis, CA, USA

[+] Now with Manila Observatory, Ateneo de Manila University campus, Quezon City, Philippines

[*] Now with Center for Environmental Remote Sensing, Chiba University, Japan

Correspondence: Maria Obiminda L. Cambaliza (mcambaliza@ateneo.edu)

Supplementary material summary: 15 Pages including Cover Page, 4 Tables, 9 Figures.

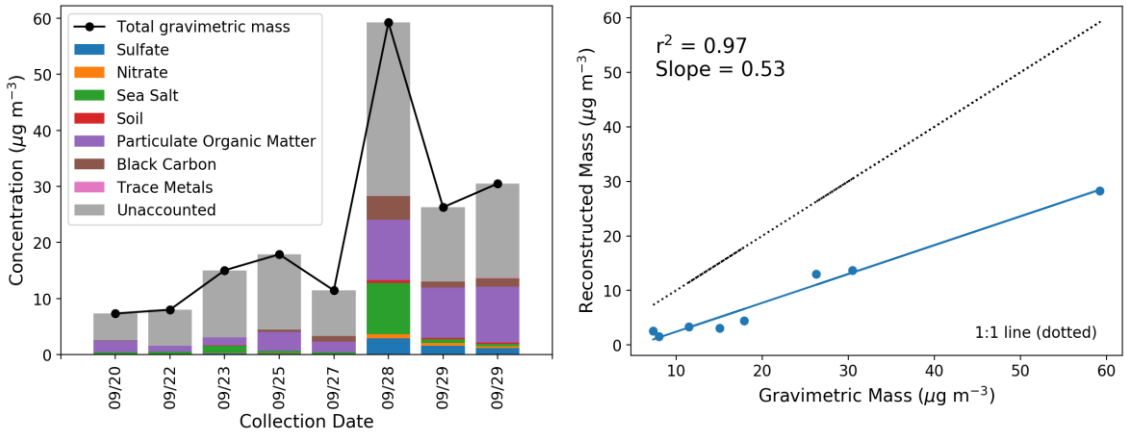

20

21 **Figure S1. (a) Contributions of $PM_{2.5}$ components (µg m^{-3}) derived from filters collected**
22 **during the cruise. (b) Linear regression (blue) of gravimetric and reconstructed masses**
23 **(µg m^{-3}) with a 1-to-1 line depicted as a dashed line (black). Methodology for the mass**
24 **reconstruction is found in Malm and Hand (2007).**

25

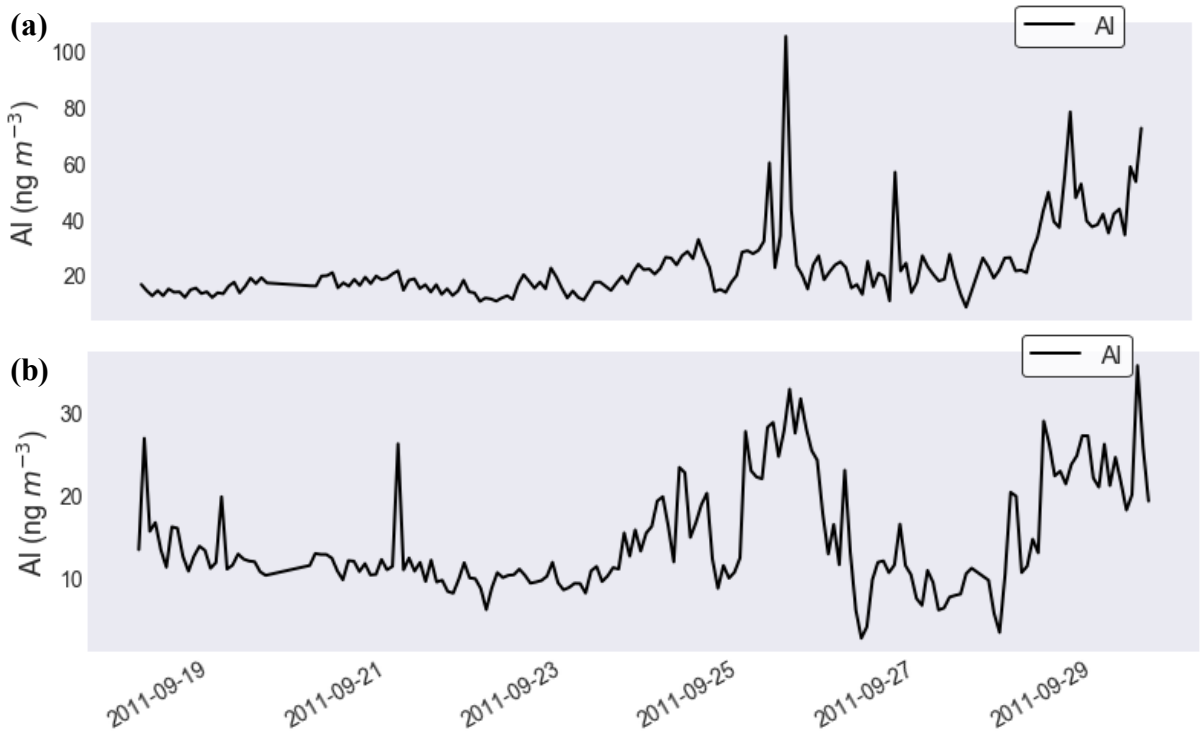

Figure S2. Time series of Al in the (a) fine and (b) ultrafine modes.

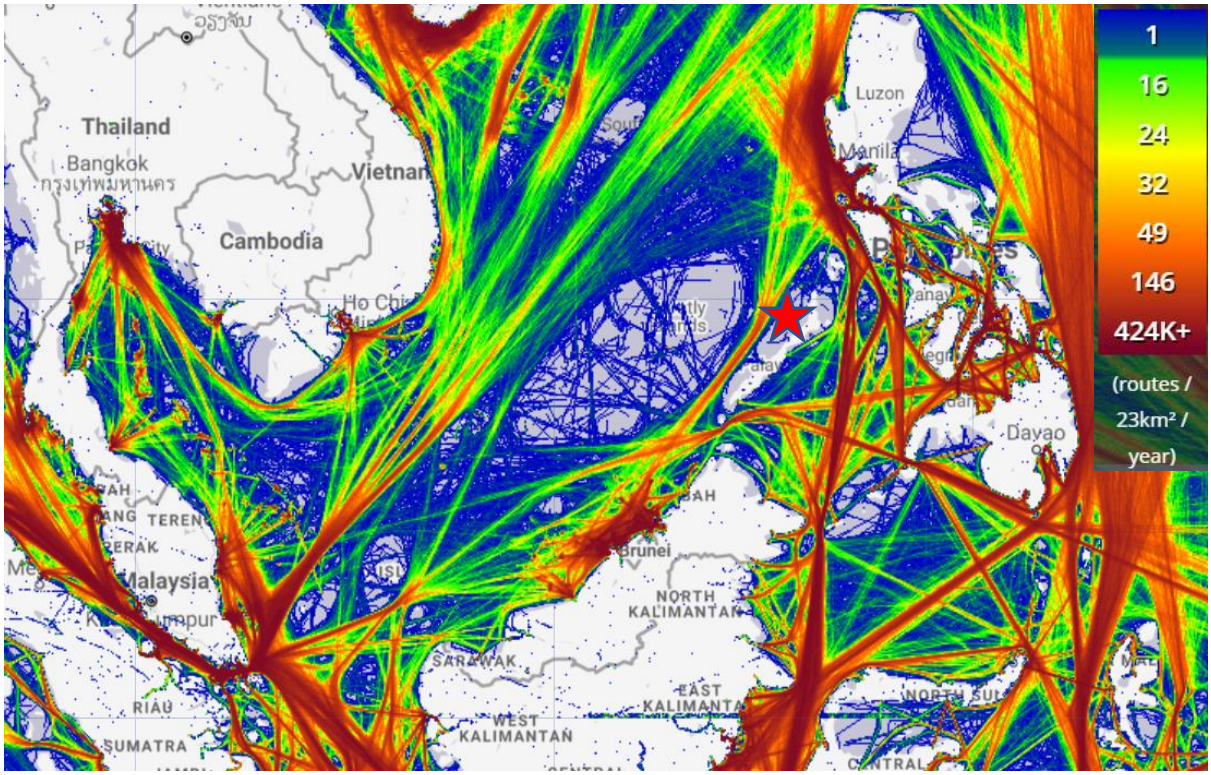

Figure S3. Ship tracks near the Palawan sampling site for 2016-2017. Red star indicates the location of the M/Y *Vasco*. Source: MarineTraffic.

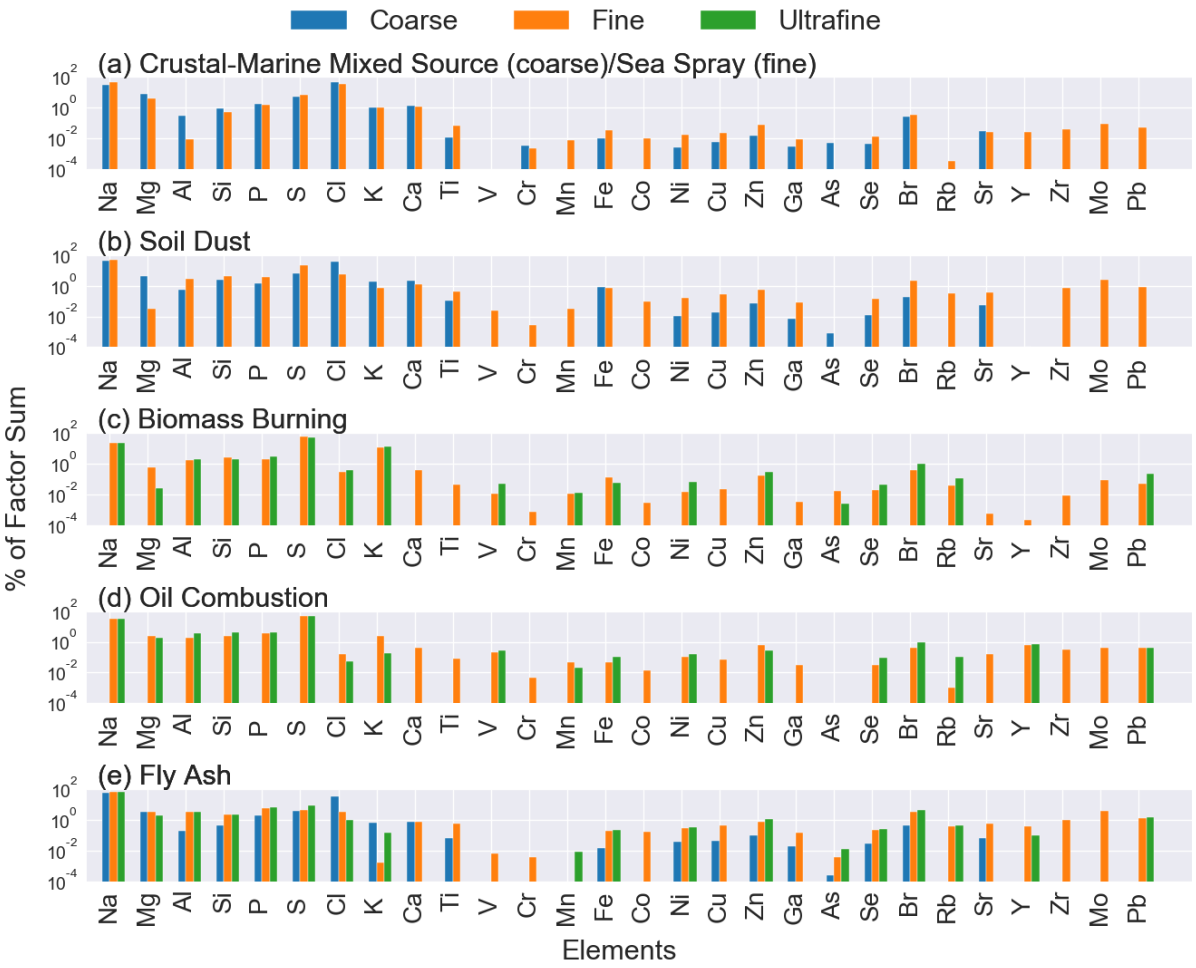

Figure S4. PMF source profiles across different size ranges displayed by percent of factor sum for (a) sea spray, (b) soil dust, (c) biomass burning, (d) oil combustion, and (e) fly ash. Coarse: Stage 1-3 (1.15-10 μm; blue), Fine: Stage 4-6 (0.34-1.15 μm; orange), Ultrafine: Stage 7-8 (0.10-0.34 μm; green).

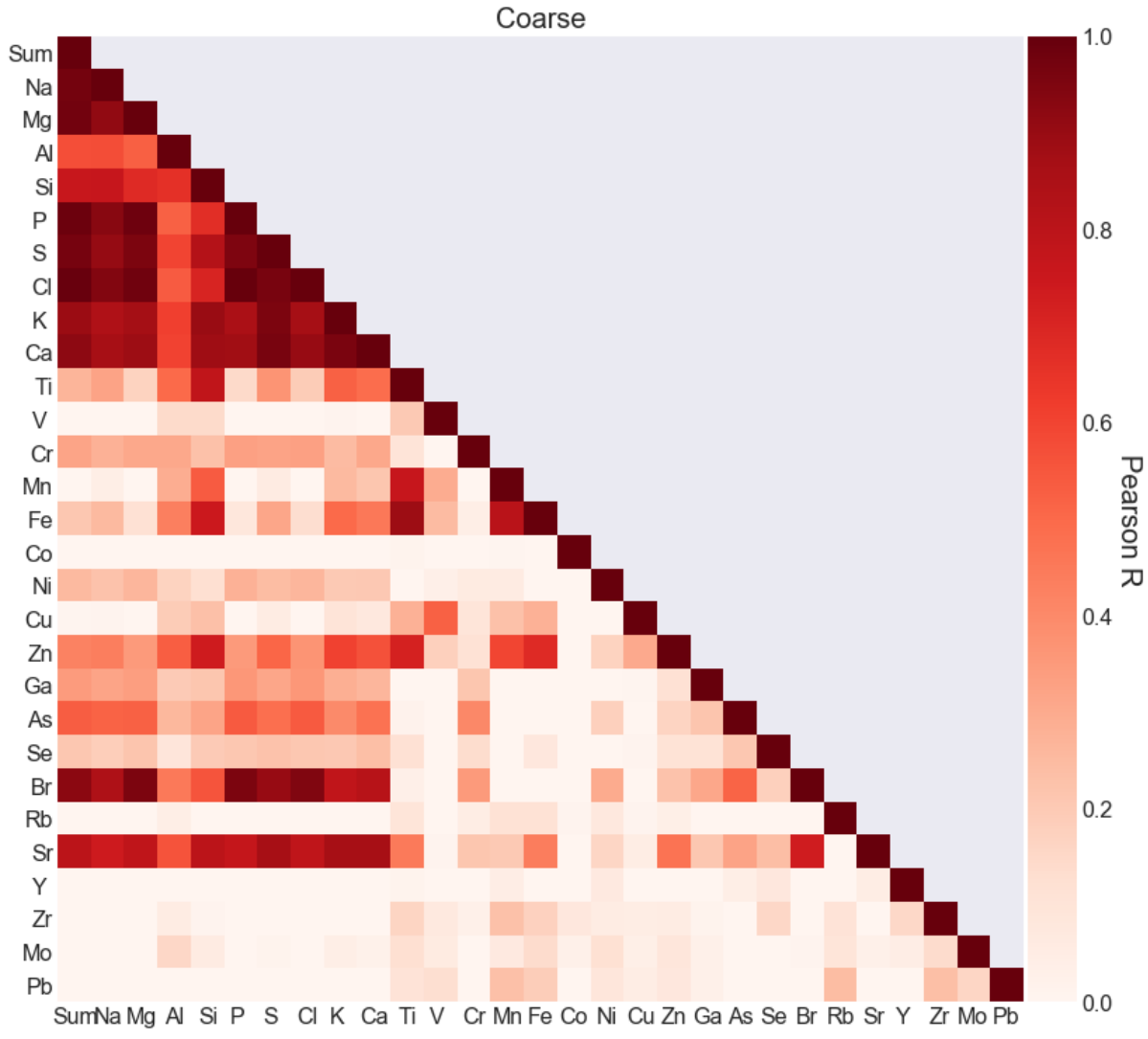

Figure S5. Correlation heatmap for the coarse mode (1.15 – 10 µm).

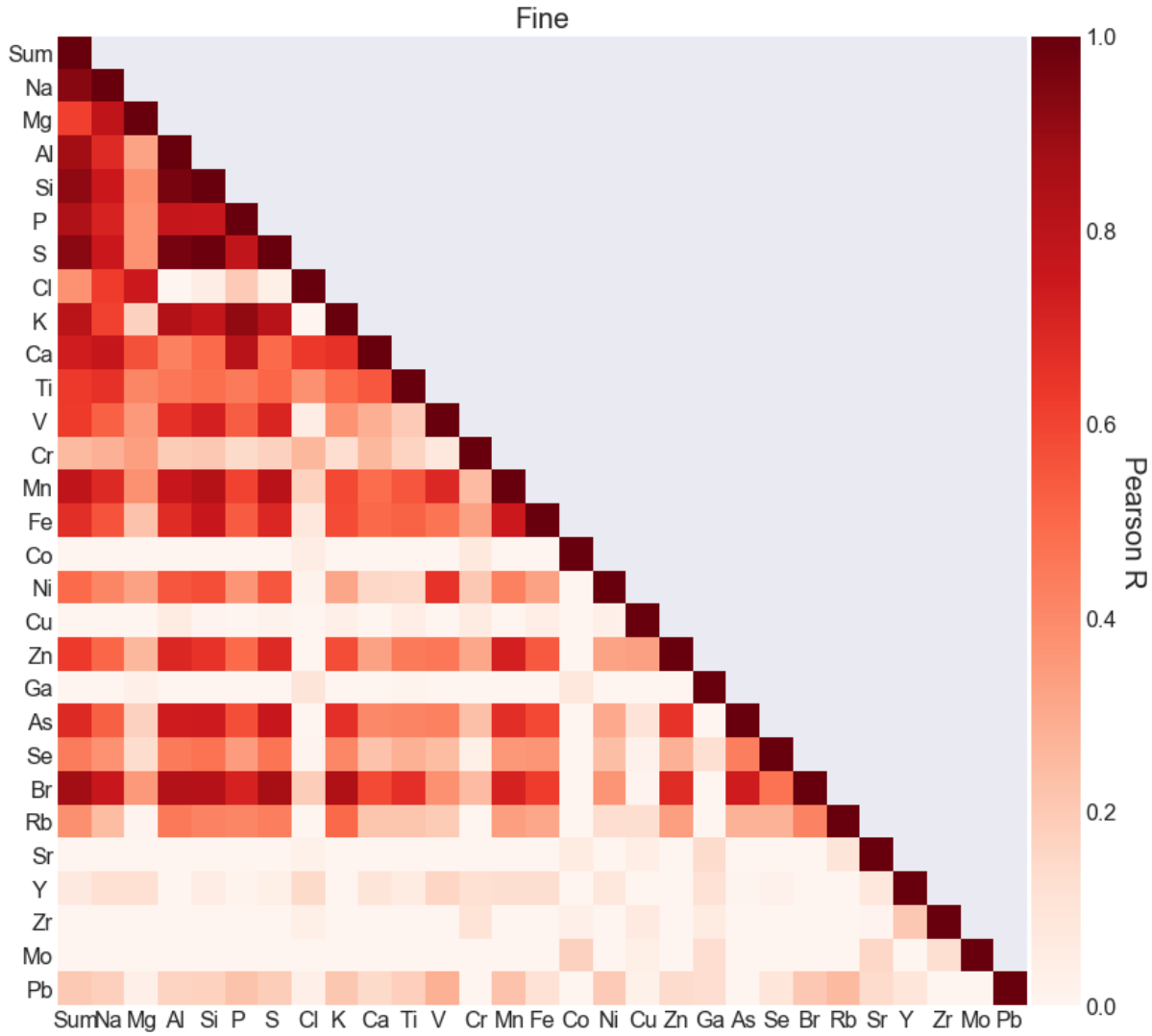

Figure S6. Correlation heatmap for the fine mode (0.34 – 1.15 µm).

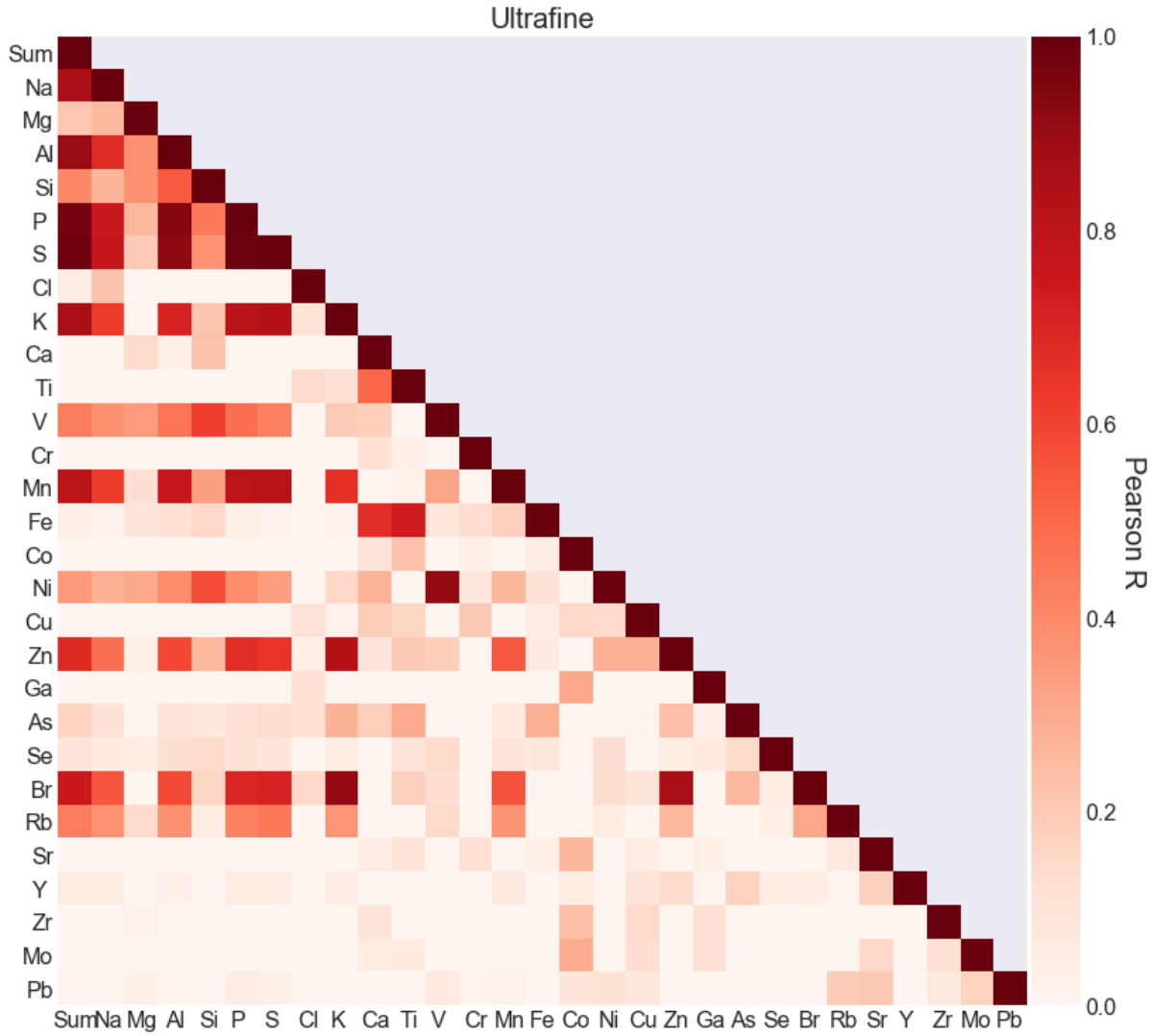

Figure S7. Correlation heatmap for the ultrafine mode (0.07-0.34 µm).

Table S1. Pearson correlation matrix for the coarse mode (1.15 - 10 µm). Correlation coefficients above 0.7 are marked in bold.

	Sum	Na	Mg	Al	Si	P	S	Cl	K	Ca	Ti	V	Cr	Mn	Fe	Co	Ni	Cu	Zn	Ga	As	Se	Br	Rb	Sr	Y	Zr	Mo	Pb
Sum	**1.00**																												
Na	**0.97**	**1.00**																											
Mg	**0.97**	**0.91**	**1.00**																										
Al	**0.57**	**0.58**	**0.53**	**1.00**																									
Si	**0.76**	**0.76**	**0.68**	**0.66**	**1.00**																								
P	**0.99**	**0.93**	**0.98**	**0.52**	**0.67**	**1.00**																							
S	**0.97**	**0.91**	**0.95**	**0.60**	**0.82**	**0.95**	**1.00**																						
Cl	**0.99**	**0.94**	**0.98**	**0.54**	**0.70**	**1.00**	**0.96**	**1.00**																					
K	**0.89**	**0.84**	**0.87**	**0.61**	**0.90**	**0.85**	**0.95**	**0.87**	**1.00**																				
Ca	**0.92**	**0.87**	**0.89**	**0.60**	**0.88**	**0.88**	**0.96**	**0.90**	**0.96**	**1.00**																			
Ti	**0.27**	**0.32**	**0.17**	**0.50**	**0.78**	**0.15**	**0.37**	**0.19**	**0.52**	**0.49**	**1.00**																		
V	**-0.11**	**-0.10**	**-0.13**	**0.14**	**0.14**	**-0.15**	**-0.05**	**-0.13**	**0.01**	**0.00**	**0.20**	**1.00**																	
Cr	**0.32**	**0.28**	**0.31**	**0.31**	**0.23**	**0.33**	**0.32**	**0.33**	**0.25**	**0.31**	**0.10**	**-0.06**	**1.00**																
Mn	**-0.03**	**0.04**	**-0.13**	**0.29**	**0.54**	**-0.15**	**0.06**	**-0.11**	**0.25**	**0.21**	**0.76**	**0.29**	**-0.08**	**1.00**															
Fe	**0.21**	**0.25**	**0.11**	**0.43**	**0.75**	**0.08**	**0.31**	**0.13**	**0.50**	**0.45**	**0.89**	**0.25**	**0.04**	**0.81**	**1.00**														
Co	**-0.07**	**-0.04**	**-0.09**	**-0.06**	**-0.06**	**-0.09**	**-0.09**	**-0.08**	**-0.10**	**-0.09**	**0.01**	**-0.04**	**-0.08**	**0.00**	**-0.02**	**1.00**													
Ni	**0.25**	**0.22**	**0.26**	**0.17**	**0.12**	**0.28**	**0.25**	**0.26**	**0.20**	**0.21**	**-0.02**	**0.03**	**0.06**	**0.06**	**-0.05**	**-0.03**	**1.00**												
Cu	**0.01**	**0.01**	**-0.02**	**0.19**	**0.23**	**-0.02**	**0.05**	**-0.01**	**0.10**	**0.08**	**0.28**	**0.52**	**0.09**	**0.23**	**0.28**	**-0.02**	**-0.02**	**1.00**											
Zn	**0.42**	**0.44**	**0.35**	**0.53**	**0.74**	**0.35**	**0.51**	**0.37**	**0.61**	**0.56**	**0.72**	**0.18**	**0.11**	**0.60**	**0.68**	**-0.03**	**0.17**	**0.30**	**1.00**										
Ga	**0.35**	**0.32**	**0.34**	**0.20**	**0.21**	**0.36**	**0.31**	**0.36**	**0.29**	**0.26**	**0.00**	**-0.04**	**0.21**	**-0.06**	**0.00**	**-0.05**	**-0.06**	**0.00**	**0.12**	**1.00**									
As	**0.53**	**0.52**	**0.52**	**0.26**	**0.32**	**0.54**	**0.48**	**0.54**	**0.40**	**0.47**	**0.02**	**-0.13**	**0.40**	**-0.09**	**-0.02**	**-0.05**	**0.18**	**-0.02**	**0.16**	**0.22**	**1.00**								
Se	**0.21**	**0.19**	**0.22**	**0.09**	**0.20**	**0.21**	**0.22**	**0.21**	**0.21**	**0.24**	**0.12**	**-0.07**	**0.14**	**-0.01**	**0.08**	**-0.07**	**-0.10**	**0.01**	**0.11**	**0.11**	**0.21**	**1.00**							
Br	**0.92**	**0.84**	**0.95**	**0.45**	**0.56**	**0.95**	**0.90**	**0.95**	**0.78**	**0.82**	**0.03**	**-0.18**	**0.35**	**-0.26**	**-0.02**	**-0.09**	**0.30**	**-0.06**	**0.23**	**0.31**	**0.51**	**0.18**	**1.00**						
Rb	**-0.17**	**-0.15**	**-0.21**	**0.04**	**-0.03**	**-0.18**	**-0.15**	**-0.18**	**-0.11**	**-0.13**	**0.10**	**-0.02**	**0.05**	**0.11**	**0.11**	**0.01**	**0.08**	**0.01**	**0.04**	**-0.09**	**-0.11**	**-0.02**	**-0.19**	**1.00**					
Sr	**0.80**	**0.74**	**0.79**	**0.56**	**0.80**	**0.77**	**0.87**	**0.79**	**0.86**	**0.86**	**0.45**	**0.01**	**0.21**	**0.20**	**0.44**	**-0.09**	**0.16**	**0.05**	**0.47**	**0.21**	**0.32**	**0.24**	**0.73**	**-0.11**	**1.00**				
Y	**-0.09**	**-0.09**	**-0.08**	**-0.07**	**-0.05**	**-0.08**	**-0.05**	**-0.09**	**-0.06**	**-0.04**	**0.01**	**-0.16**	**-0.02**	**0.04**	**-0.01**	**-0.09**	**0.07**	**-0.10**	**-0.05**	**-0.08**	**0.04**	**0.08**	**-0.07**	**-0.14**	**0.05**	**1.00**			
Zr	**-0.15**	**-0.10**	**-0.20**	**0.05**	**0.01**	**-0.18**	**-0.17**	**-0.17**	**-0.11**	**-0.13**	**0.16**	**0.07**	**0.03**	**0.23**	**0.17**	**0.08**	**0.05**	**0.05**	**0.05**	**0.01**	**-0.10**	**0.16**	**-0.18**	**0.11**	**-0.13**	**0.15**	**1.00**		
Mo	**-0.02**	**-0.03**	**-0.01**	**0.15**	**0.06**	**-0.03**	**0.01**	**-0.03**	**0.04**	**0.03**	**0.12**	**0.06**	**-0.04**	**0.07**	**0.14**	**0.03**	**0.12**	**0.04**	**0.09**	**0.03**	**-0.11**	**-0.03**	**0.01**	**0.10**	**0.03**	**0.04**	**0.14**	**1.00**	
Pb	**-0.33**	**-0.32**	**-0.35**	**-0.01**	**-0.13**	**-0.34**	**-0.30**	**-0.34**	**-0.23**	**-0.28**	**0.10**	**0.13**	**-0.08**	**0.23**	**0.19**	**-0.09**	**0.09**	**0.05**	**0.08**	**0.03**	**-0.48**	**-0.26**	**-0.34**	**0.24**	**-0.13**	**-0.02**	**0.24**	**0.16**	**1.00**

Table S2. Pearson correlation matrix for the fine mode (0.34 – 1.15 µm). Correlation coefficients above 0.7 are marked in bold.

	Sum	Na	Mg	Al	Si	P	S	Cl	K	Ca	Ti	V	Cr	Mn	Fe	Co	Ni	Cu	Zn	Ga	As	Se	Br	Rb	Sr	Y	Zr	Mo	Pb
Sum	**1.00**																												
Na	**0.93**	**1.00**																											
Mg	**0.61**	**0.79**	**1.00**																										
Al	**0.88**	**0.68**	**0.32**	**1.00**																									
Si	**0.92**	**0.75**	**0.39**	**0.96**	**1.00**																								
P	**0.84**	**0.71**	**0.37**	**0.77**	**0.76**	**1.00**																							
S	**0.93**	**0.75**	**0.37**	**0.97**	**0.98**	**0.78**	**1.00**																						
Cl	**0.37**	**0.62**	**0.75**	**-0.08**	**0.05**	**0.20**	**0.04**	**1.00**																					
K	**0.80**	**0.61**	**0.17**	**0.83**	**0.78**	**0.91**	**0.81**	**-0.02**	**1.00**																				
Ca	**0.73**	**0.77**	**0.57**	**0.43**	**0.49**	**0.81**	**0.49**	**0.63**	**0.66**	**1.00**																			
Ti	**0.63**	**0.66**	**0.41**	**0.46**	**0.48**	**0.45**	**0.51**	**0.38**	**0.50**	**0.55**	**1.00**																		
V	**0.63**	**0.52**	**0.35**	**0.66**	**0.72**	**0.53**	**0.70**	**0.05**	**0.37**	**0.29**	**0.20**	**1.00**																	
Cr	**0.25**	**0.28**	**0.33**	**0.19**	**0.21**	**0.14**	**0.18**	**0.26**	**0.13**	**0.26**	**0.17**	**0.07**	**1.00**																
Mn	**0.79**	**0.69**	**0.38**	**0.76**	**0.82**	**0.60**	**0.81**	**0.17**	**0.59**	**0.49**	**0.55**	**0.69**	**0.25**	**1.00**															
Fe	**0.67**	**0.56**	**0.22**	**0.68**	**0.76**	**0.54**	**0.69**	**0.08**	**0.58**	**0.50**	**0.52**	**0.47**	**0.32**	**0.75**	**1.00**														
Co	**-0.43**	**-0.34**	**-0.12**	**-0.44**	**-0.47**	**-0.42**	**-0.47**	**0.04**	**-0.40**	**-0.29**	**-0.20**	**-0.42**	**0.07**	**-0.43**	**-0.45**	**1.00**													
Ni	**0.49**	**0.41**	**0.33**	**0.55**	**0.57**	**0.37**	**0.55**	**0.02**	**0.32**	**0.15**	**0.15**	**0.65**	**0.20**	**0.43**	**0.33**	**-0.20**	**1.00**												
Cu	**-0.04**	**-0.09**	**-0.13**	**0.06**	**0.01**	**-0.02**	**0.02**	**-0.19**	**0.03**	**-0.10**	**0.04**	**-0.01**	**0.06**	**-0.07**	**0.04**	**0.00**	**0.03**	**1.00**											
Zn	**0.63**	**0.50**	**0.26**	**0.69**	**0.66**	**0.49**	**0.68**	**0.00**	**0.58**	**0.33**	**0.45**	**0.46**	**0.31**	**0.72**	**0.55**	**-0.36**	**0.32**	**0.33**	**1.00**										
Ga	**-0.11**	**-0.05**	**0.03**	**-0.15**	**-0.17**	**-0.13**	**-0.15**	**0.09**	**-0.15**	**-0.10**	**0.02**	**-0.09**	**-0.07**	**-0.12**	**-0.18**	**0.08**	**-0.01**	**-0.06**	**-0.04**	**1.00**									
As	**0.69**	**0.53**	**0.17**	**0.73**	**0.74**	**0.57**	**0.76**	**-0.03**	**0.67**	**0.40**	**0.42**	**0.43**	**0.23**	**0.67**	**0.59**	**-0.33**	**0.30**	**0.10**	**0.66**	**-0.23**	**1.00**								
Se	**0.44**	**0.37**	**0.13**	**0.45**	**0.47**	**0.35**	**0.47**	**0.01**	**0.41**	**0.22**	**0.28**	**0.24**	**0.04**	**0.36**	**0.36**	**-0.17**	**0.23**	**0.02**	**0.28**	**0.12**	**0.43**	**1.00**							
Br	**0.88**	**0.76**	**0.35**	**0.83**	**0.82**	**0.71**	**0.86**	**0.19**	**0.84**	**0.58**	**0.67**	**0.38**	**0.25**	**0.71**	**0.62**	**-0.32**	**0.36**	**0.01**	**0.68**	**-0.10**	**0.74**	**0.47**	**1.00**						
Rb	**0.38**	**0.24**	**0.01**	**0.45**	**0.42**	**0.41**	**0.44**	**-0.13**	**0.50**	**0.22**	**0.22**	**0.19**	**-0.01**	**0.33**	**0.31**	**-0.15**	**0.13**	**0.13**	**0.34**	**-0.13**	**0.28**	**0.28**	**0.42**	**1.00**					
Sr	**-0.18**	**-0.14**	**-0.08**	**-0.17**	**-0.19**	**-0.21**	**-0.19**	**0.03**	**-0.21**	**-0.14**	**-0.06**	**-0.05**	**-0.10**	**-0.10**	**-0.11**	**0.06**	**-0.03**	**0.04**	**-0.04**	**0.14**	**-0.21**	**-0.01**	**-0.16**	**0.09**	**1.00**				
Y	**0.07**	**0.12**	**0.12**	**-0.01**	**0.04**	**0.01**	**0.04**	**0.14**	**-0.07**	**0.09**	**0.06**	**0.16**	**0.12**	**0.13**	**0.13**	**-0.10**	**0.08**	**-0.14**	**-0.04**	**0.11**	**0.01**	**0.02**	**-0.02**	**-0.22**	**0.08**	**1.00**			
Zr	**-0.13**	**-0.12**	**-0.01**	**-0.14**	**-0.13**	**-0.08**	**-0.15**	**0.04**	**-0.14**	**-0.03**	**-0.04**	**-0.05**	**0.10**	**-0.08**	**-0.01**	**0.03**	**-0.02**	**0.06**	**-0.06**	**0.06**	**-0.13**	**-0.02**	**-0.18**	**-0.11**	**0.01**	**0.21**	**1.00**		
Mo	**-0.27**	**-0.27**	**-0.21**	**-0.17**	**-0.23**	**-0.20**	**-0.22**	**-0.21**	**-0.19**	**-0.27**	**-0.11**	**-0.13**	**-0.22**	**-0.19**	**-0.23**	**0.17**	**-0.03**	**0.04**	**-0.16**	**0.13**	**-0.21**	**-0.16**	**-0.23**	**-0.07**	**0.15**	**-0.02**	**0.12**	**1.00**	
Pb	**0.20**	**0.18**	**0.03**	**0.17**	**0.17**	**0.22**	**0.19**	**0.03**	**0.21**	**0.14**	**0.18**	**0.28**	**-0.03**	**0.23**	**0.11**	**-0.14**	**0.20**	**0.03**	**0.14**	**0.13**	**-0.07**	**0.09**	**0.20**	**0.25**	**0.14**	**0.09**	**-0.11**	**-0.01**	**1.00**

Table S3. Pearson correlation matrix for the ultrafine mode (0.07-0.34 µm). Correlation coefficients above 0.7 are marked in bold.

	Sum	Na	Mg	Al	Si	P	S	Cl	K	Ca	Ti	V	Cr	Mn	Fe	Co	Ni	Cu	Zn	Ga	As	Se	Br	Rb	Sr	Y	Zr	Mo	Pb
Sum	**1**																												
Na	**0.85**	**1**																											
Mg	**0.21**	**0.25**	**1**																										
Al	**0.9**	**0.68**	**0.38**	**1**																									
Si	**0.4**	**0.27**	**0.38**	**0.54**	**1**																								
P	**0.97**	**0.75**	**0.26**	**0.94**	**0.45**	**1**																							
S	**0.98**	**0.77**	**0.2**	**0.91**	**0.37**	**0.98**	**1**																						
Cl	**0.05**	**0.22**	**-0.29**	**-0.3**	**-0.15**	**-0.1**	**-0.06**	**1**																					
K	**0.86**	**0.63**	**-0.01**	**0.71**	**0.22**	**0.81**	**0.83**	**0.1**	**1**																				
Ca	**-0.04**	**-0.04**	**0.15**	**0.03**	**0.23**	**-0.01**	**-0.07**	**-0.02**	**-0.05**	**1**																			
Ti	**-0.02**	**-0.04**	**-0.1**	**-0.04**	**0**	**-0.04**	**-0.06**	**0.14**	**0.12**	**0.51**	**1**																		
V	**0.44**	**0.38**	**0.34**	**0.47**	**0.62**	**0.48**	**0.43**	**-0.07**	**0.2**	**0.18**	**-0.09**	**1**																	
Cr	**-0.11**	**-0.11**	**-0.03**	**-0.09**	**-0.06**	**-0.12**	**-0.1**	**-0.05**	**-0.11**	**0.11**	**0.03**	**-0.06**	**1**																
Mn	**0.8**	**0.63**	**0.12**	**0.76**	**0.33**	**0.8**	**0.81**	**-0.04**	**0.66**	**-0.02**	**0.03**	**0.32**	**-0.03**	**1**															
Fe	**0.04**	**0.02**	**0.09**	**0.11**	**0.16**	**0.04**	**0.02**	**-0.02**	**0.02**	**0.67**	**0.73**	**0.09**	**0.13**	**0.17**	**1**														
Co	**-0.62**	**-0.53**	**-0.12**	**-0.55**	**-0.21**	**-0.59**	**-0.62**	**-0.06**	**-0.51**	**0.1**	**0.22**	**-0.34**	**0.03**	**-0.51**	**0.04**	**1**													
Ni	**0.35**	**0.28**	**0.31**	**0.39**	**0.58**	**0.39**	**0.33**	**-0.07**	**0.15**	**0.27**	**-0.04**	**0.91**	**0.08**	**0.26**	**0.11**	**-0.25**	**1**												
Cu	**-0.09**	**-0.09**	**-0.19**	**-0.14**	**-0.16**	**-0.11**	**-0.11**	**0.11**	**0.02**	**0.19**	**0.16**	**-0.16**	**0.2**	**-0.02**	**0.05**	**0.15**	**0.14**	**1**											
Zn	**0.68**	**0.48**	**0.04**	**0.59**	**0.25**	**0.67**	**0.64**	**0.03**	**0.82**	**0.09**	**0.2**	**0.19**	**-0.01**	**0.54**	**0.07**	**-0.32**	**0.28**	**0.28**	**1**										
Ga	**-0.23**	**-0.15**	**-0.08**	**-0.29**	**-0.2**	**-0.25**	**-0.25**	**0.11**	**-0.16**	**-0.19**	**-0.06**	**-0.12**	**-0.08**	**-0.24**	**-0.23**	**0.31**	**-0.13**	**-0.04**	**-0.17**	**1**									
As	**0.17**	**0.11**	**-0.04**	**0.1**	**0.08**	**0.12**	**0.13**	**0.12**	**0.28**	**0.18**	**0.3**	**-0.01**	**-0.03**	**0.07**	**0.28**	**-0.05**	**-0.02**	**0.01**	**0.23**	**0.03**	**1**								
Se	**0.09**	**0.07**	**0.06**	**0.12**	**0.14**	**0.11**	**0.09**	**-0.06**	**0.05**	**-0.01**	**0.1**	**0.14**	**-0.04**	**0.1**	**0.08**	**0.01**	**0.13**	**-0.11**	**0.05**	**0.07**	**0.14**	**1**							
Br	**0.75**	**0.55**	**-0.1**	**0.58**	**0.16**	**0.69**	**0.71**	**0.16**	**0.91**	**-0.03**	**0.17**	**0.13**	**-0.07**	**0.56**	**-0.01**	**-0.38**	**0.13**	**0.1**	**0.86**	**-0.08**	**0.26**	**0.05**	**1**						
Rb	**0.44**	**0.37**	**0.14**	**0.38**	**0.05**	**0.42**	**0.45**	**-0.09**	**0.36**	**-0.16**	**-0.1**	**0.14**	**-0.03**	**0.37**	**-0.13**	**-0.24**	**0.06**	**-0.08**	**0.26**	**-0.04**	**-0.09**	**0.04**	**0.31**	**1**					
Sr	**-0.21**	**-0.14**	**-0.04**	**-0.19**	**-0.12**	**-0.2**	**-0.21**	**0**	**-0.22**	**0.05**	**0.09**	**-0.16**	**0.11**	**-0.2**	**0.03**	**0.26**	**-0.14**	**0.05**	**-0.16**	**0.03**	**-0.11**	**-0.07**	**-0.17**	**0.07**	**1**				
Y	**0.06**	**0.06**	**-0.12**	**0.03**	**0**	**0.05**	**0.06**	**0**	**0.05**	**-0.13**	**-0.07**	**-0.09**	**-0.07**	**0.07**	**-0.08**	**0.06**	**-0.07**	**0.09**	**0.14**	**-0.06**	**0.17**	**0.05**	**0.05**	**-0.18**	**0.17**	**1**			
Zr	**-0.33**	**-0.28**	**0.02**	**-0.29**	**-0.14**	**-0.32**	**-0.33**	**0.01**	**-0.26**	**0.1**	**-0.01**	**-0.15**	**0**	**-0.33**	**-0.12**	**0.24**	**-0.06**	**0.15**	**-0.16**	**0.12**	**-0.12**	**0**	**-0.22**	**-0.19**	**0**	**-0.02**	**1**		
Mo	**-0.27**	**-0.26**	**-0.08**	**-0.25**	**-0.07**	**-0.26**	**-0.28**	**-0.01**	**-0.2**	**0.06**	**0.07**	**-0.14**	**-0.02**	**-0.25**	**-0.01**	**0.29**	**-0.08**	**0.13**	**-0.04**	**0.12**	**-0.04**	**-0.13**	**-0.08**	**-0.04**	**0.16**	**-0.07**	**0.12**	**1**	
Pb	**0.01**	**-0.04**	**0.04**	**0.01**	**-0.01**	**0.05**	**0.03**	**-0.03**	**-0.05**	**-0.06**	**-0.14**	**0.06**	**0.01**	**0.02**	**-0.18**	**0.09**	**0.11**	**0.08**	**-0.01**	**0**	**-0.53**	**-0.08**	**0.01**	**0.19**	**0.21**	**-0.1**	**0.07**	**0.17**	**1**

Table S4. Comparison of ratio-slopes and r^2 correlations of various elements with stage 7-8 Si.

	18-19 Sept			*19-30 Sept*		
	Ratio-slope	R^2	Intercept	Ratio-slope	R^2	Intercept
P	0.06	0.76	16.36	0.83	0.96	10.45
S	1.73	0.73	11.67	22.26	0.94	-84.65
Al	0.11	0.61	9.4	0.81	0.92	3.47

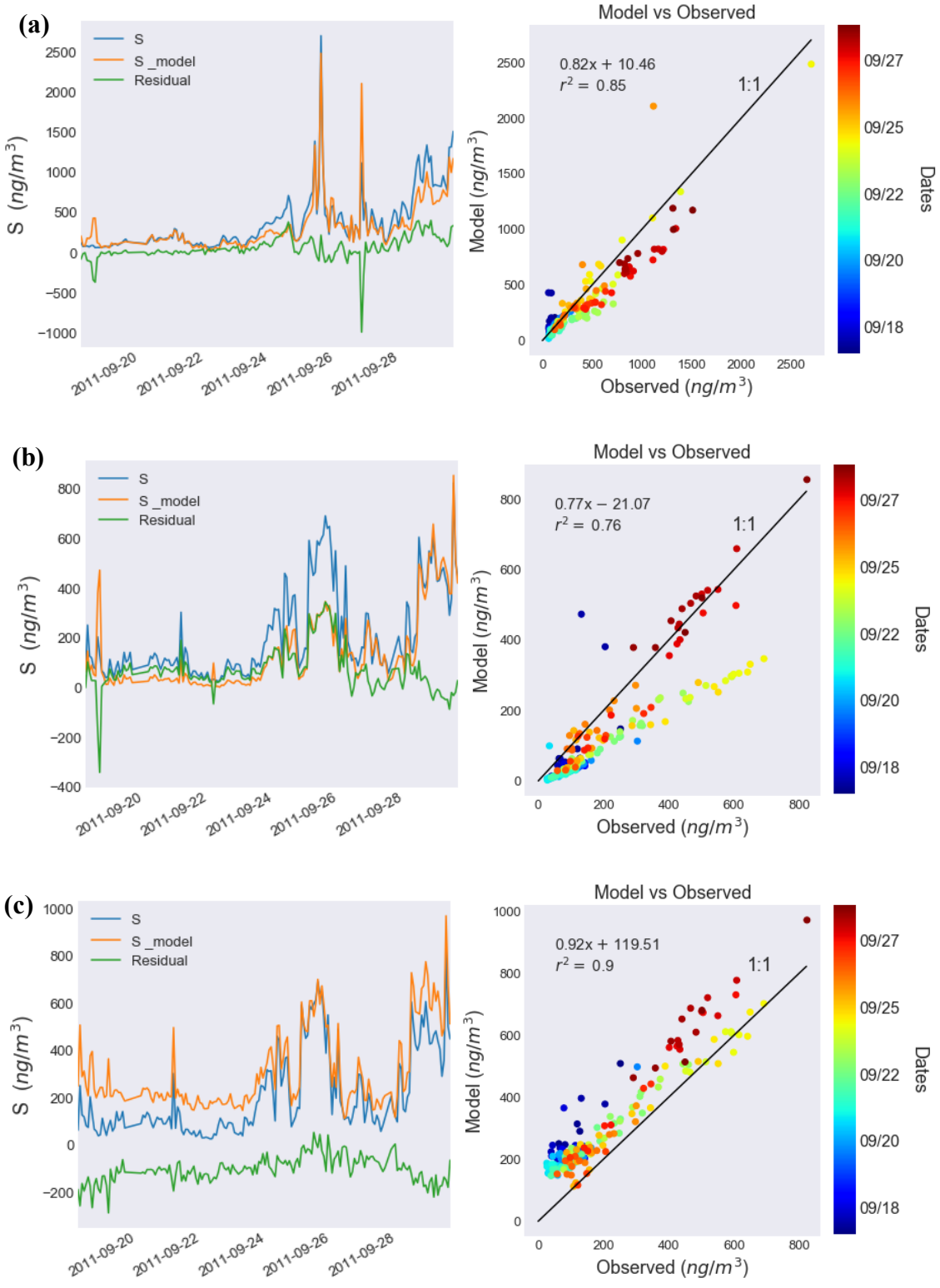

Figure S8. Multiple linear regression time series plots predicting S using tracers K and V in the (a) fine mode, (b) ultrafine mode, and (c) with the addition of Al in the model for the ultrafine mode. The residual is plotted in green, defined as the difference between the actual and modelled concentrations of S. Color bar indicates the time of sampling.

Multiple linear regression analysis description

Having origins in both oil combustion (Balasubramanian et al., 2003; Han et al., 2006; Santoso et al., 2010) and biomass burning (Artaxo et al., 1998; Han et al., 2006; Reid et al., 2015), S serves as a general indicator combustion (Atwood et al., 2012). Multiple linear regression was used with S as the dependent variable to determine contributions from biomass burning and oil combustion in the fine and ultrafine modes. One key assumption is that variations in S can be attributed to biomass burning and oil combustion, represented by their tracers K and V, respectively.

Strong correlations, slopes near unity, and low y-intercepts in the linear regression plots of actual and modelled S indicate that K and V are good predictors of S, particularly in the fine mode (Fig. S7a). However, the model underestimates the concentration of ultrafine S between 24 to 26 September (Fig. S7b). The underestimation may be due to an additional source of ultrafine S that is independent of biomass burning and oil combustion.

To further investigate additional elements that may explain the model's underestimation, residual values between the modelled and actual concentrations of S were used to identify elements that correlated strongly with the residual. In the ultrafine mode, Al was found to correlate strongly with the residual. Upon adding Al to the model, the model was observed to better capture variance in S, specifically between 24 and 26 September (Fig. S7c) which was significantly underestimated when only K and V were included in the model (Fig. S7b). This addition creates a positive discrepancy of the model over the actual concentration of S which indicates source of Al distinct from S in the ultrafine mode. Although the addition of Al improves the model's prediction between 24 and 26 September, we consider K and V generally sufficient predictors of S.

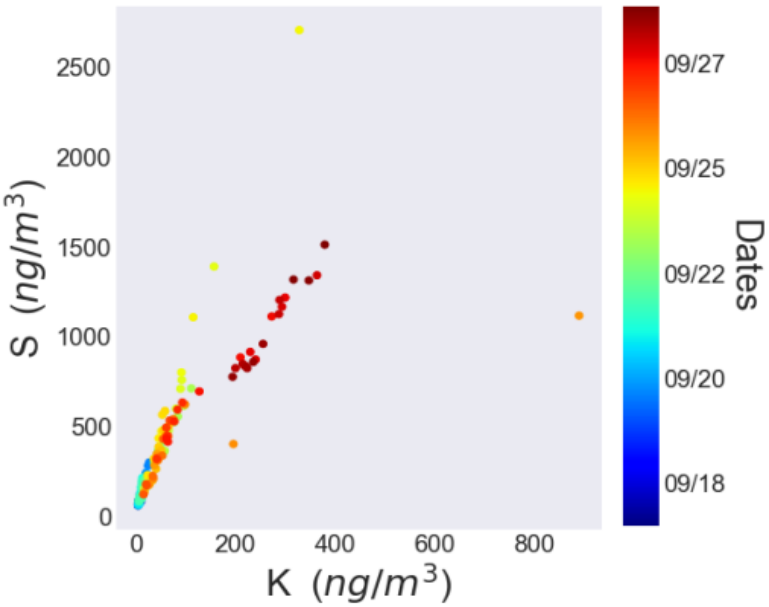

Figure S9. Linear regression of S and K in the fine mode (0.34 – 1.15 µm), colored by date.